



UNIVERSITY OF THE  
WITWATERSRAND,  
JOHANNESBURG

**Establishing and characterizing organoid cultures from colon tissue of South African individuals**

by

**Thea-Leonie du Plessis**

**(1824202)**

**Dissertation**

Submitted in fulfilment of the requirements for the degree

**Master of Science**

in

**Molecular and Cell Biology**

in the Faculty of Science, University of the Witwatersrand, Johannesburg, South Africa

Supervisor:

Professor Mandeep Kaur

June 2024

## Declaration

I declare that this dissertation is my own, unaided work. It is being submitted for the Degree of Master of Science at the University of the Witwatersrand, Johannesburg. It has not been submitted before for any degree or examination at any other University.

A handwritten signature in black ink, appearing to be 'Raa', written over a horizontal line.

(Signature of candidate)

4 June 2024 at Alberton

## **Acknowledgements**

I would like to thank my supervisor, Professor Kaur, for all her guidance and help throughout the writing of this proposal, as well as her continuous support, patience and kind words of motivation throughout the period of being my supervisor.

I would like to extend a special thank you to my mentor, Naaziyah Abdulla for her continuous support, guidance and mentorship throughout my MSc degree.

I would also like to thank each of my lab colleagues in GH519 for the continued support and guidance.

I would also like to thank the NRF for funding, CPRR grant number: 129356.

Lastly, I would like to thank my mother, fiancé, friends and extended family for always believing, supporting and pushing me to reach my goals.

## Table of Contents

Declaration .....	2
Acknowledgements .....	3
List of Figures .....	6
List of Tables .....	7
List of Equations .....	7
Annexures .....	7
List of Symbols .....	8
Nomenclature .....	10
List of outputs .....	15
1. Abstract .....	16
2. Introduction .....	17
2.1. Cancer and the global statistics .....	17
2.2. Colorectal Cancer .....	17
2.2.1. Colorectal Cancer in South Africa .....	17
2.2.2. Colorectal Cancer Staging and Treatments .....	18
2.2.3. Colorectal Cancer Development .....	22
2.2.3.1. Molecular Pathways Defining Colorectal Cancer .....	23
2.2.3.1.1. CIN Pathway .....	23
2.2.3.1.2. MSI Pathway .....	24
2.2.3.1.3. CIMP Pathway .....	24
2.3. Culture Models to Study Cancer .....	27
2.3.1. Intestinal Organoids .....	32
2.3.1.1. Intestinal Organoid Applications .....	33
2.3.1.2. Organoid Culture Validation Techniques .....	36
2.3.1.3. Intestinal Structure and Cell Types .....	37
2.3.1.3.1. Intestinal Stem Cells .....	38
2.3.1.3.1.1. Absorptive Cells of the Intestinal Tract .....	38
2.3.1.3.1.2. Secretory Cells of the Intestinal Tract .....	39
3. Aim and Objectives .....	41
3.1. Aim .....	41

3.2.	Objectives.....	41
3.3.	Hypothesis.....	41
3.4.	Project Workflow.....	41
4.	Methodology.....	44
4.1.	Ethical Clearance and Informed Patient Consent.....	44
4.2.	Patient Sample Collection.....	44
4.3.	Organoid Culturing.....	44
4.3.1.	Freezing and storage of Tissue samples.....	44
4.3.2.	Isolation of Human Colonic Crypts from Fresh Tissue.....	45
4.3.2.1.	Isolation of human crypts from frozen tissue.....	45
4.3.3.	Counting and plating of Isolated Human Colon Crypts.....	46
4.3.4.	Generation of in-house organoid media.....	47
4.3.5.	Organoid Passaging.....	51
4.4.	Reverse-Transcriptase Quantitative Polymerase Chain Reaction (RT-qPCR).....	51
4.4.1.	RNA Extraction.....	52
4.4.2.	cDNA synthesis.....	53
4.4.3.	RT-qPCR.....	54
4.5.	Immunofluorescence procedure and analysis.....	57
4.6.	Data Analysis.....	59
5.	Results.....	59
5.1.	Organoid Generation.....	59
5.1.1.	Patient Sample Collection Data.....	59
5.1.2.	Optimization of Organoid Seeding Density.....	62
5.2.	Comparing Organoid Growth using STEMCELL™ Technologies media and in-house prepared Organoid Media.....	64
5.2.1.	Organoid Growth Monitoring across days at Passage 0.....	66
5.2.2.	Organoid Sub-culturing and Growth Monitoring across Passages.....	69
5.3.	Protocol generating organoids from frozen tissue biopsies.....	73
5.4.	Organoids Accurately Recapitulate Genetic Composition and Spatial Localization of Cell Types in Primary Tissue.....	76
5.4.1.	Identification of the most suitable protocol to isolate RNA from organoids.....	76
5.5.	Genetic Composition of Cell Types present in Normal Tissue is Recapitulated in Non-cancerous Organoids.....	79

6.	Discussion.....	85
6.1.	Success of Organoid Culture is Inherently Dictated by the Concentration of Reconstituted BME and Seeding Density of Organoids .....	86
6.2.	Components in organoid media and their effects on organoid growth and morphology	89
6.3.	Inherent Sample variation and its Effects on Organoid Growth .....	93
6.4.	Organoids Recapitulate Cell Types Present in the Original Tissue and Spatial Localization.....	94
6.5.	Successes of this study .....	97
6.6.	Limitations of organoids and this study .....	97
6.7.	Future research and recommendations.....	99
7.	Conclusion.....	103
8.	Annexure 1 .....	104
8.1.	Reconstitution Methodologies for Reagents .....	104
8.2.	Agarose Gel Electrophoresis RT-qPCR Optimization.....	106
9.	References .....	108

## List of Figures

Figure 1:	Treatments strategies per stage of colorectal cancer. ....	22
Figure 2:	Molecular Pathways involved in Colorectal Cancer Development.....	26
Figure 3:	Intestinal organoid development. ....	33
Figure 4:	Structure of the intestinal crypt and villi with intestinal cell types of interest. ....	38
Figure 5:	Project workflow. ....	43
Figure 6:	Organoid growth of N-B043 of non-cancerous and C-B043 cancer organoids in STEMCELL™ Technologies organoid media vs. in-house prepared media. ....	65
Figure 7:	Monitoring organoid growth to identify key development steps.. ....	67
Figure 8:	Monitoring non-cancerous organoid growth across several days in culture at p0. ....	68
Figure 9:	Monitoring the organoids in TrypLE to identify optimal TrypLE incubation time. ....	70
Figure 10:	Organoid growth during p1, p2 and p3. ....	71
Figure 11:	Failure of cancer organoid growth from fresh tissue biopsies. ....	72
Figure 12:	Comparison of non-cancerous organoid growth from N-B046 frozen tissue biopsy..	73
Figure 13:	Growth monitoring of cancer organoids in culture from frozen tissue biopsies. ....	76
Figure 14:	Characterising non-cancerous organoid cell composition using RT-qPCR in comparison to matched tissue. ....	80
Figure 15:	Representative immunofluorescent images of non-cancerous and cancerous organoids in comparison to previously published literature. ....	84

## List of Tables

Table 1: CRC TMN classification system that is commonly used with reference to CRC disease stage (Adapted from AJCC Cancer Staging Manual (Sung and Sung, 2010)).....	19
Table 2: Comparisons between 2D cell culture, Spheroids and Organoids.....	29
Table 3: Components required for organoid media generation with stock and final concentrations as well as functions of each component.....	49
Table 4: Volumes of RevertAidFirst Strand cDNA Synthesis reagents for cDNA synthesis. ....	54
Table 5: Volumes required for the SensiFast™ SYBR® No-ROX kit for qPCR. ....	55
Table 6: Primer sequences for the genes of interest with β-Actin (ACTB).....	55
Table 7: The Three-step cycling parameter that will be used for qPCR.....	56
Table 8: The primary and secondary antibodies used for immunofluorescence and their respective ratios. ....	58
Table 9: Patient sample collection data. ....	60
Table 10: Table summarising the number of crypts to seed per dome and the more robust BME to use for organoid culture .....	62
Table 11: Comparisons of procured media vs. generating in-house media.....	64
Table 12: Comparison across three different RNA isolation protocols tested.....	78
Table 13: The $2^{-\Delta\Delta C_t}$ values obtained for each gene per sample when comparing the organoids to the tissue samples.....	81
Table 14: Media composition comparisons across 8 different protocols .....	90
Table 15: Variables to consider when generating organoids and the recommendations based on this experimental design. ....	101

## List of Equations

Equation 1: Calculation to determine the average number of crypts.....	46
Equation 2: Calculation performed to calculate the log fold change from generated qPCR data	57

## Annexures

Table S 1: Reagents and concentrations required to generate the media for sample collection.	104
Table S 2: Reagents and concentrations required to generate tissue dissociation buffer (TDB)	104
Table S 3: Reagents and concentration required to generate collagenase IV digestion buffer...	105
Table S 4: Reagents and concentrations required to generate Complete Intesticult™ Organoid medium (non-cancerous organoid media). ....	105
Table S 5: Reagents and concentrations required to make Basal Intesticult™ Organoid Growth Medium (cancer organoid media).....	105
Table S 6: Reagents and volumes used to make washing solution for organoid immunofluorescence.....	105
Supplementary Figure 1: Representative gel images for PCR optimization.....	106

## List of Symbols

$\alpha$	Alpha
$\beta$	Beta
$\kappa$	Kappa
$\mu$	Micro
©	Copyright
™	Trademark
®	Registered Trademark
$\mu\text{L}$	Microliter
$\mu\text{M}$	Micromolar
$\mu\text{g}$	Microgram
mM	Millimolar
mL	Millilitre
mV	Millivolts
mg	Milligram
M	Molar
g	Gram
x	Times
x g	g force (Relative centrifugal force)
%	Percentage
<	Less than

>	Greater than
°C	Degrees Celsius
nm	Nanometre
nM	Nanomolar
ng	Nanogram
rpm	Revolutions per minute
L	Litre
I	One
II	Two
III	Three
IV	Four
dH <sub>2</sub> O	Distilled water
mmol/L	Millimole per litre
w/v	Weight per volume
ΔΔCt	Delta delta cycle threshold

## Nomenclature

2D	2-Dimensional
3D	3-Dimensional
5-FU	5-Fluorouracil
18q	Long arm of chromosome 18
Alk	Anaplastic lymphoma kinase
<i>APC</i>	Adenomatous polyposis coli gene
<i>BAX</i>	Bcl-2-associated X protein
<i>BCL2</i>	B-cell lymphoma 2
<i>BME</i>	Basement membrane extract
<i>BSA</i>	Bovine Serum Albumin
<i>BRAF</i>	v-raf murine sarcoma viral oncogene homolog B1
<i>CAP</i>	Capecitabine
<i>CAPOX</i>	Capecitabine and Oxaliplatin
<i>CAPIRI</i>	Capecitabine and Irinotecan
<i>CAR</i>	Chimeric antigen receptor
<i>cDNA</i>	Complementary DNA
<i>CHGA</i>	Chromogranin A
<i>c-MYC</i>	Cellular myelocytomatosis
<i>CI</i>	Confidence Interval
<i>CIN</i>	Chromosomal Instability pathway
<i>CIMP</i>	CpG Island Methylator pathway
<i>CpG</i>	Linear dinucleotide of Cytosine and guanine

CO <sub>2</sub>	Carbon dioxide
Cq/ct	Quantitative cycle/threshold cycle
CRC	Colorectal cancer
CRISPR/Cas9	Clustered regularly interspaced short palindromic repeats-associated protein 9
DAPI	4',6 – diamidino – 2 – phenylindole
DMEM	Dulbecco's modified eagle medium
DNA	Deoxyribonucleic acid
dNTP	Deoxynucleotide triphosphate
D-PBS	Dulbecco's phosphate buffered saline
ECM	Extra-cellular matrix
EDTA	Ethylenediamine tetraacetic acid
EGF	Epidermal Growth Factor
EpCAM	Epithelial cell adhesion molecule
FBS	Fetal bovine serum
FGF-2	Fibroblast growth factor 2
FOLFOX	5-Fluorouracil and Oxaliplatin
FOLFIRINOX	5-Fluorouracil, irinotecan, oxaliplatin and leucovorin
FOXFIRI	5-Fluorouracil and Irinotecan
GTC	Guanidium Thiocyanate lysis buffer
H&E	Haematoxylin and eosin
HEPES	4-(2-hydroxymethyl)-1-piperazineethanesulfonic acid
IGF-1	Insulin-like growth factor 1

IGF2R	Insulin-like growth factor 2 receptor
IRI	Irinotecan
Ki-67	Nuclear protein Ki-67
<i>KRAS</i>	Kirsten rat sarcoma gene
LGR5	Leucine-rich repeat-containing G-protein coupled receptor 5
<i>LYZ</i>	Lysozyme gene
MAPK	Mitogen-activated protein kinase
MKi-67	Marker of Proliferation
<i>MLH1</i>	MutL homolog 1
MMR	DNA mismatch repair
mRNA	Messenger ribonucleic acid
MSH3	MutS Homolog 3
MSH6	MutS Homolog 6
MSI	Microsatellite instability pathway
mTOR	Mammalian target of rapamycin
MTT	3-(4,5-Dimethylthiazol-2-yl)-2,5-diphenyltetrazolium bromide
<i>MUC2</i>	Mucin 2 gene
NF- $\kappa$ B	Nuclear factor kappa B
OX	Oxaliplatin
P0	Passage zero
P1	Passage one
P2	Passage two
PCR	Polymerase Chain Reaction

PBS	Phosphate buffered saline
pH	Potential of hydrogen
PI3K	Phosphoinositide 3-kinase
PTEN	Phosphatase and tensin homolog
qPCR	Quantitative Polymerase Chain Reaction
Raf-MEK-ERK	Rat sarcoma-mitogen-activated protein kinase-extracellular-signal-regulated kinase
rRNA	Ribosomal ribonucleic acid
RNA	Ribonucleic acid
ROCK	Rho-associated protein kinase inhibitor
RT-PCR	Real-time polymerase chain reaction
RT-qPCR	Real-time quantitative polymerase chain reaction
SARS-Covid-2	Severe acute respiratory syndrome coronavirus 2
Sc-RNA	Single-cell ribonucleic acid
SMAD2	Mothers against decapentaplegic homolog 2
SMAD4	Mothers against decapentaplegic homolog 4
SYBR	N',N'- dimethyl - N - [4 - (E) - (3 - methyl - 1,3 - benzothiazol - 2 - ylidene) methyl ] - 1 - phenylquinolin - 1 - ium -2 - y] - N - propylpropane - 1,3 - diamine
TE	Tris and Ethylenediamine tetraacetic acid
TGF- $\beta$	Transforming Growth Factor beta
TGFBR2	Transforming growth factor, beta receptor II
TME	Tumour microenvironment

TNM	Tumour, nodes, metastasis
<i>TP53</i>	Tumour protein 53 gene
UV	Ultraviolet
V600E	Valine substituted by glutamic acid at amino acid 600
<i>VILI</i>	Vilin 1 gene
Wnt	Wingless-related integration site
Wnt3A	Wnt Family Member 3A
Y-276324	ROCK inhibitor

## List of outputs

### Publication:

du Plessis, T. L., Abdulla, N. and Kaur, M. (2023). ‘The utility of 3D models to study cholesterol in cancer: Insights and future perspectives’, *Frontiers in Oncology*, 13(April), pp. 1–16. doi: 10.3389/fonc.2023.1156246.

### Conferences and Poster Presentations:

- Molecular Biosciences Research Thrust 2022 1 December 2022, University of the Witwatersrand  
  
(Poster) Title: Establishing colorectal cancer (CRC) organoid cultures to delineate biological mechanisms of tumorigenesis in a South African CRC patient cohort.  
  
Authors: Abdulla, N., Du Plessis, T-L., Bebington, B.D. and Kaur, M.
- Pan African Cancer Research Institute – International Cancer Meeting 26 February 2023 – 1 March 2023 University of Pretoria  
  
(Poster) Title: Establishing and Validating Colorectal Cancer (CRC) Organoid Cultures from a South African Patient Cohort  
  
Authors: Abdulla, N., Du Plessis, T-L., Aronson, R.S., Bebington, B.D., Kaur, M.
- Society for Advanced Cell Culture and Modelling for Africa 9<sup>th</sup> – 11<sup>th</sup> October 2023 North-West University  
  
(Poster) Title: Establishing and Characterizing Colorectal Cancer (CRC) Organoid Cultures from South African Patients.  
  
Authors: Abdulla, N., Aronson, R., Du Plessis, T-L, Bebington B.D. and Kaur, M
- Organ Modelling and 3D Cell Culture Conference 2024 (Hosts - Discovery by Oxford Global) 18-19 March 2024, London  
  
(Poster) Title: Establishing and characterizing organoid cultures from South African Patients  
  
Authors: Abdulla, N., Du Plessis, T-L., Aronson, R., Bebington, B.D. and Kaur, M

## 1. Abstract

Colorectal cancer (CRC) has been poorly studied in South Africa, with limited studies on disease progression and development. Studies that have investigated CRC in South Africa have indicated that there is racial disparity between different racial groups that may be attributed to alternative developmental pathways, differences in genetic compositions or CRC initiators that result in these different clinical presentations. Furthermore, the lack of population-based studies substantiates the need for more intensive CRC research. A particular model used to study cancer in general is the use of two-dimensional (2D) cell cultures, which have provided novel insight into many cancers and their development processes. However, these models lack the complex biology observed *in vivo*. One such model that is gaining research interest is the use of three-dimensional (3D) organoid cultures. Organoids are derived from stem cells and are able to self-organize and mimic the corresponding organ from which they were derived. Research has indicated that organoids are able to maintain cell-type heterogeneity as well as gene expression levels that resemble the organ of origin. Therefore, this project aimed at standardizing a protocol to establish and characterise colorectal organoid cultures from South African patient-derived tissues. Patient samples were obtained from individual patients with informed consent and were processed to generate organoids. The morphology of the organoids was monitored across several days and across passages. Once the organoids had reached maturity and were at passage 2, characterization was performed using real-time quantitative polymerase chain reaction (RT-qPCR) and immunofluorescence which indicated that the genetic composition and spatial localization of cell types of interest in non-cancerous tissue was recapitulated in the organoids. Based on these observations, it is proposed that organoids could be a promising model to investigate CRC disease development and progression and potentially search for novel therapeutics. This project has established the protocols for growing and characterizing organoids from African samples and provides baseline data, and outlines the complexities and issues involved in growing organoid cultures for the future studies.

## **2. Introduction**

### **2.1. Cancer and the global statistics**

Cancer is a growing burden in all developing and developed countries. As of 2020, the GLOBOCAN cancer statistics estimated 19.3 million new cancer cases and 10 million cancer deaths (Sung *et al.*, 2021). This places cancer as one of the leading causes of death worldwide with a projected 47% increase in the number of cases (28.4 million cancers cases) by the year 2040 (Sung *et al.*, 2021). Colorectal cancer (CRC) has been identified as the third commonly diagnosed cancer type (10% contribution to newly diagnosed cancer cases) and is the second leading cause of cancer deaths (9.4% contribution to cancer-related deaths) worldwide (Sung *et al.*, 2021). The estimated number of new CRC cases in 2020 was 1.9 million and 935 000 deaths (Sung *et al.*, 2021). The increasing incidence of CRC may be attributed to changes in lifestyle choices and factors such as excess weight, low physical activity and changes in diet, all of which are independently associated with CRC risk (Siegel *et al.*, 2021; Sung *et al.*, 2021).

### **2.2. Colorectal Cancer**

#### **2.2.1. Colorectal Cancer in South Africa**

CRC has been poorly studied in South Africa, with limited studies on disease progression and development (McCabe *et al.*, 2020). In 2020, there were 66 198 cases and 42 875 deaths recorded (Sharma *et al.*, 2022). According to the South African Cancer Registry, CRC is the second diagnosed cancer type in men and third in woman, and is the fifth most frequently diagnosed cancer type in the country (CANSAs, 2023). Furthermore, South African populations have different clinical presentations in comparison to those observed globally (McCabe *et al.*, 2020). Intriguingly, the cancer disparity between South African racial groups is well-defined, where the African population present with earlier onset of CRC before the age of 50 and the white population present with later onset of CRC (McCabe *et al.*, 2020). Due to the potentially different development pathways, genetic make-up or initiators of CRC that result in the different clinical presentations, this substantiates the need for more intensive research on CRC development and progression in South Africa.

Significant efforts have been made to improve patient prognosis over the last decade. Notably, surgical resection of the primary tumour and chemotherapeutic combinations have contributed significantly to patient survival (Brand *et al.*, 2018). It has been recorded that the 5-year overall survival rates for South African CRC patients are 93.2% for stage I, 72.1 – 84.7% for stage II, 52.3 – 83.4% for stage III and 8.1% for stage IV cancers (Brand *et al.*, 2018). However, 20 – 25% of patients, at initial diagnosis, are classified with metastatic form of the disease (Misiakos *et al.*, 2011; Valderrama-Treviño *et al.*, 2017; Brand *et al.*, 2018; Hossain *et al.*, 2022). Therefore, palliative chemotherapy with possible surgical resection (based on the metastatic site) are the only therapeutic options to improve patient survival. On average, CRC is a slow growing cancer that requires approximately 10 years to progress from an early adenoma to established CRC and a further 9 years (on average) to metastasize (Brand *et al.*, 2018; Nguyen and Duong, 2018). Once metastasis has occurred, prominent sites include, but are not limited to, the lungs, liver, lymph nodes and possible blood vessel metastasis (Misiakos *et al.*, 2011; Valderrama-Treviño *et al.*, 2017; Brand *et al.*, 2018; Hossain *et al.*, 2022). Furthermore, approximately 30% of patients, that were not diagnosed with the metastatic form of disease, may develop metastatic CRC and approximately 50% of patients have been reported to develop drug resistance resulting in limited therapeutic availability (Dallas *et al.*, 2009; Hu *et al.*, 2016; Khan *et al.*, 2021; Zhu *et al.*, 2021). Therefore, the establishment of early screening platforms and alternative therapeutic regimes are crucial avenues to explore in an attempt to target this disease.

### **2.2.2. Colorectal Cancer Staging and Treatments**

Tumour, Nodes and Metastasis (TNM) classification system is the standard method to determine CRC tumour stage (gross appearance) and grade (microscopic appearance) (Table 1) to assess prognosis and guide treatment regimens (Wang *et al.*, 2020). This classification evaluates the primary tumour (T), presence or absence of lymph node metastasis (N) and if distant metastasis (M) formed, as well as providing a numerical measurement that indicates tumour size, extent of regional lymph node spread and the number of metastatic sites (Quirke *et al.*, 2007).

**Table 1: CRC TMN classification system that is commonly used with reference to CRC disease stage (Adapted from AJCC Cancer Staging Manual (Sung and Sung, 2010))**

CRC Stage	TMN Grading Categories	Description
	Tx	Primary tumour cannot be assessed
	T0	No evidence of primary tumour
0	Tis	Carcinoma in situ – intramucosal carcinoma
	N0	No regional lymph nodes metastasis
	M0	No evidence of distant metastasis
I	T1	Tumour grown through muscularis mucosa and into the submucosa
	OR	
	T2	Tumour grown into the muscularis propria
	N0	No regional lymph nodes metastasis
	M0	No evidence of distant metastasis
IIA	T3	Tumour invades perirectal tissue through muscularis propria
	N0	No regional lymph nodes metastasis
	M0	No evidence of distant metastasis
IIB	T4a	Tumour penetrates the visceral peritoneum surface
	N0	No regional lymph nodes metastasis
	M0	No evidence of distant metastasis
IIC	T4b	Tumour directly invades or adheres to other organs and structures
	N0	No regional lymph nodes metastasis
	M0	No evidence of distant metastasis
IIIA	T1	Tumour grown through muscularis mucosa and into the submucosa
	OR	
	T2	Tumour grown into the muscularis propria
	N1	Metastasis in one to three regional lymph nodes
	OR	
	N1c	Tumour deposits in the subserosa or mesentery without regional node metastasis
	M0	No evidence of distant metastasis
	OR (other potential grading)	
	T1	Tumour grown through muscularis mucosa and into the submucosa
	N2a	Metastasis in four – six regional lymph nodes
M0	No evidence of distant metastasis	
IIIB	T3	Tumour invades perirectal tissue through muscularis propria
	OR	
	T4a	Tumour penetrates the visceral peritoneum surface
	N1	Metastasis in one to three regional lymph nodes
	OR	

	N1c	Tumour deposits in the subserosa or mesentery without regional node metastasis
	M0	No evidence of distant metastasis
	OR (other potential grading)	
	T2	Tumour grown into the muscularis propria
	OR	
	T3	Tumour invades perirectal tissue through muscularis propria
	N2a	Metastasis in four – six regional lymph nodes
	M0	No evidence of distant metastasis
	OR (other potential grading)	
	T1	Tumour grown through muscularis mucosa and into the submucosa
	OR	
	T2	Tumour grown into the muscularis propria
	N2b	Metastasis in seven or more regional lymph nodes
	M0	No evidence of distant metastasis
IIIC	T4a	Tumour penetrates the visceral peritoneum surface
	N2a	Metastasis in four – six regional lymph nodes
	M0	No evidence of distant metastasis
	OR (other potential grading)	
	T3	Tumour invades perirectal tissue through muscularis propria
	OR	
	T4a	Tumour penetrates the visceral peritoneum surface
	N2b	Metastasis in seven or more regional lymph nodes
	M0	No evidence of distant metastasis
	OR (other potential grading)	
	T4b	Tumour directly invades or adheres to other organs and structures
	N1	Metastasis in one to three regional lymph nodes
	OR	
	N2	Metastasis present in four or more regional lymph nodes
M0	No evidence of distant metastasis	
IVA	Any T	Cancer may or may not have grown through the wall of the colon or rectum
	Any N	Cancer may or may not have spread to nearby lymph nodes
	M1a	Metastasis confined to one organ or site (liver, lung, ovary or nonregional ganglia)
IVB	Any T	Cancer may or may not have grown through the wall of the colon or rectum
	Any N	Cancer may or may not have spread to nearby lymph nodes
	M1b	Metastasis in more than one organ or site in the peritoneum
IVC	Any T	Cancer may or may not have grown through the wall of the colon or rectum
	Any N	Cancer may or may not have spread to nearby lymph nodes
	M1c	Metastasis to parts of peritoneum and may or may not have spread to distant organs or lymph nodes

Therapeutic options that are available for CRC patients are largely dependent on the stage of diagnosis. The initial intervention is surgical resection, which is combined with chemotherapy or radiotherapy pre- or post-surgery (Figure 1) (Khiavi *et al.*, 2019). Chemotherapy is generally administered, despite its limitations, such as patient resistance, toxicity, adverse drug reactions and unsatisfactory response rates (McQuade *et al.*, 2017; Patil *et al.*, 2017). Approximately 25% of CRC cases are diagnosed at advanced stages and an additional 20% acquire metachronous metastasis (Hossain *et al.*, 2022). Current chemotherapeutic regimes may be single-agent and multiple-agent regimes. The most commonly used single-agent regime is 5-Fluorouracil (5-FU), whereas multiple-agent first-line therapy regimes may include a combination of 5-FU + oxaliplatin (OX) (FOLFOX), 5-FU + irinotecan (IRI) (FOXFIRI), capecitabine (CAP) + OX (CAPOX) or CAP + IRI (CAPIRI) (Hossain *et al.*, 2022). An additional regimen used for advanced or metastatic CRC is FOLFIRINOX (5-FU + OX + IRI + leucovorin), which combines three chemotherapeutics with leucovorin (Lamarca *et al.*, 2020; Sakr *et al.*, 2020). The addition of leucovorin is used to enhance the therapeutic effects and toxicity of 5-FU (Groves *et al.*, 2021). Additionally, 5-FU resistance is a major concern as approximately 40% of patients are resistant to 5-FU and the overall response rate in patients with late stage CRC is 10-15% (Vodenkova *et al.*, 2020). Therefore, further investigations for optimal treatment strategies with desired response rates are desired.

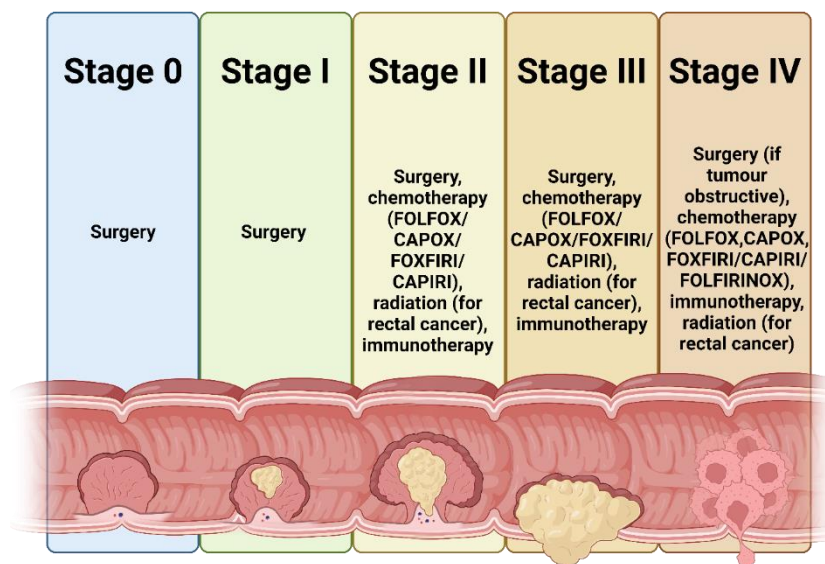


**Figure 1: Treatments strategies per stage of colorectal cancer.** The most commonly used therapeutic intervention for stage 0 – I CRC is surgical removal of the polyp. Several treatment interventions are available for stage II and III including surgical removal of the growth with pre- or post-surgery chemotherapeutics, radiation and combinations thereof depending on the site of development. The two chemotherapeutic combinations often administered is FOLFOX or CAPOX. Additionally, immunotherapy may also be administered. In Stage IV CRC patients, surgery is only performed if the tumour causes an obstruction but combinations of chemotherapies (FOLFOX, CAPOX, FOXFIRI and FOLFIRINOX) are generally administered, radiation therapy in combination with chemotherapy depending on site of development and immunotherapy. (Figure created using BioRender and adapted from Rodrigues and Correia, 2023)

### **2.2.3. Colorectal Cancer Development**

The development of CRC begins with epithelial cells acquiring a series of genetic and epigenetic alterations that confer to hyperproliferation (Nguyen and Duong, 2018; Hossain *et al.*, 2022). CRC development is largely attributed to various mutations in genes associated with deoxyribonucleic acid (DNA) repair mechanisms, tumour suppressor genes and oncogenes (Mármol *et al.*, 2017). Approximately 70% of CRC cases are classified as sporadic and being associated with a broad range of mutations in vital signalling genes resulting in a very heterogeneous cancer type (Mármol *et al.*, 2017). The development of sporadic CRC tends to follow a specific succession of mutations that result in the progression from an adenoma to an adenocarcinoma (Fearon and Vogelstein, 1990; Mármol *et al.*, 2017). The most widely accepted model of the adenoma-carcinoma sequence was developed by Fearon and Vogelstein in 1990 (Smit *et al.*, 2020; Hong *et al.*, 2021). The adenoma-carcinoma sequence is defined by a set of recurrent driver mutations, specifically in Adenomatous polyposis coli (*APC*), Kirsten ras viral oncogene homolog (*KRAS*), Suppressor of Mothers Against Decapentaplegic 4 (*SMAD4*) and tumour suppressor protein 53 (*TP53*) genes (Smit *et al.*, 2020).

Mutations that accumulate in these genes ultimately drive the progression towards sporadic CRC (Smit *et al.*, 2020). These driver mutations deregulate specific cell signalling pathways, leading to oncogenic transformation and metastasis (Smit *et al.*, 2020). Particularly, mutations in *APC* or v-raf murine sarcoma viral oncogene homolog B1 (*BRAF*) oncogene are described as the initiating events required to produce adenomas or serrated polyps, respectively (Nguyen *et al.*, 2020).

Subsequent events that occur will vary depending on the specific molecular pathway that is engaged.

### **2.2.3.1. Molecular Pathways Defining Colorectal Cancer**

The three major molecular pathways that are associated with CRC pathogenesis are the chromosomal instability (CIN), microsatellite instability (MSI) and CpG island methylator phenotype (CIMP) pathway. The most observed pathway is the CIN pathway, which is reported in approximately 85% of CRC cases, characterised by chromosomal numbers and structural alterations (Nguyen and Duong, 2018; Hoevenaar *et al.*, 2020; Malki *et al.*, 2021). MSI is the second most common pathway, constituting 15 – 20% of CRC cases, where alterations in the number of repetitive DNA microsatellites throughout the genome sequence are present (Nguyen and Duong, 2018; Malki *et al.*, 2021). The third pathway is the CIMP pathway, where a high density of methylated genes are observed in approximately 17% of CRC cases (Nguyen and Duong, 2018; Nguyen *et al.*, 2020).

#### **2.2.3.1.1. CIN Pathway**

The CIN pathway is characterized by high rates of gains or losses of whole or sections of chromosomes (Nguyen and Duong, 2018; Nguyen *et al.*, 2020). As a result, aneuploidy tumours and loss of heterozygosity is observed, as well as telomere dysfunction, alterations in chromosome segregation and alterations to DNA damage response mechanisms (Mármol *et al.*, 2017; Nguyen *et al.*, 2020). Additionally, the CIN pathway presents mutations in *APC*, *KRAS*, *SMAD2/SMAD4* (through 18q loss) and lastly *TP53* (Nguyen and Duong, 2018; Nguyen *et al.*, 2020) (Figure 2). Mutations in *APC* result in increased cell proliferation and the activation of *KRAS* that further leads to increased cell survival and inflammation as well as contributes to increased cell proliferation (Mármol *et al.*, 2017; Nguyen *et al.*, 2020). Loss of chromosome 18q in approximately 70% of CRC cases affecting *SMAD2* and *SMAD4* genes localized in 18q21.1 which are two tumour suppressor genes and encode signal transducers for transforming growth factor-beta (TGF- $\beta$ ) (Nguyen and Duong, 2018). Alterations in *SMAD2* and *SMAD4* may result in resistance to TGF- $\beta$  and contribute to tumorigenesis (Nguyen and Duong, 2018). Mutations/loss of *TP53* is common in CRC (43.28%) and assists in tumour progression as it is a transcription factor that regulates genes involved in DNA repair, cell cycle arrest, apoptosis, senescence and metabolism in response to stress (Nguyen and Duong, 2018; Malki *et al.*, 2021). The loss of *TP53* allows for damaged

genetic material to be propagated to daughter cells resulting in the transition from adenoma to carcinoma (Nguyen and Duong, 2018). When karyotypic abnormalities are combined with the accumulation of mutations in tumour suppressor genes and oncogenes, it activates signalling pathways that are critical for CRC initiation and progression.

#### **2.2.3.1.2. MSI Pathway**

The MSI pathway is characterized by defects in DNA mismatch repair (MMR) that is caused by mutation, inactivation or by epigenetic silencing of CpG island hyper-methylation of the MutL homolog 1 (*MLH1*) gene promoter (Malki *et al.*, 2021). The function of the DNA MMR system is to repair a single base pair mismatch that is incorporated into microsatellites during DNA synthesis to maintain genomic stability but alterations result in genomic instability (Malki *et al.*, 2021). Furthermore, CRC cases that present with the MSI pathway also harbour a mutation in *BRAF* that encodes a valine to glutamic acid substitution at amino acid 600 (V600E) resulting in increased cell proliferation and inflammation (Caputo *et al.*, 2019; Nguyen *et al.*, 2020). Additionally, mutations occur in transforming growth factor beta receptor 2 (*TGFBR2*), insulin-like growth factor 2 receptor (*IGF2R*) and B-cell lymphoma 2 (BCL-2)-associated X protein (*BAX*) resulting in increased cell proliferation and survival (Nguyen and Duong, 2018). *TGFBR2* is an important gene that encodes a protein that prevents colon epithelial cell proliferation but the accumulation of mutations in *TGFBR2* inactivates the receptor consequently promoting cell proliferation (Nguyen *et al.*, 2020). *BAX* is a pro-apoptotic gene that belongs to the BCL2 family that present with frameshift mutations resulting in the silencing of *BAX* and suppression of apoptosis (Nguyen and Duong, 2018). Furthermore, the insulin-like growth factor 2 (*IGF2*) gene is parentally imprinted and often loss of imprinting or aberrant imprinting can lead to its overexpression, increased cell proliferation and CRC development (Kasprzak and Adamek, 2019). Consequently, genomic instability and the accumulation of mutations in critical signalling pathways result in the development and progression of CRC (Figure 2).

#### **2.2.3.1.3. CIMP Pathway**

The CIMP pathway contains a high density of hyper-methylated genes in promoter regions that results in loss of gene expression (Malki *et al.*, 2021). CRC tumours that present with the CIMP pathway are shown to have mutations in *BRAF* and hyper-methylation of *MLH1* (Nguyen and Duong, 2018; Nguyen *et al.*, 2020). Inactivation of *MLH1* leads to the induction of MSI, followed

by additional mutations in MutS homolog 3 (*MSH3*), MutS homolog 6 (*MSH6*), *BAX*, *IGF2R* and phosphatase and tensin homolog (*PTEN*) (Malki *et al.*, 2021). This results in the development of dysplasia and cellular transformation (Malki *et al.*, 2021). The CIMP pathway is also a precursor for the serrated pathway, which gives rise to serrated polyps (Nguyen *et al.*, 2020). The serrated pathway is not completely characterized but a distinguished trait of this pathway is the activation of V600E mutation in *BRAF* (Nguyen *et al.*, 2020). This mutation in *BRAF* results in the constitutive activation of the mitogen-activated protein kinase – extracellular signal regulated kinase (MAPK-ERK) pathway and uncontrolled cell division (Nguyen *et al.*, 2020). Furthermore, the serrated pathway exhibits high levels of CpG island methylation, particularly those that are upstream from tumour suppressor genes that result in gene silencing and tumour formation (Nguyen *et al.*, 2020) (Figure 2).

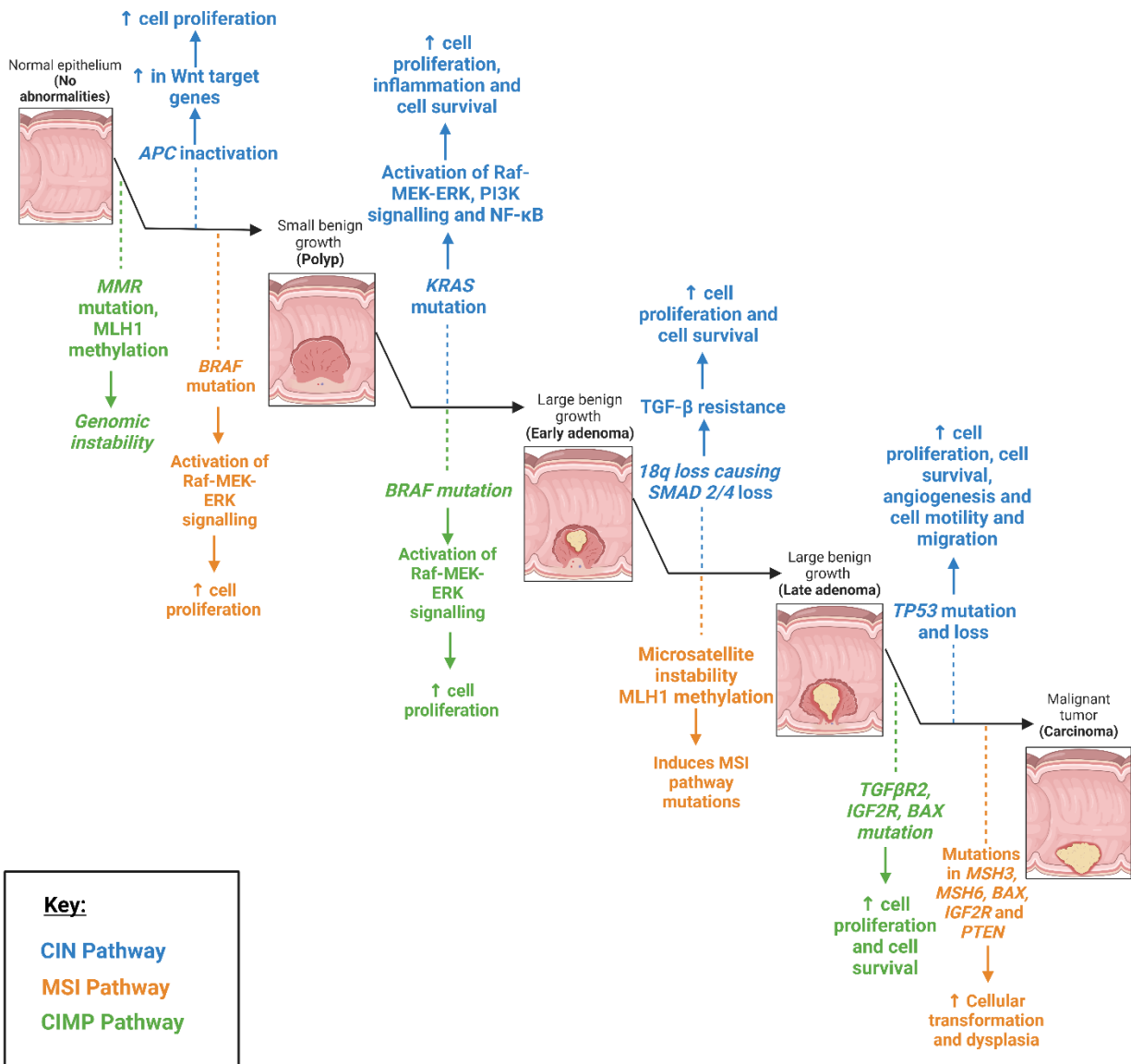


**Figure 2: Molecular Pathways involved in Colorectal Cancer Development.** The most commonly observed pathway in CRC is the CIN pathway (shown in blue). This pathway presents with mutations in APC, KRAS, TP53 and loss of 18q affecting SMAD 2 and SMAD 4. The genetic mutations result in increased cell proliferation through the activation of Wnt target genes and the activation of KRAS mutations. Mutations in KRAS result in constitutive activation of rapidly accelerated fibrosarcoma/mitogen activated protein kinase/extracellular signal regulated kinase (Raf-MEK-ERK) pathway, phosphoinositide 3 kinase (PI3K) signalling via mammalian target of rapamycin (mTOR) and transcription factor nuclear factor kappa light chain enhancer of

activated B cells (NF- $\kappa$ B). The second pathway that is observed is the MSI pathway (shown in orange) that is characterised by defects in DNA mismatch repair. These defects are due to mutation, inactivation or by epigenetic silencing of CpG island hypermethylation of MLH1 and genomic instability. Genomic instability results in the downstream mutations of BRAF and the activation of Raf-MEK-ERK activation that causes increase cell proliferation. When a late adenoma is formed, mutations in TGFBR2, IGF2R and BAX occur, which will ultimately result in the development of malignant tumours. The least commonly observed pathway is the CIMP pathway (shown in green), which is characterised by containing a high-density of hypermethylated genes particularly in promoter regions of MMR and MLH1. This results in loss of gene expression and eventually genomic instability. Mutations then occur that results in increased cell proliferation due to Raf-MEK-ERK activation. Inactivation of MLH1 ultimately leads to the induction of microsatellite instability followed by additional mutations in MSH3, MSH6, BAX, IGF2R and PTEN that causes increase cellular transformation and dysplasia. (Figure generated using BioRender)

### **2.3. Culture Models to Study Cancer**

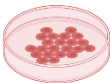


To study the complex gene networks and interactions that cancer utilizes, researchers make use of various *in vitro* models. The most used culture models include two-dimensional (2D) cell culture, followed by three-dimensional (3D) spheroids, and as of late, organoids. The development of 2D cell culture was a major advancement in allowing the improved understanding of cell biology, tissue morphology and most importantly, disease development and drug mechanisms (Kapałczyńska *et al.*, 2016). The abundance of cell lines have been well established and characterised facilitating ease of use and minimal cost, which have allowed for numerous studies involving cancer biology (Yan *et al.*, 2018; D'Costa *et al.*, 2020). 2D cell lines may also be easily manipulated to study drug resistance but their lack of complexity and integration of multiple pathways do not recapitulate the human tissue architecture in its entirety, resulting in an oversimplified model (Yan *et al.*, 2018; D'Costa *et al.*, 2020). Therefore, scientists have explored 3D culture models that mimic disease pathophysiology as a robust alternative. Comparisons amongst these models is shown in Table 2.

Spheroids are generated in a 3D culture by growing spherical cell aggregates derived from single-cell suspensions on low-attachment culture plates, in suspension culture or in a gel or agar

(Białkowska *et al.*, 2020; Nazari, 2020). Spheroids are also self-assembled forming a “mass” due to the close proximity of the cells, allowing for the accumulation of cell-generated collagen for spheroid anchorage (Han *et al.*, 2021; Pape *et al.*, 2021). Spheroid models are more complex than 2D culture methods as their advanced culture capabilities allows them to mimic tumour features. These features include mimicking cell-cell adhesion, cell-extracellular matrix (ECM) interactions, physio-chemical gradients, as well as gene expression patterns resembling those of the original tumour (Franchi-Mendes *et al.*, 2021). Limitations of spheroids are developing and maintaining spheroids in their uniform structure, a larger number of cells are required for spheroids to form efficiently and that ratios of different cells types in the spheroid cannot be controlled when co-culturing with other cell types (Biju *et al.*, 2023). An alternative 3D model to spheroids are organoids, which are more complex and robust in nature.

Organoids are characterised as advanced 3D cultures due to their self-organizing capabilities and have been derived from pluripotent stem cells or adult stem cells, which are able to mimic the *in vivo* organ from which they were derived (Sato *et al.*, 2009; Tuveson and Clevers, 2019). Furthermore, their culture is comprised of growth in a basement membrane matrix and is supplemented with various growth factors to mimic the stem cell niches and provide a representation of the differentiated cell-type heterogeneity present in particular organs (Sato *et al.*, 2009; Tuveson and Clevers, 2019). In a more complex format, organoids are also derived from adult stem cells that comprise individual patient’s tissue, allowing for a more personalized medicine approach towards cancer patients. The applications of organoid culture include, but are not limited to, drug screening, modelling of disease development, biobanking and pre-clinical models (Clevers, 2016; Yan *et al.*, 2018; Boonekamp *et al.*, 2020; Rizzo *et al.*, 2021). Additionally, organoid culture has aided in studying drug metabolism and response, cell differentiation and gene expression levels that largely resemble the organ from which they were derived, as well as led to new insights in the field of drug discovery due to the incorporation of the ECM (Jensen and Teng, 2020; Kim *et al.*, 2020).

**Table 2: Comparisons between 2D cell culture, Spheroids and Organoids**

	<u>2D Culture</u> Cell Culture	<u>3D Culture</u>		<u>References</u>
		Spheroids 	Organoids 	
<b>Accessibility</b>	Easily accessible as well-established culture reagents and cell lines are readily available.	Cellular sources and reagents are available making this model accessible.	More novel method, accessibility remains limited due to specific reagent suppliers and tissue availability from patients.	(Zhao, 2023)
<b>Cost to maintain cultures</b>	Relatively cheap to maintain due to commercially available reagents and assays.	Lower cost in comparison to organoids.	More expensive due to fewer commercially available reagents. Can be costly to initiate and develop cultures.	(Kapałczyńska <i>et al.</i> , 2016; Jensen and Teng, 2020)
<b>Well-established culture protocols</b>	Well-established and standardized protocols available for a variety of cell lines and assays. Examples of assays include cell viability 3-(4,5-Dimethylthiazol-2-yl)-2,5-diphenyltetrazolium bromide (MTT), cytotoxicity (trypan blue) and cell death (APOPercentage™ (Biocolor Ltd, UK)) assays.	A number of well-established protocols available (suspension culture and scaffold culture) but use may be dependent on experiment type. Examples of assays are cell invasion and migration, immunofluorescence, spheroid formation assay and calcein AM assay.	Some well-established protocols available but no standardized protocols available. Assay examples used in organoids are CellTiter-Glo® (Promega, USA) for viability, EdU assay for proliferation and imaging assays using fluorescence.	(Ryu <i>et al.</i> , 2019; Kim <i>et al.</i> , 2020; Zhao, 2023)
<b>Time expenditure to establish culture</b>	Few hours to a few days.	Few days to a few weeks.	Few weeks to a few months.	(Khetan and Burdick, 2010; Baker and

				Chen, 2012; Chen <i>et al.</i> , 2012)
<b>Patient-specific &amp; cellular sources</b>	Yes, can be generated from patient primary cells or an established single cell-line.	Yes, can be generated from patient primary cells or established cell-lines can be used.	Yes, patient tissue samples are digested, and specific cell-types harvested to generate organoids.	(Gunti <i>et al.</i> , 2021)
<b>Cellular characteristics</b>	Cells are grown as monolayers only allowing for the expansion in two-dimensions. This results in the cells having a flat and elongated shape.	Cells are grown as aggregates and in layers allowing them to maintain their natural 3D shape as it would occur <i>in vivo</i> .		(Mseka <i>et al.</i> , 2007; Costa <i>et al.</i> , 2016; Kapałczyńska <i>et al.</i> , 2016; Langhans, 2018; Yamada <i>et al.</i> , 2022)
<b>Cell proliferation rates</b>	Cell proliferation occurs at unnatural rates with cells often at the same stage of growth.	Cell proliferation rates are more natural with cells sometimes at different stages of growth, as would be seen <i>in vivo</i> .		(Ravi <i>et al.</i> , 2015; Langhans, 2018)
<b>Gene and protein expression levels</b>	Expression levels differ vastly different in comparison to <i>in vivo</i> systems.	Expression levels have been shown to closely resemble those seen <i>in vivo</i> .		(Ravi <i>et al.</i> , 2015; Costa <i>et al.</i> , 2016; Kapałczyńska <i>et al.</i> , 2016; Langhans, 2018)
<b>Sensitivity to drugs</b>	Cells present with minimal resistance to drugs that may result in successful outcomes to administered drugs, which may not be a true representation of cellular response.	Cells present more resistance to administered drug treatments, resulting a more holistic overview to drug response and metabolism <i>in vivo</i> .		(Haisler <i>et al.</i> , 2013; Imamura <i>et al.</i> , 2015; Langhans, 2018)

<b>Tumour microenvironment (TME)</b>	Single cell types are often cultured which limits tumour heterogeneity. Additionally, no ECM substance is often present that limits cell-cell interactions to between one cell type. Therefore, does not accurately represent the TME.	Multiple cell types are often cultured together allowing for more tumour heterogeneity to be observed. ECM substrates are often used and cell-cell interactions can be observed between different cell types and the ECM. Therefore, the TME is more accurately represented.	(Hoarau-Véchet <i>et al.</i> , 2018; Barbosa <i>et al.</i> , 2022)
<b>Usage, analysis &amp; reproducibility</b>	Easy to use and results and analysis is easily understandable. Easily reproducible.	Usage can vary from user-to-user and from experiments. Analysis of 3D structures can be difficult to perform and reproducibility remains inconsistent. This is also due to patient-to-patient disparities.	(Hickman <i>et al.</i> , 2014; Booi <i>et al.</i> , 2019; Kim <i>et al.</i> , 2020)

### 2.3.1. Intestinal Organoids

The term “organoid” was first used in 1987 to describe *in vitro* cultures derived from neuroblastomas and the lung, as well as the culture of tissue fragments from epithelial tissues that were separated from the stroma using mechanical and enzymatic digestion and grown in different types of 3D gels (Simian and Bissell, 2017; Almeqdadi *et al.*, 2019). These gels were collagen-rich or laminin-rich and the tissue fragments produced organ-like structures (Simian and Bissell, 2017). However, as of 2012, the Intestinal Stem Cell Consortium published nomenclature guidelines, which stated that the term “organoid” is used for cultures that contain multiple cell types, including mesenchymal and epithelial cell types (Almeqdadi *et al.*, 2019). As research started to shift from 2D culture to 3D culture, a milestone in the development of organoid culture was achieved in 2009 by Sato *et al.*, which showed that single leucine-rich repeat containing G protein-coupled receptor 5 (LGR5)-expression adult intestinal stem cells are capable of forming 3D intestinal organoids in Matrigel® (Sato *et al.*, 2009; Almeqdadi *et al.*, 2019). This was the first report of establishing 3D organoid culture, particularly from mice and this led the way for subsequent organoid work on intestinal organoids. Intestinal organoids are derived from the intestinal epithelium and when derived from humans, they are termed human intestinal organoids and function as “mini-guts” (Sato and Clevers, 2013). Intestinal organoids are generated by differentiation from human pluripotent stem cells or by harvesting intestinal crypts from biopsies taken from individuals (Taelman *et al.*, 2022) and may be used to study disease development and responses to drug treatments. This project focuses on the generation of intestinal organoids derived from human tissue biopsies. Culturing of intestinal organoids is made possible by isolating harvested intestinal crypts and culturing them in Matrigel®, which allows the intestinal organoids to develop a 3D morphology (Sato and Clevers, 2013). The Matrigel® functions as a mimic for the basal lamina that is rich in laminin and collagen, and is particularly useful for stem cells as it retains the stem cells in an undifferentiated state (Hughes *et al.*, 2010; Sato and Clevers, 2013). Additionally, the media used to culture intestinal organoids also assists in maintaining the stem cells as it is supplemented with a combination of growth factors, such as R-spondin, epidermal growth factor (EGF), and Noggin (Sato and Clevers, 2013). This combination ensures stem cell proliferation and maintains the stem cell niche with the addition of a Wnt ligand (Wnt3a), which will further maintain the crypt base columnar epithelial cells that give rise to the various intestinal cell types (Sato and Clevers, 2013). The general growth pattern of human intestinal organoids is illustrated in Figure 3 (Sato and Clevers, 2013).

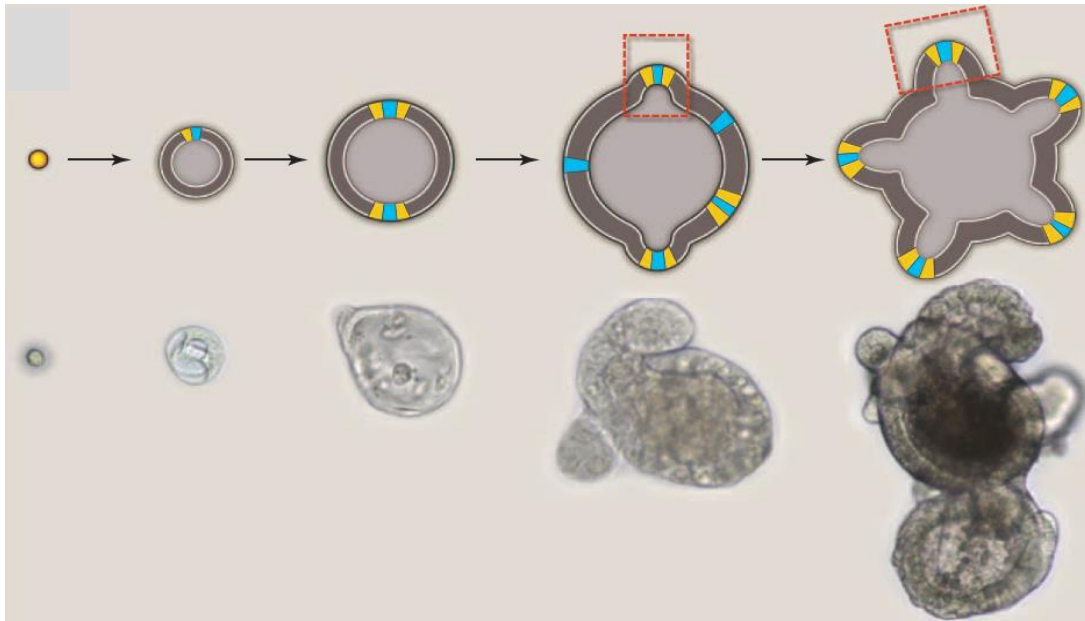


**Figure 3: Intestinal organoid development.** At day 0, the initial growth of the organoid presents as a single stem cell that will progress to form a cyst-like structure. The cyst-like structure is comprised of proliferating progenitor cells and a central lumen that will increase in size. Between days 3 and 4, budding of the cyst-like structure will appear, which marks the development of a crypt. Crypts present as budding structures around the central lumen and will progress to become larger. Organoids will reach maturity between days 7 and 10 in culture, where the structure of the organoid resembles that of the intestine. The lumen will also progress to become darker as this is the region in which villi will develop and dead cells are shed towards the lumen (Figure adopted from Sato and Clevers, 2013).

### 2.3.1.1. Intestinal Organoid Applications

The use and applications of intestinal organoids is a growing research topic that has seen a plethora of literature being published. Current applications of organoids have included, but limited to, are investigating microorganism interactions with patient-derived organoids, gene editing applications and drug screening.

Several microorganisms have been used in organoid based studies to delineate their associations with intestinal diseases. From as early as 2015, co-culturing organoids with bacteria have been used to understand microbiome interactions that result in gastrointestinal diseases. Co-culture is defined as culturing multiple cell types, either directly or indirectly within the same culture environment (Yuan *et al.*, 2023). Currently, studies performed on *Clostridium* (Engevik *et al.*, 2014; Leslie *et al.*, 2015), *Helicobacter pylori* (Schlaermann *et*

*al.*, 2016; Morey *et al.*, 2018; Yao and Smolka, 2019; Maubach *et al.*, 2022), *Escherichia coli difficile* (In *et al.*, 2016; Karve *et al.*, 2017; Pleguezuelos-Manzano *et al.*, 2020; Pradhan *et al.*, 2020) and *Listeria* (Zhou, Zhang, *et al.*, 2022; Zhou, Zou, *et al.*, 2022) have been co-cultured with intestinal organoids and have illustrated the effects on stem cell repair, inflammation, cancer initiation and epithelial barrier function. Viruses have also been co-cultured with intestinal organoids, specifically, human noroviruses (Ramani *et al.*, 2014; Chen *et al.*, 2022; Ettayebi *et al.*, 2022; Mboko *et al.*, 2022) that cause nonbacterial acute gastroenteritis and severe acute respiratory syndrome coronavirus 2 (SARS-CoV-2) as half of patients presented with gastrointestinal symptoms (Krüger *et al.*, 2021). Therefore, the novel development of intestinal organoids has allowed for a more humanised model to study microorganisms. Apart from studies co-culturing microorganisms with organoids, gene editing has also been incorporated, specifically clustered regularly interspaced short palindromic repeats-associated protein 9 (CRISPR/Cas9) (Tian *et al.*, 2023). In a study performed by Schwank and colleagues (2013), CRISPR/Cas9 was applied to modify genes of stem cells from the intestinal stem cells of patients with cystic fibrosis (Schwank *et al.*, 2013). The authors demonstrated that the corrected allele inserted into the patient-derived organoids via CRISPR/Cas9 was expressed and fully functional, which provided a proof of concept for gene correction (Schwank *et al.*, 2013). Gene knock in and knock out applications have also been performed using the CRISPR/Cas9 system. In 2015, two independent groups targeted *KRAS*, *APC*, *p53* and *SMAD4* to introduce mutations in human intestinal organoids (Drost *et al.*, 2015; Matano *et al.*, 2015). These organoids were then transplanted into mice to develop into tumours and the authors could ascertain the levels of differentiation and invasive behaviour depending on the number of genes that were altered (Drost *et al.*, 2015; Matano *et al.*, 2015). This allowed for a better understanding of CRC development and progression. Moreover, the immune system is another avenue to consider due to the use of immunotherapy as a treatment for CRC.

In efforts to study immune system interactions, researchers have utilized the co-culture of specific immune cells with intestinal organoids. Some of the immune cells that have been co-cultured with intestinal organoids are macrophages, T-cells, natural killer cells and neutrophils. In a study performed by Noel and colleagues (2017), the authors utilized intestinal organoids to study epithelial cell-macrophage interactions and the innate immune response to bacterial infections (Noel *et al.*, 2017). The use of T-cells derived from human peripheral blood mononuclear cells have also been used to study cancer T-cell interactions (Dijkstra *et al.*, 2018). Dijkstra and colleagues (2018), investigated the tumour-specific T-cell-based targeting

at a patient specific level as an avenue for personalized medicine to induce tumour-specific T-cell killing of tumour organoids (Dijkstra *et al.*, 2018). Investigating the effects of chimeric antigen receptor (CAR) natural killer cells has also been performed, where the authors co-cultured CRC organoids with EGF variant III – CAR natural killer-92 cells to identify and select suitable target antigens, as well as assessed the anticancer activity of CAR-natural killer 92 cells (Schnalzger *et al.*, 2019). An additional application was to determine the effects of matrices on neutrophil infiltration into organoids (Gjorevski *et al.*, 2020). Gjorevski *et al.*, (2020), using organ-on-a-chip applications to investigate inflammation and develop a model that can be utilized for inflammatory diseases (Gjorevski *et al.*, 2020). As a result, co-culturing patient-derived organoids with immune cells have allowed for novel developments in understanding immune system interactions in an *in vitro* format. As intestinal organoids are derived from patient tissue, it allows for the application of personalised medicine, particularly using drug screening.

The use of intestinal organoids for drug screening is also becoming a popular research topic with researchers developing screening platforms for a variety of intestinal diseases. One of the earliest drug screening applications involved the drug screening on 22 organoid lines using 83 experimental drugs (Van De Wetering *et al.*, 2015). Their results illustrated that the tumour organoids of different genetic backgrounds have effects on drug sensitivities (Van De Wetering *et al.*, 2015). Additionally, the authors verified that the cancer derived organoids retained the heterogeneity of the original tumour to indicate that the use of patient-derived models is a valuable tool for drug screening (Van De Wetering *et al.*, 2015). In a study performed by Vlachogiannis and colleagues (2018), the authors evaluated the feasibility of patient-derived intestinal organoids derived from metastatic cancer as a drug screening tool (Vlachogiannis *et al.*, 2018). A library of 55 drugs were used to screen the derived organoids and their results indicated that the organoids showed 100% sensitivity, 93% specificity, 88% positive prediction and 100% negative prediction (Vlachogiannis *et al.*, 2018). This data was generated based on *ex vivo* treatment responses to correlate the robustness of organoids recapitulating *in vivo* drug responses (Vlachogiannis *et al.*, 2018). The aforementioned advancements in intestinal organoid applications have led to novel research since their development in 2009. However, an important aspect to consider prior to utilizing organoids for a vast number of experiments is to perform characterization and validation to ensure robust and reliable results.

### 2.3.1.2. Organoid Culture Validation Techniques

An important aspect of organoid culture, once the culture has been established, is to validate the culture by characterizing organoid structure and function (Zhao *et al.*, 2022). Validation techniques can be separated on the basis of whether the structure or function is being investigated. For organoid structure validation, simple techniques such as bright-field imaging or immunofluorescent staining can be performed (Zhao *et al.*, 2022).

Bright-field microscopy and imaging can be used for quantification of organoids, such as by counting the number of organoids and monitoring organoid culture progression (Fei *et al.*, 2022). Additionally, bright-field microscopy can be used for morphological measurement, such as size, shape and growth in both healthy and diseased organoids, which can be used to track disease progression (Fei *et al.*, 2022). Immunohistochemical and immunofluorescence imaging can be further used to validate organoid cultures by using specific cell marker antibody staining (Zhao *et al.*, 2022). This method can provide an overview of the spatial distribution and proportion of specific cell types (Zhao *et al.*, 2022). Additionally, histopathological staining can also validate the organoid cultures in comparison to the original tissue as it has been proven that histological features are conserved (Gu *et al.*, 2023).

For organoid function validation, a plethora of techniques are available such as colorimetric assays, calcium signalling or luciferase assays, but the simplest validation methods are polymerase chain reaction (PCR), single-cell RNA (sc-RNA) sequencing or immunofluorescent imaging (Zhao *et al.*, 2022). Real-time quantitative PCR (RT-qPCR) is one of the easiest and fastest methods to validate organoid cultures against marker genes for cell identity and allows for the characterization of gene expression levels which can be compared to the tissue of origin to evaluate the degree of similarity (Zhao *et al.*, 2022; Calà *et al.*, 2023). An additional technique that can be used to evaluate gene expression and validate the cell type heterogeneity in organoid culture is sc-RNA sequencing, which allows for analysis of the transcriptome at single-cell level (Jovic *et al.*, 2022). The cell types from the organoids identified in sc-RNA sequencing are then compared to the cell types in the corresponding tissue to evaluate the degree of similarity (Zhao *et al.*, 2022). Immunofluorescence can be used to investigate the protein content of specific markers and can be compared to the tissue of origin as well (Calà *et al.*, 2023). This technique can also be used to assist in understanding the localization of cell types within organoids, as well as determine interactions between those cells (Bergdorf *et al.*, 2021). Therefore, performing both structural and functional validation of organoid culture is

important to gauge a holistic view and allows for the identification of important intestinal cell types required in the intestinal organoids.

### 2.3.1.3. Intestinal Structure and Cell Types

The inner lining of the intestine is comprised of villi with invaginations that are used to maximise absorption of nutrients (Figure 4). Crypts constitute the base of the villi and contain various intestinal stem cells that contribute to self-renewal of the intestinal epithelium. These stem cells (crypt base columnar cells) give rise to the different cell types present in the human gut and it can be divided into absorptive cells and secretory cells (Boonekamp *et al.*, 2020). The absorptive cells in the crypt are constituted of enteroendocrine cells, whereas the secretory cells are constituted of Paneth cells, goblet cells, tuft cells and enteroendocrine cells (Figure 4). Each cell type differs in abundance and location along the crypt-villus axis (Boonekamp *et al.*, 2020). Furthermore, each cell type presents with a particular genetic makeup that confers upon these cells' specific functions. This molecular signature is utilized to characterise the cells and confirm the presence of each cell type in the intestine. This can be extended to characterising the organoids in culture to confirm that intestinal organoids are being grown.

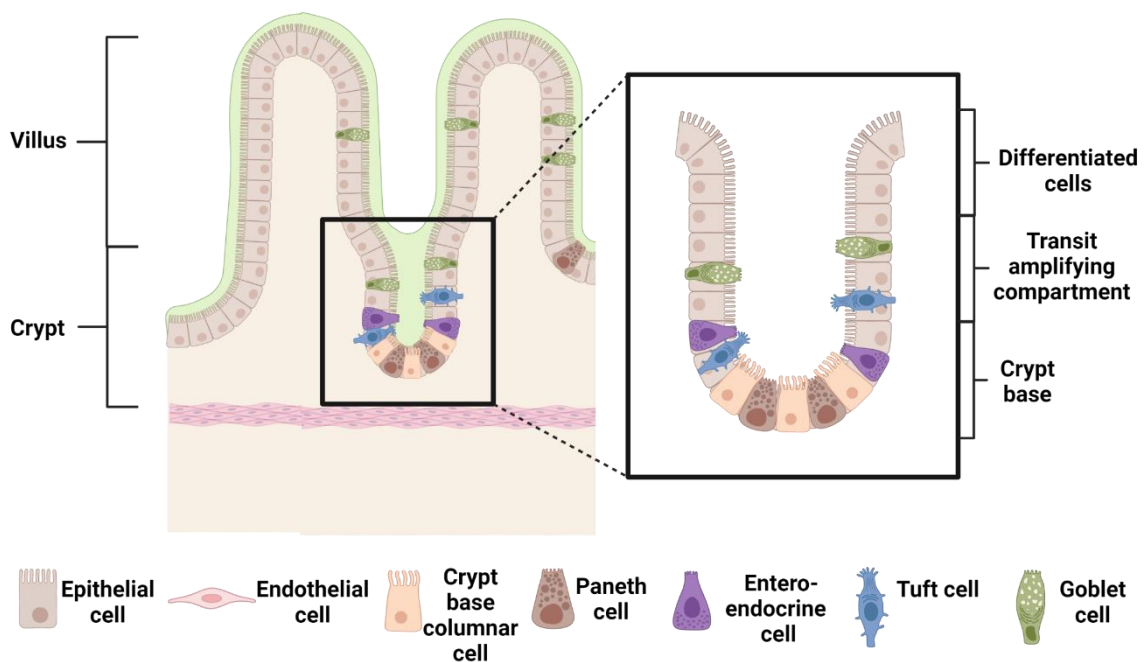


**Figure 4: Structure of the intestinal crypt and villi with intestinal cell types of interest.** The crypt forms the basic functional unit of the intestine as it has been described as the site for stem cells and where cell renewal occurs. When in homeostasis, the stem cells (crypt base columnar epithelial cells) are restricted to the stem cell niche in the crypt base. The transit amplifying region is where the progeny of stem cells will rapidly divide and terminal differentiation will occur in the upper region where fully differentiated cells will eventually be shed into the lumen and the process repeats. Crypt base columnar cells are the intestinal stem cells that will give rise to absorptive cells (enterocytes) and secretory cells (Paneth cells, enteroendocrine cells, tuft cells and goblet cells) that are involved in immune responses, chemoreception and hormone secretion. (Figure created using BioRender and adapted from

#### **2.3.1.3.1. Intestinal Stem Cells**

A major cell type present in the crypt of the intestine is crypt-base columnar cells. These cells continuously divide and give rise to the other cell types present in the crypt (Bonis *et al.*, 2021). This cell type has been shown to express a particular target gene of the Wnt pathway, namely, *LGR5* (Bahrami *et al.*, 2017). *LGR5* encodes an orphan-G-protein-coupled receptor that presents with a large leucine-rich extracellular domain, which has been found to be expressed in CRC and is exclusively expressed in the intestine as it marks the stem cells present (Barker *et al.*, 2007; Bahrami *et al.*, 2017). In addition to *LGR5*, the proliferation marker Ki-67 (expressed by the *MKi-67* gene), has also been shown to be expressed in crypt base columnar cells (Bahrami *et al.*, 2017; Boonekamp *et al.*, 2020). As crypt base columnar cell progress towards the villi of the intestine, they differentiate and give rise to either absorptive cells or secretory cells.

##### **2.3.1.3.1.1. Absorptive Cells of the Intestinal Tract**

Enterocytes are the absorptive cell type that is derived from crypt base columnar cells. These cells are particularly involved in digestion by ensuring uptake of ions, water, vitamins, as well as the absorption of unconjugated bile salts (Miron and Cristea, 2012). These cells are able to perform their digestive function as they contain high concentrations of digestive enzymes that breakdown proteins and carbohydrates that results in their absorption (Ali *et al.*, 2020). Furthermore, enterocytes are responsible for maintaining the integrity of the intestinal epithelial barrier (Ali *et al.*, 2020). This function is attributed to the ability of enterocytes being able to sample luminal agents through pattern recognition receptors, which is the first line of defense against pathogens (Vitale *et al.*, 2016). Therefore, this cell type assists in affecting

immune responses apart from its absorption and digestion functions. Secretory cell types are also vital in the intestinal tract as they assist in the solubilization and dilution of nutrients which are crucial in maintaining intestinal homeostasis.

#### **2.3.1.3.1.2. Secretory Cells of the Intestinal Tract**

There are four cell types that constitute secretory cells, these are Paneth cells, goblet cells, tuft cells and enteroendocrine cells. These cell types perform different functions that assist in maintaining intestinal homeostasis and proliferation as the intestinal tract requires strict spatial organization and continuous cell turnover for normal functioning (Bonis *et al.*, 2021).

Paneth cells are located in the crypts present in the small intestine and are secretory epithelial cells that secrete antimicrobial proteins (Lueschow and McElroy, 2020). Their main function is to initiate immune responses against invasive pathogens, as well as to maintain the stem cell niche to ensure self-renewal and proliferation of the intestinal epithelium (Bel *et al.*, 2017; Yu *et al.*, 2020). Paneth cells are able to maintain the stem cell niche as they provide essential Notch ligands, EGF and Wnt signals for proliferation to occur (Bonis *et al.*, 2021). Furthermore, Paneth cells are able to initiate immune responses due to their ability to secrete lysozyme (LYZ) that is controlled by the expression of the *LYZ* gene that digests bacterial cell walls (Mei *et al.*, 2020). Another cell type that is involved directly with immune responses is goblet cells due to their secretion of mucin that lines the intestinal tract.

Goblet cells are another secretory cell type present in the intestine but are specifically secretory progenitor cells with the primary function of secreting mucin (Dao and Le, 2021). The gene responsible for the secretion of mucin is the mucin 2 gene (*MUC2*) and results in a protective mucus layer in the digestive tract (Dao and Le, 2021). The importance of this mucus layer is to eliminate any microbes or chemicals that may cause damage to the intestinal tract and therefore functions in the activation of an immune response (Herath *et al.*, 2020). Another cell type that is found on these mucosal surfaces are tuft cells (Iqbal *et al.*, 2023). Tuft cells are a rare cell type that are derived from *LGR5* and are specifically involved in chemoreception and immune responses (Hendel *et al.*, 2022). Tuft cells are comprised of actin filaments cross-linked by actin-binding protein, Villin 1 (*VIL1*) (Esmaeilniakooshkghazi *et al.*, 2020). *VIL1* proteins are a result of the expression of *VILI*, which can be used as a marker to identify tuft cells that are present in the intestinal tract (Esmaeilniakooshkghazi *et al.*, 2020). A cell type that shares similarities to tuft cells are enteroendocrine cells (Du *et al.*, 2023), which is the last secretory cell type present in the intestinal tract.

Enteroendocrine cells function in the secretion of hormones associated with food digestion and absorption, as well as effecting immune responses in the presence of microbial metabolites (Worthington *et al.*, 2018). As enteroendocrine cells play a role in mediating the homeostasis of the immune system, they may contribute to chronic inflammation, consequently implicating this cell type in inflammatory bowel diseases such as Crohn's disease and Ulcerative Colitis, which can increase the risk of CRC development (Worthington *et al.*, 2018). Additionally, studies have indicated that Chromogranin A (*CHGA*) levels function as a marker of enteroendocrine cells (Worthington *et al.*, 2018; Watanabe, 2021). *CHGA* is classified as a soluble glycoprotein stored with hormones and neuropeptides in secretory granules of most endocrine cells and is also a precursor for various biologically active peptides and granulogenic protein that regulates the storage and secretion of hormones and peptides (Laguerre *et al.*, 2020).

In addition to the above-mentioned cell types and associated genes that may serve as markers to identify CRC organoids, Epithelial cell adhesion molecule (*EpCAM*) is another gene of interest. *EpCAM* is expressed in epithelial cells, as well as a range of stem cells as it mediates cell-to-cell adhesion, regulates proliferative gene expression and the maintenance of self-renewal and pluripotent phenotype (Huang *et al.*, 2018). As the intestine is comprised of epithelial cells that have differentiated into epithelial cell types (goblet, enteroendocrine cells, Paneth cells and enterocytes), evaluating the expression of *EpCAM* will validate the presence of epithelial cells in the intestinal tract (Wright, 2012). Therefore, the identification of these markers in the organoid cultures would validate successful formation of intestinal organoids.

Throughout the twentieth century, the use of cell lines and animal models have proven to be quite successful in studies trying to understand disease development, progression, drug metabolism and drug resistance. However, extrapolating these results to humans has not always been accurate due to various reasons, one of which includes patient-to-patient genetic differences. Furthermore, some molecular processes that occur in the human body cannot be recapitulated in these models, such as testing the efficacy of drugs (Kim *et al.*, 2020). The development of 3D culture models, such as organoids, may hold promise in overcoming these issues. Organoids are histologically indistinguishable from the organ it was grown from and may bridge the gap between *in vitro* response and clinical response, as well as understanding patient-specific disease biology (Sato *et al.*, 2009; Fujii *et al.*, 2018). Therefore, this allows the potential of 3D cultures to be extended to current biological research in a more physiologically relevant patient-based approach. Currently, the published research on organoids and CRC in

South Africa is very limited. Therefore, the novelty of this project and the impact it may have on future CRC studies in a South African patient cohort could lead to a more personalised medicine approach to CRC treatment.

### **3. Aim and Objectives**

#### **3.1. Aim**

The aim of this study was to standardise a protocol to establish and characterize colorectal organoid cultures from South African patient-derived tissues.

#### **3.2. Objectives**

1. Optimize the culture conditions and maintenance of intestinal crypt organoids from patient-derived tissue.
2. Characterize the culture of intestinal crypt organoids using RT-qPCR assessing genes specific to intestinal composition, i.e., *LGR5*, *VIL1*, *MUC2*, *EpCAM*, *MKi67*, *LYZ* and *CHGA*.
3. Characterize the culture of intestinal crypt organoids using immunofluorescence assessing proteins specific to intestinal composition, i.e. *VIL1*, *MUC2*, *EpCAM*, and *Ki67*.

#### **3.3. Hypothesis**

It is hypothesised that the intestinal crypts that were extracted and cultured to form organoids will be those from the colon and express the genes specific to intestinal composition.

#### **3.4. Project Workflow**

The methodology that was employed in this project has been outlined in Figure 5. Ethical clearance for this project was obtained from the Human Research Ethics Committee of the University of the Witwatersrand (Ethics clearance number: M210233) and informed consent was obtained from each patient to use their samples in this project. Patient-derived non-cancerous and CRC samples were utilized to produce 3D organoids. The samples from individuals with varying stages of CRC were used. A biopsy of normal tissue (distal site) and of tumour tissue (cancer) was collected from patients. For culture and characterization of organoids derived from non-cancerous tissue (referred to as non-cancerous organoids in the text), five patient samples were used. For culture and characterization of organoids derived from the tumour/cancerous tissue (referred to as cancer organoids in text), six samples were used. The crypts were isolated from the patient biopsies and the organoids were grown (passage p0) and passaged (p1). Monitoring of culture growth was also performed during culture and

during passaging to ascertain organoid morphology from each patient using brightfield inverted phase contrast microscopy. RNA extraction from the non-cancerous samples was performed only from second passage (p2) to allow for stabilization of the organoids, followed by complementary DNA (cDNA) synthesis and RT-qPCR. The purpose of RT-qPCR was to validate that the organoids that were grown are those from the colon and the genes of interest that were used to validate the organoids included: *EpCAM*, *VIL1*, *MUC2*, *LGR5*, *MKi67*, *CHGA* and *LYZ*. The combination of these gene markers is unique to CRC, hence, their use. Additionally, immunofluorescence was performed on the non-cancerous organoids to assess the localization of the proteins from the genes of interest, as well as to visually confirm their expression. Monitoring of cancerous organoid growth was also performed during culture and immunofluorescence was performed as a proof of concept to assess VIL1, EpCAM, Ki-67 and MUC2 protein localization.

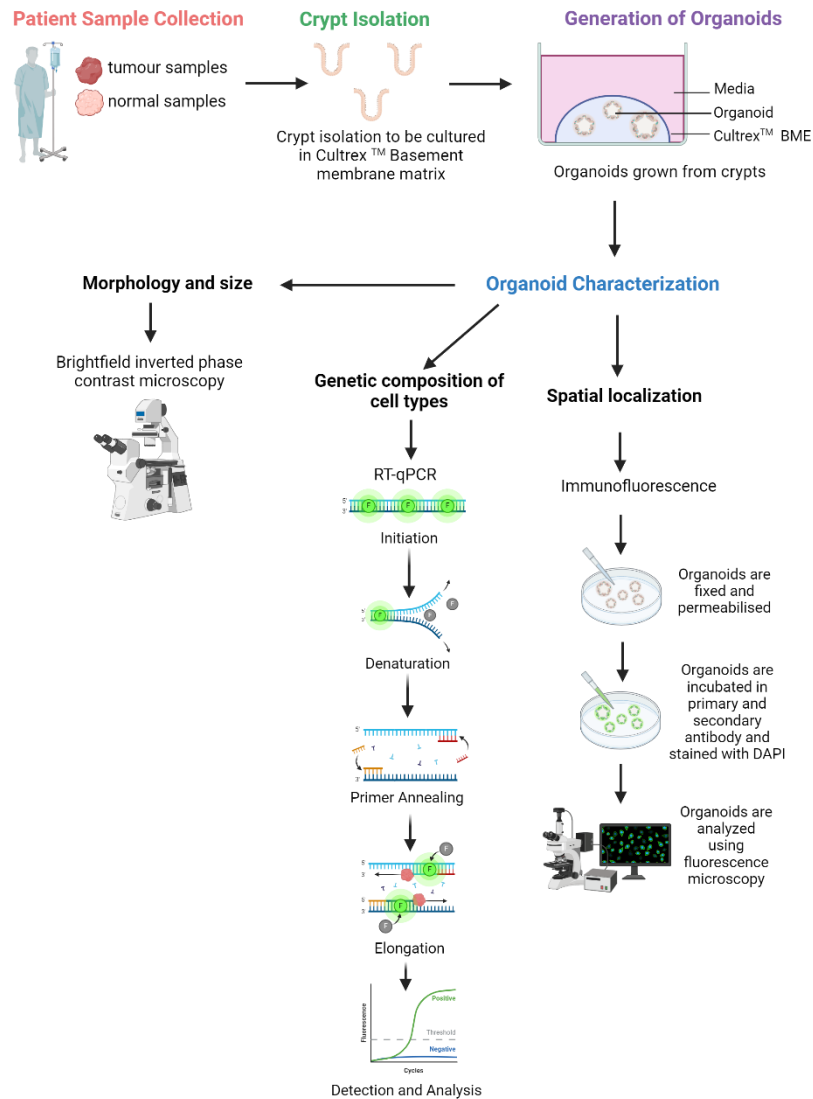


**Figure 5: Project workflow.** Patient samples were collected from the Wits Donald Gordan Hospital (Ethics clearance number: M210233). The samples collected were those derived from the tumour and a matched normal tissue from a distal site in the colon. The samples were then taken back to the laboratory for processing, which included digestion of the tissue by mechanical and enzymatic digestion. The crypts obtained from the tissue were counted and seeded in Cultrex™ Basement Membrane Extract (BME) and once solidified media was added. The organoids were passaged once optimal size and culture density was reached and when passage 2 was reached, the organoids were subjected to RNA extraction for RT-qPCR and immunofluorescence for characterization. (Figure created using BioRender)

## **4. Methodology**

### **4.1. Ethical Clearance and Informed Patient Consent**

Ethics clearance was obtained from the Human Research Ethics Committee (Medical) of the University of the Witwatersrand to perform sample collection from the Wits Donald Gordon Centre (Parktown, Johannesburg) (Ethics clearance number: M210233). The patients were under no obligation to partake in the study and those that chose to partake signed an informed consent form that they understood and were willing to partake. The patients were also required to complete a short questionnaire to obtain personal information (such as age, gender, weight and height), familial history of CRC, dietary information, symptoms that led to onset of CRC and any treatment regimens or other medications. The data obtained was kept anonymous throughout and patient records were assigned an internal file number. This also ensured anonymity of the patient samples when culturing the organoids to prevent bias.

### **4.2. Patient Sample Collection**

A tumour sample and matched normal healthy control tissue were collected from nine randomly selected patients. The samples were collected from the Wits Donald Gordon Medical Centre (Parktown, Johannesburg) by Dr Brendan Bebington (Head, Colorectal Unit). The media preparation for sample collection can be found in Table S1 in Annexure 1.

### **4.3. Organoid Culturing**

#### **4.3.1. Freezing and storage of Tissue samples**

Following the surgical procedure, specimens were placed in their respective 50 mL falcon tubes labelled: normal (about 15 cm away from the tumour site), and tumour core, respectively, with the internal patient file number. The collection falcon tubes contained the components in Table S1 with the addition of Primocin™. Primocin™ is a broad-spectrum antibiotic used to prevent contamination from microbes (Marinucci *et al.*, 2022). All the samples collected were kept on ice and immediately taken to our laboratory for processing. The samples were either frozen and stored or processed for crypt isolation. The tissue samples were washed twice with 10 mL of ice-cold D-PBS (Thermo Fisher Scientific, USA) that was supplemented with Primocin™ (2 µL/1 mL of D-PBS) in a 10 mL petri plate. The samples were then cut into smaller tissue fragments using a sharp Iris curved scissor (dissection kit component) (Lasec, RSA). One tissue fragment from each sample type (normal or tumour core) were each placed into separate 2 mL cryovial (NEST Biotec, China) that was snap frozen using liquid nitrogen and stored in liquid nitrogen. Additionally, a tissue fragment from each sample type was stored in Recovery™ Cell

Culture Freezing Medium (Thermo Fisher Scientific, USA) and stored at  $-80^{\circ}\text{C}$  in Mr Frosty (Thermo Fisher Scientific, USA). The next day, the samples were removed from  $-80^{\circ}\text{C}$  and stored in liquid nitrogen until use.

### **4.3.2. Isolation of Human Colonic Crypts from Fresh Tissue**

The tissue samples were washed twice with 10 mL of ice-cold D-PBS (Thermo Fisher Scientific, USA) that was supplemented with Primocin™ (2  $\mu\text{L}$ /1 mL of D-PBS) in a 10 mL petri plate. The tissue samples were cut into smaller fragments using a sharp Iris curved scissor (dissection kit component) (Lasec, RSA) for mechanical digestion and were transferred to an Eppendorf tube containing 2 mL of tissue dissociation buffer. The Eppendorf tubes were incubated at  $37^{\circ}\text{C}$  in a water bath for 1 hour and at 15-minute intervals the contents resuspended 20 times to ensure adequate mechanical and enzymatic digestion of the tissue. The tissue dissociation buffer was prepared prior to collection of the samples and the reagents and quantities used to prepare this buffer are defined in Table S2 in Annexure 1. The function of the tissue dissociation buffer is to dissociate the cells and crypts from the tissue samples. The main components of the tissue dissociation buffer are DMEM, HEPES, Fetal bovine serum (FBS) (Lasec, RSA), dispase (Thermo Fisher Scientific, USA), and Collagenase (Thermo Fisher Scientific, USA). The function of combining DMEM, HEPES and FBS was to form the base of the buffer, HEPES was used to control the pH of the buffer with DMEM and FBS providing nutrients to the cells to prevent excessive cell death during the process. Dispase was added as it gently dissociated cells with minimal damage from the tissue sample. The collagenase aided in the detachment of the cells from the tissue samples as it hydrolyses collagen. Once the 1-hour incubation period surpassed, the mixture was filtered using a 70  $\mu\text{M}$  strainer (Corning, USA) into a 15 mL falcon tube (Corning, USA). The 70  $\mu\text{M}$  strainer excludes debris and other unwanted cell types. Once the entire mixture was filtered, a volume of 10 mL D-PBS was added to wash the filter as some crypts may have adhered to the strainer. The flow-through was centrifuged at  $400 \times g$  using the swing bucket rotor Allegra X-30R centrifuge (Beckman Coulter, USA) for 5 minutes at  $4^{\circ}\text{C}$  and the supernatant was discarded. A volume of 2 mL DMEM with 1% bovine serum albumin (BSA) was used to resuspend the pellet and was kept on ice until the Cultrex™ was thawed.

#### **4.3.2.1. Isolation of human crypts from frozen tissue**

Previously collected samples were stored in Recovery™ Cell Culture Freezing Medium (Thermo Fisher Scientific, USA) and kept in liquid nitrogen. Prior to collecting the tissue samples stored in liquid nitrogen, collagenase II digestion buffer was made by dissolving 5 mg

of collagenase II in 450  $\mu\text{L}$  of organoid media. The samples were then collected from liquid nitrogen. The cryovial with the tissue sample was thawed in a 37 °C water bath for 1 minute and the tissue was transferred to a 35 mm x 12 mm petri plate (NEST Biotec, China) and washed once with D-PBS. The tissue was then transferred to the Eppendorf tube with 450  $\mu\text{L}$  of the collagenase II digestion buffer and mechanically digested by cutting the tissue into smaller fragments. The composition for the collagenase digestion buffer is defined in Table S3 in Annexure 1. The Eppendorf tube was then closed and transferred to a tube rotator (Rotomini™, Benchmark Scientific, USA) and incubated at 37 °C for 30 minutes for a maximum period of 90 minutes (sample dependent). Once the majority of the tissue was completely dissociated, the sample was processed as per 4.3.1 where the solution was strained using a 70  $\mu\text{M}$  strainer (Corning, USA) into a 15 mL falcon tube (Corning, USA).

### **4.3.3. Counting and plating of Isolated Human Colon Crypts**

The total number of crypts present in the sample were counted before seeding the crypts by aliquoting three 10  $\mu\text{L}$  droplets of the crypt mixture into a 35 mm x 12 mm petri plate (NEST Biotec, China). Crypts were manually counted using an inverted light microscope (Leica DMIL LED Inverted Microscope (Leica Microsystems, Germany)) and the number of crypts present in each aliquot was recorded and averaged. The calculations that were performed are illustrated below (equation 1):

#### **Equation 1: Calculation to determine the average number of crypts**

$$\text{Aliquot 1 (10 } \mu\text{L)} + \text{Aliquot 2 (10 } \mu\text{L)} + \text{Aliquot 3 (10 } \mu\text{L)} = x$$

$$x \div 3 = \text{Average number of crypts (in 10 } \mu\text{L)}$$

$$\text{Average number of crypts (in 10 } \mu\text{l)} \times 200 \text{ (dilution factor)} = \text{total number of crypts in the 2000 } \mu\text{L (2 mL) sample}$$

A recommended number of crypts that may be plated in each culture dome is 1000 crypts per dome to prevent the culture being plated too densely, increased cell death at the core of the dome and eventual collapse of the dome. The samples were then centrifuged at 500 x g for 5 minutes at room temperature and the supernatant discarded. A final, diluted concentration of 10 mg/mL of Cultrex™ Reduced Growth Factor Basement Membrane Extract, Type 2, Select (R&D systems, USA) was added to the pellet. The Cultrex™ functions as a reconstituted

basement membrane matrix. It is a gelatinous protein mixture derived from Engelbreth-Holm-Swarm mouse sarcoma cells and is used due to the fact that it retains the stem cells in an undifferentiated state (Hughes *et al.*, 2010). Furthermore, Cultrex™ specifically contains laminin, entactin, type IV collagen, proteoglycans and growth factors secreted by the mouse sarcoma cells (Prince *et al.*, 2022). To resuspend the pellet, the mixture was mixed by slowly resuspending (20 times) the sample to avoid the introduction of air bubbles. This step was performed on ice to prevent the solidification of the Cultrex™. Cultrex™ remains liquid at temperatures of below 4 °C but solidifies at room temperature as the matrix proteins polymerise. Approximately 6-7 domes that consisted of a mixture of 10 µL of crypt solution and Cultrex™ was added to each well on a pre-warmed 24-well plate (Corning, USA) (at 37 °C overnight to assist in solidification of the domes) to form domes. Tips were pre-coated with DMEM and 1 % BSA by aspirating in the solution prior to contact with crypt solution) to prevent the crypts from adhering to the tips. The plate was placed back into the 37 °C incubator for 30 minutes to allow for the domes to solidify. While the domes solidify, 4 mL of complete Intesticult™ Organoid Growth Medium (STEMCELL™ Technologies, Canada) (Refer to Table S4 for non-cancerous organoids and Table S5 for cancerous organoids in Annexure 1) was prepared at room temperature and placed into a 37 °C water bath.

The volumes in Table S4 and Table S5, Annexure 1, varied depending on the number of organoids to be cultured but the Intesticult™ Organoid Growth Medium Basal media (composition not stated, patented formulation) and Intesticult™ Organoid Growth Medium Organoid Supplement (composition not stated, patented formulation) must be added in a 1:1 ratio and the 4 mL of complete medium is sufficient for 8-wells in a 24-well cell culture plate (Corning Inc, USA). Primocin™ was the antibiotic used to ensure absence of growth of microbes and the Rho-kinase (ROCK) inhibitor (Sigma Aldrich, UK) was added as it enables the maintenance of stem cell phenotype. Once the domes solidified, 500 µL of the complete Intesticult™ Organoid Growth Medium was pipetted down the wall of each well containing the organoid domes. The plate was placed back into the cell culture incubator at 37 °C with 5 % CO<sub>2</sub> and the organoids were allowed to develop and grow and media was changed every second day.

#### **4.3.4. Generation of in-house organoid media**

Due to restrictions in media related to cost, shipping and closure of the local distributor it was sought to generate the media in-house. The required reagents to generate the media are listed in Table 3 along with the stock solution concentration that was made when reconstituted as per

manufacturers' recommendations. The final concentrations used for each component are also listed in Table 3, which were used to calculate the final volumes to add to produce the complete medium. The function of each component is also listed in Table 3.

**Table 3: Components required for organoid media generation with stock and final concentrations as well as functions of each component**

Reagent	Stock Solution Concentration	Final Concentration	Function
Advanced DMEM/F12 (Thermo Fisher Scientific, USA)	1 x	1 x	Forms the basal media for the organoids and contains essential nutrients for cell growth.
GlutaMAX (Thermo Fisher Scientific, USA)	100 x	1 x	Used to substitute for L-glutamine to ensure efficient energy metabolism and high-growth yields.
HEPES (Thermo Fisher Scientific, USA)	1 M	10 mM	Organic buffer agent.
B27 (Thermo Fisher Scientific, USA)	50 x	1 x	Supplement that assists with growth and maintenance of stem cells and is an FBS alternative for organoid media.
EGF (Sigma Aldrich, UK)	500 ug/mL	50 ng/mL	Stimulates the proliferation of different cell types by activating the EGF receptor tyrosine kinase that activates the Ras-RAF-MEK-ERK MAPK and PI3K-mTOTR pathways.
R-spondin 1 (Thermo Fisher Scientific, USA)	100 ug/mL	500 ng/mL	Wnt agonist and induces proliferation.
Noggin (Sigma Aldrich, UK)	10 ug/mL	100 ng/mL	Inhibits bone morphogenic protein signalling that would result in differentiation.
Gastrin I (Sigma Aldrich, UK)	100 uM	10 nM	Stimulates gastric acid secretion and has a mitogenic effect on gastric cells.
Prostaglandin E2 (Sigma Aldrich, UK)	100 uM	10 nM	Promotes optimal organoid growth and induces higher levels of cell proliferation.
A83-01 (Sigma Aldrich, UK)	5 mM	500 nM	Inhibitor SMAD2 phosphorylation and maintains self-renewal and proliferation of stem cells.
Niacinamide (Sigma Aldrich, UK)	1 M	10 mM	Suppresses the activity of sirtuins and promotes organoid forming efficiency.

n-Acetylcysteine (Sigma Aldrich, UK)	500 mM	1,25 mM	An antioxidant and has mucolytic and anti-inflammatory properties.
SB202190 (Sigma Aldrich, UK)	10 mM	3 uM	Inhibitor of p38 mitogen-activated protein kinase and stabilises human pluripotent stem cells.
Recombinant Human Wnt3a (Biotechne, USA)	10 ug/mL	100 ng/mL	Used to promote proliferation of stem cells.
N-2 Supplement (Thermo Fisher Scientific, USA)	100 x	1 x	Used to increase viability and health of cell types during culture.
ROCK inhibitor (Sigma Aldrich, UK)	10 mM	10 uM	Prevents anoikis and cell death of single cells.
Primocin™ (InvivoGen, France)	50 mg/mL	2.5 mg/mL	Antibiotic that is used to prevent microbe contamination.

*\*Note: Culture medium required for cancer organoid growth does not include the component Recombinant Human Wnt3a. Media recipe was obtained from Andrew Beggs Laboratory, University of Birmingham, UK.*

### **4.3.5. Organoid Passaging**

Primary culture was performed 7-10 days after initial organoid seeding. This was to give the organoids sufficient time to stabilise and grow and mature in culture. The culture plate was initially pre-warmed in a 37 °C incubator overnight prior to the seeding of the primary culture. The culture media was removed from the initial culture plate and the domes were washed with 500 µL of cold D-PBS and was subsequently removed. A volume of 500 µL of Cultrex™ organoid harvesting solution (R&D Systems, USA) (composition not disclosed, patented formulation) was added and the organoids were detached by gently loading the organoid harvesting solution in the well. Cultrex™ organoid harvesting solution is a non-enzymatic solution that depolymerizes the matrix that enables the harvesting of the organoids from the Cultrex™ domes. The mixture was transferred to a 2 mL Eppendorf tube and resuspended (20 times) and incubated on ice for 90 minutes to ensure adequate digestion of the Cultrex™ domes. To remove the Cultrex™ and organoid harvesting solution, the Eppendorf tube was centrifuged for 8 minutes at 500 x g and the supernatant discarded. The organoid pellet was resuspended in TrypLE (300 µL per well) (Thermo Fischer Scientific, USA) and the tube was placed into a 37 °C water bath for 3 minutes as this is the optimal temperature for the action of TrypLE to dissociate the organoids. Once the incubation period had surpassed the tube was centrifuged at 500 x g for 5 minutes at room temperature and the supernatant was discarded. Subsequently, a volume of 1 mL ice-cold DMEM and 1 % BSA was added to each tube using a pre-coated (with culture media) pipette tip to resuspend the digested organoids. The crypts were counted using previously described formula in 4.3.2. Once the crypt count was completed and the average number of crypts were obtained, the sample was then centrifuged at 500 x g for 5 minutes at room temperature and the supernatant was discarded and crypt seeding was performed as per section 4.3.2.

## **4.4. Reverse-Transcriptase Quantitative Polymerase Chain Reaction (RT-qPCR)**

RT-qPCR allows for the sensitive, specific and reproducible quantification of nucleic acids (Arya *et al.*, 2005). This method detects and measures the gene products generated during each PCR cycle, which is directly proportional to the amount of template cDNA prior to the beginning of the PCR process (Arya *et al.*, 2005). The fluorescence emission during the PCR reaction is detected in real-time and is used to construct amplification plots using the fluorescence emission (Arya *et al.*, 2005). This methodology was applied to characterise the

organoids using specific marker genes of interest as it is classified as a method of characterization, particularly for organoids to identify the presence or absence of a specific cell type (Zhao *et al.*, 2022).

#### **4.4.1. RNA Extraction**

Ribonucleic acid (RNA) extraction was performed using the Omega Bio-tek E.Z.N.A.® Total RNA kit I (Omega bio-tek, USA). All the steps were performed at room temperature and the steps that required centrifugation were performed at 20-25 °C employing a standard benchtop microcentrifuge (Sigma Zentrifugen, Germany, model 1-14). To obtain sufficient RNA from the organoids, five 10 µL domes were combined in a 2 mL Eppendorf tube.

The media was removed from the wells and the domes were washed with 300 µL of ice-cold D-PBS. The D-PBS was removed and 350 µL of GTC lysis buffer (common formulation found: 4 M guanidinium thiocyanate, 25 mM sodium citrate (pH 7.0), 0.5 % (w/v) sarcosyl (N-lauroylsarcosine) and 0.1 M 2-mercaptoethanol, kit formulation is not specified) was placed in each well. The tips were then pre-coated with 1 % BSA and DMEM and the organoid/lysis buffer solution was resuspended 20 times. The suspension was vortexed for 30 seconds to dislodge the cells and centrifuged for 5 minutes at 12 000 x g. The lysate was transferred to an RNA homogenizer Mini Column that was inserted into a 2 mL Eppendorf tube. This was then centrifuged for 1 minute at 12 000 x g. The column was discarded, and 1 volume (equal to that of the filtrate, i.e., 350 µL) of 70 % ethanol was added to the filtrate. This was then vortexed for 20 seconds and 700 µL of the solution was transferred to a HiBind RNA column that was placed in a new 2 mL collection tube. The sample was centrifuged for 1 minute at 10 000 x g and the filtrate was discarded. This was repeated until the entire sample had been used. A volume of 500 µL of RNA wash buffer I was added and centrifuged for 30 seconds at 10 000 x g. The filtrate was discarded and 500 µL of RNA wash buffer II that was diluted with 100 % ethanol in the column. The column was centrifuged for 1 minute at 10 000 x g and the filtrate was discarded. The collection tube was reused, and a second RNA wash buffer II step was performed as before. The empty spin column was then centrifuged at 12 000 x g for 8 minutes to dry the column and prevent excess ethanol from being eluted with the RNA. A volume of 40 µL of RNase free water as added to the column that was inserted into a new collection tube. This was centrifuged for 2 minutes at 12 000 x g to elute the RNA. The extracted RNA was then assessed and quantified (ng/µL) using the Nanodrop 1000 spectrophotometer (Thermo Fisher Scientific, USA). and the integrity of RNA was assessed using agarose gel electrophoresis.

The purity ratio of  $A_{260}/A_{280}$  provides an indication of the presence of protein contaminants, as well as any other contaminants that absorb light in the UV region. RNA has an absorption maximum at 260 nm. The desired ratio is approximately 2.0 and hence extracted RNA that coincides with this value was used in downstream applications. The  $A_{260}/A_{230}$  ratio provides an indication of the presence of salt contamination and the desired ratio required from the extracted RNA would be 1.8 for downstream applications. Following quantification using the above spectrophotometric measurements, the integrity of each of the RNA samples was evaluated through agarose gel electrophoresis.

This was performed through the combination of 500 ng/ $\mu$ L of RNA with 2  $\times$  RNA loading dye (Thermo Scientific Scientific, USA) and loaded onto a 1% (w/v) agarose gel. The gel was prepared by combining 0.5 g of agarose powder (Benchmark Scientific, USA) with 50 mL of 1  $\times$  Tris (Sigma Aldrich, UK)-borate (Calbiochem, USA) ethylenediamine tetraacetic acid (EDTA) (Sigma Aldrich, UK) (TBE buffer), and 0.5 mg/mL of ethidium bromide (Thermo Fisher Scientific, USA). The gels were electrophoresed for 60 minutes at 100 V and viewed using the ChemiDoc™ MP system (Bio-Rad, USA). Intact RNA was used for cDNA synthesis or stored at -80 °C until required for subsequent experiments.

#### **4.4.2. cDNA synthesis**

RevertAidFirst Strand cDNA Synthesis kit (Thermo Fisher Scientific, USA) was used to convert the extracted RNA to cDNA. Table 4 illustrates the volumes of RevertAidFirst Strand cDNA Synthesis reagents that were added with the extracted RNA for cDNA synthesis. The Oligo-dT18 primers allowed cDNA synthesis and provided a copy of the messenger ribonucleic acid (mRNA) present. The deoxynucleotide triphosphate (dNTP) mix allowed for extension of the cDNA as the mix contains the nucleotides present in DNA. The RevertAid M-MuLV reverse transcriptase synthesized the cDNA from the extracted RNA and the DNase/nuclease-free water was added to make up the final volume of the reaction as it is free from DNases and nucleases that could potentially degrade the cDNA that was synthesized. The reagents were combined in a 200  $\mu$ L PCR tube, gently mixed and centrifuged briefly prior to the incubation at 42 °C for 1 hour and termination at 70 °C for 5 minutes using the MultiGene PCR machine (Labnet International, UK).

**Table 4: Volumes of RevertAidFirst Strand cDNA Synthesis reagents for cDNA synthesis.**

Reagent	Volume ( $\mu\text{L}$ )
Template RNA	Volume dependent on RNA concentration (2 $\mu\text{g}$ in this case)
Oligo-dT18 primer	1
Nuclease-free water	To make a volume of up to 12 $\mu\text{l}$ after template RNA added
<b>Master Mix</b>	
5 $\times$ Reaction Buffer	4
RiboLock RNase Inhibitor	1
10 mM dNTP Mix	2
RevertAid M-MuLV RT	1
Total volume for reaction	20

The final volume per sample was 20  $\mu\text{L}$ . The volume of RNA required for the reaction was also dependent on the extracted RNA concentration. The cDNA was then used in RT-qPCR or stored at  $-20\text{ }^{\circ}\text{C}$  ( $-80\text{ }^{\circ}\text{C}$  for long-term storage) until required.

#### 4.4.3. RT-qPCR

The purpose of RT-qPCR was to quantify the amplification of the number of targeted gene (Ho-Pun-Cheung *et al.*, 2009). In this study, the expression level of the following genes was measured: *EPCAM*, *MUC2*, *VIL1*, *LYZ*, *LGR5*, *MKi67* and *CHGA*, which are defined markers of colon cell composition as explained in the section 2.3.1.3. These genes were used to confirm that the organoids that were cultured are in fact those of the colon or intestinal organoids. The SensiFAST™ SYBR® No-ROX (Meridian Bioscience, USA) kit was used to determine the expression of these genes. N',N'- dimethyl – N – [4 – (E) – (3 – methyl – 1,3 – benzothiazol – 2 – ylidene) methyl ] – 1 – phenylquinolin – 1 – ium -2 – y] – N – propylpropane – 1,3 – diamine (SYBR) green is described as a fluorescent cyanine dye that is capable of intercalating into double-stranded DNA. This process occurs during the annealing and extension steps of the PCR reaction. Due to this, the detection of SYBR green (Cq/Ct; which is the initial detection of SYBR green) is directly correlated to the amount of template and extension during the RT-qPCR process. This also allowed for the determination of change in relative mRNA expression of the aforementioned genes of interest to that of the control samples. using the  $-2^{\Delta\Delta Ct}$  (delta-delta Ct) Livak method (Livak and Schmittgen, 2001). This method was used to determine the relative target quantity (fold change) in the samples by measuring the

amplification of the target genes and reference gene. This was performed for each of the genes in the organoids and the tissue and the  $\Delta\Delta Ct$  was calculated by subtracting the  $\Delta Ct$  values of each gene of the tissues from the  $\Delta Ct$  values of each gene in the organoids. Therefore, the expression ratio is calculated as a fold change by taking the negative log of the  $\Delta\Delta Ct$  (Equation 2). The reaction volumes that were required for each of the reaction components are expanded on in Table 5 and the final volume of reagents together with the cDNA amounted to 10  $\mu L$ . The primers used were selected from the PrimerBank database (<http://pga.mgh.harvard.edu/primerbank/>). Primer sequences were validated to target the correct gene, have a GC content of 35-65%, length of 18-22 base pairs and an amplicon length of 70-140 base pairs using the UCSC *In-silico* PCR Genome Browser (<https://genome.ucsc.edu/cgi-bin/hgPcr>), NCB-Primer-BLAST website (<https://www.ncbi.nlm.nih.gov/tools/primer-blast/>) and the Integrated DNA technologies (IDT) OligoAnalyzer™ Tool (<https://eu.idtdna.com/pages/tools/oligoanalyzer>). Primer sequences were synthesised by Integrated DNA Technologies (Whitehead Scientific, RSA) and their sequences listed in Table 6. The 3-step cycling parameters are shown in Table 7 and were set on the Bio-Rad CFX-96 system (Bio-Rad, USA) and the Cq/Ct values were generated using the CFX Maestro software (Bio-Rad, USA).

**Table 5: Volumes required for the SensiFast™ SYBR® No-ROX kit for qPCR.**

Reagent	Volume ( $\mu L$ )	Final Concentration
2 x SensiFast™ SYBR® No-ROX mix	5.0	1 x
10 $\mu M$ Forward Primer	0.4	400 nM
10 $\mu M$ Reverse Primer	0.4	400 nM
cDNA Template	2.0	1000 ng/ $\mu L$
dH <sub>2</sub> O	2.2	-
Final Volume	<b>10.0</b>	-

**Table 6: Primer sequences for the genes of interest with  $\beta$ -Actin (ACTB).**

Gene	Sequence (5'-3')	Optimized Annealing temperature (°C)	GC Content (%)
<i>EpCAM</i> (Forward)	TGATCCTGACTGCGATGAGAG	61.1	52.4
<i>EpCAM</i> (Reverse)	CTTGTCTGTTCTTCTGACCCC	61.1	52.4

<i>MUC2</i> (Forward)	GAGGGCAGAACCCGAAACC	60.6	63.2
<i>MUC2</i> (Reverse)	GGCGAAGTTGTAGTCGCAGAG	60.6	57.1
<i>VILI</i> (Forward)	AGAGCTGGTACCTGTGGATTCC	57.0	54.5
<i>VILI</i> (Reverse)	TGCCCTGCCAAACGTAGAG	57.0	57.9
<i>LGR5</i> (Forward)	CCTTCCAACCTCAGCGTCTT	60.6	55.0
<i>LGR5</i> (Reverse)	AGGGATTGAAGGCTTCGCAA	60.6	50.0
<i>LYZ</i> (Forward)	CTTGTCCTCCTTTCTGTTACGG	53.0	50.0
<i>LYZ</i> (Reverse)	CCCCTGTAGCCATCCATTCC	53.0	60.0
<i>MKi67</i> (Forward)	ACGCCTGGTTACTATCAAAGG	60.0	45.5
<i>MKi67</i> (Reverse)	CAGACCCATTTACTTGTGTTGGA	60.0	43.5
<i>CHGA</i> (Forward)	TGTAGTGCTGAACCCCCACC	62.0	60.0
<i>CHGA</i> (Reverse)	CTCTCGCCTTTCCGGATCT	62.0	57.9
<i>ACTB</i> ( $\beta$ -Actin) (Forward)	CATGTACGTTGCTATCCAGGC	56.0	55.0
<i>ACTB</i> (Reverse)	CTCCTTAATGTCACGCACGAT	56.0	57.1

**Table 7: The Three-step cycling parameter that will be used for qPCR.**

Cycles	Temperature (°C)	Duration	PCR Step
1	95	2 minutes	Polymerase activation
45	95	6 seconds	Denaturation
	57.1	10 seconds	Annealing
	72	20 seconds	Extension

*ACTB* was used as a reference gene as it is constitutively expressed in all cells and therefore by including it in the RT-qPCR reaction it allows for normalisation of the results. Normalising the results, allowed for accurate determination of the expression levels of the aforementioned genes from the tumour organoids and non-cancerous organoids. In addition to these positive

controls, a no-template control was used as a negative control from the cDNA synthesis procedure. The function of a no-template control was to ensure that the amplification is not from other contaminants.  $-2^{\Delta\Delta Ct}$  was calculated using the below formula (equation 2):

**Equation 2: Calculation performed to calculate the log fold change from generated qPCR data**

Ct values were generated by the thermocycler.

(Each replicate value is then averaged and averaged data is plotted on the graphs)

$$\Delta CT = CT(\text{target gene}) - CT(\text{reference gene})$$

This was calculated for each gene in the tissues and the organoids and these were used in the equation below:

$$\Delta\Delta CT = \Delta CT(\text{organoids}) - \Delta CT(\text{tissue})$$

To calculate the log fold change:  $2^{-\Delta\Delta Ct}$

## 4.5. Immunofluorescence procedure and analysis

The principle of immunofluorescence is based on antigen-antibody binding using fluorescent detection. This technique uses the binding of specific antibodies to the protein of interest (such as EpCAM, MUC2, VIL1 or Ki-67, in this study) and a secondary antibody that is conjugated to a fluorophore. When the sample is exposed to a certain wavelength using a fluorescent microscope, the fluorophore will absorb light at its excitation wavelength and the fluorophore will emit light at its emission wavelength and can be seen visually. This technique allows for the detection and localization of the proteins of interest within the organoids.

The Cultrex™ domes were digested as mentioned above in 4.3.4 as the organoids need to be in suspension for antibody binding. The media from the wells was discarded and replaced with 300 µL of organoid harvesting solution (Biotechne, USA) and the plate incubated on ice at 4 °C for 90 minutes. The solution was transferred to a 2 mL Eppendorf tube and subsequently centrifuged for 8 minutes at 500 x g at room temperature. Following centrifugation, the supernatant was discarded. The harvested organoids were resuspended in 1 mL of 4 % paraformaldehyde (Sigma Aldrich, UK) to fix the organoids and incubated for 30 minutes while the tube was inverted several times at 10 minutes intervals. The organoid suspension was centrifuged for 5 minutes at 1000 x g and the paraformaldehyde was removed and the organoid pellet was washed using 1 mL of washing solution (D-PBS+ 0.1% Tween-20 (Sigma Aldrich, UK) + 1% BSA (VWR, USA)), the contents and volumes for the washing

solution can be found in Table S6 Annexure 1. All washing steps were performed twice and was completed for each subsequent step. The organoids were pelleted again by centrifugation for 5 minutes at 1000 x g. A volume of 1 mL of 0.2 % Triton-X-100 was added to the pellet and resuspended to permeabilise the organoids. Triton-X-100 was incubated for 30 minutes at room temperature and the tube was inverted 10 times at 10 minutes intervals. Once the incubation period surpassed, the solution was centrifuged for 5 minutes at 1000 x g to pellet the organoids. Subsequently, the pelleted organoids were incubated in 600 µL of blocking solution (5 % BSA in PBS) for 60 minutes on a tube rotator (Roto-mini™, Benchmark Scientific, USA) to prevent non-specific binding of the antibodies to the organoids. Thereafter, the organoids were pelleted, washed and resuspended in 200 µL of primary antibody. The ratios and volumes per primary antibody are mentioned in Table 8. Primary antibody was incubated overnight at 4 °C on a tube rotator and once the incubation period had surpassed the primary antibody/organoid solution was pelleted by centrifugation at 1000 x g for 5 minutes and washed. The pelleted organoids were resuspended in 200 µL of secondary antibody for 2 hours at room temperature on a tube rotator, in the dark. The organoids were then pelleted, washed and incubated in 4',6 – diamidino – 2 – phenylindole (DAPI) (Thermo Fisher Scientific, USA) for 10 minutes in the dark on a tube rotator. Subsequently, the organoids were pelleted, washed and resuspended in fluoromount mounting solution (Merck, USA). A volume of 20 µL of the organoid suspension was pipetted onto a glass slide and a coverslip placed on top. The organoids were then viewed using the Flويد™ Cell Imaging Station (Thermo Fisher Scientific, USA) at 40X magnification on the blue channel (wavelengths of 420-495nm) to visualise DAPI, red channel (wavelengths of 620-700nm) to visualise Ki-67 and the green channel (wavelengths of 500-550nm) to visualise LYZ, VIL1 and MUC2. All secondary antibodies used were fluorescently tagged.

**Table 8: The primary and secondary antibodies used for immunofluorescence and their respective ratios.**

<b>Antibody</b>	<b>Ratio (antibody: PBS)</b>
Vil1(conjugated primary antibody) (Santa Cruz Biotechnology, USA)	1: 50
EpCAM primary antibody (R&D systems, USA)	1: 50
EpCAM secondary antibody – AlexaFluor™ 488 donkey anti-goat IgG (Thermo Fisher Scientific, USA)	1: 100

Muc2 primary antibody (Santa Cruz Biotechnology, USA)	1: 100
Muc2 secondary antibody - AlexaFluor™ 488 donkey anti-mouse IgG (Thermo Fisher Scientific, USA)	1: 100
Ki-67 primary antibody (R&D systems, USA)	1: 50
Ki-67 secondary antibody – Texas Red™ goat anti-rabbit IgG (Thermo Fisher Scientific, USA)	1: 100

## 4.6. Data Analysis

The statistical method used to analyse the RT-qPCR data was a paired t-test which was used to compare the tissue and organoid means as the two samples are correlated. A statistically significant p-value was  $< 0.05$  based on the difference between triplicate results whereas a p-value  $> 0.05$  was regarded as being statistically non-significant. Prior to performing the paired t-test the delta CT values that were obtained were first analysed to determine whether the data was normally distributed. The methods used to determine the distributions of the data was the Shapiro-Wilk normality test and a Kolmogorov-Smirnov normality test with Dallal-Wilkinson-Lilie for p-value. GraphPad Prism 8 and Microsoft Excel © 2016 was used to perform the statistical analysis and to construct the relevant graphs.

## 5. Results

### 5.1. Organoid Generation

#### 5.1.1. Patient Sample Collection Data

The patient samples used are illustrated in Table 9 along with their internal file number, gender, ethnicity, age, chemotherapeutic status and disease stage classification.

**Table 9: Patient sample collection data.**

Internal File Number	Gender	Ethnicity	Site Detected	Family History of CRC	Age of Diagnosis	Chemotherapy	Tumour Grade	Tumour Size (mm)	Nodes Involved	TNM Classification	Staging
<b>Non-cancerous Samples used</b>											
N-B020	Male	White	Proximal ascending colon	No	74	No	Low-grade adenocarcinoma	35 x 30 x 10	2	T4aN1bM0	IIB
N-B026	Female	White	Rectum	Yes, father	39	No	Early intramucosal adenocarcinoma	8 x 6 x 5	11	-	-
N-B027	Female	White	Colon	Yes, maternal grandfather	55	No	Low-grade adenocarcinoma	40 x 10	0	T3aN0M0	Stage IIA
N-B046	Male	White	Rectum	No	68	No	Invasive low-grade adenocarcinoma	35 x 51 x 12	1	T2AN1bM0	Stage IIIA
N-B043	Male	African	Colon	No	80	No	Invasive low-grade adenocarcinoma	50 x 50 x 22	1	T4aN0M0	Stage IIB


**Cancer Samples used**

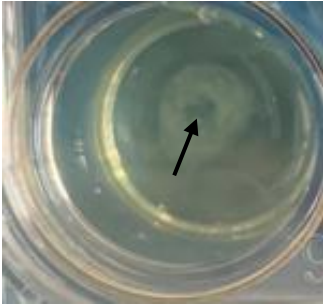
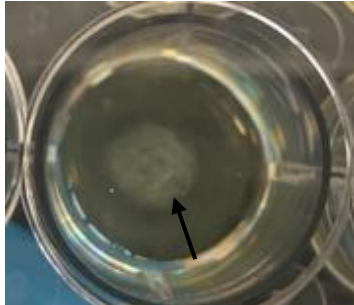
C-B026	Female	White	Rectum	Yes, father	39	No	Early intramucosal adenocarcinoma	8 x 6 x 5	11	-	-
C-B033	Male	White	Colon	Yes	53	No	Low-grade adenocarcinoma	25 x 15 x 5	5	T3aN2aM0	Stage IIB
C-B042	Male	White	Caecum	Yes	38	No	High-grade adenocarcinoma	30 x 25 x 20	5	T4aN2aM0	Stage IIC
C-T005	Male	White	Rectum	No	57	No	Invasive low-grade adenocarcinoma	80 x 55 x 30	0	T2N0M0	Stage I
C-T006	Female	White	Colon	No	69	Yes (12 rounds)	Low grade adenocarcinoma	20 x 20	7	T3cN2bM0	Stage IIC
C-B043	Male	African	Colon	No	80	No	Invasive low-grade adenocarcinoma	50 x 50 x 22	1	T4aN0M0	Stage IIB

### 5.1.2. Optimization of Organoid Seeding Density

A variety of literature recommends different crypt numbers, ranging from 200 – 1000 crypts per dome (Sato *et al.*, 2009, 2011; Verhoeckx *et al.*, 2015; Dijkstra *et al.*, 2018; Fujii *et al.*, 2018; Vlachogiannis *et al.*, 2018; Conder *et al.*, 2020; Vonk *et al.*, 2020). Therefore, the required number of crypts per dome and the gel substance used to form the domes had to be standardized. Crypts in either Geltrex™ or Cultrex™ were seeded according to Table 10 and monitored over several days.

**Table 10: Table summarising the number of crypts to seed per dome and the more robust BME to use for organoid culture**

Number of Crypts	Geltrex™	Cultrex™	Cause	Sample images
200	Domes collapse within 2 – 3 days	Domes collapse within 4 – 5 days	Domes are too sparsely seeded, affects the factors produced by organoids and media to allow for proper expansion.	 <p><i>Note: arrow indicates pieces of Cultrex™ BME pieces from the dome that remains</i></p>
300	Domes collapse within 2 – 3 days	Domes collapse after 1 week	Domes are too sparsely seeded, affects the factors produced by organoids and media to allow for proper expansion.	
400	Domes collapse within 2 – 3 days	Domes collapse after 1 week		
500	Domes collapse within 4 – 6 days	Domes shrinks after 1 week and start collapsing	Domes are too sparsely seeded. Affects the factors produced by organoids and media to allow for	

600	Domes collapse within 4 – 6 days	Domes shrinks after 1 week and start collapsing	proper expansion. Geltrex™ is primarily used for 2D cell culture assays, whereas Cultrex™ is optimized for organoid growth and expansion	 <p><i>Note: arrow indicates collapse of Cultrex™ BME dome from the centre</i></p>
700	Domes collapse after 7 days	Domes hold for 1 – 2 weeks	Geltrex™ is primarily used for 2D cell culture assays, whereas Cultrex™ is optimized for organoid growth and expansion. Enough crypts were seeded in Cultrex™ domes to ensure enough nutrients from media and factors from media and organoids	 <p><i>Note: arrow indicates Cultrex™ BME dome that remains at higher crypt seeding densities</i></p>
800	Domes collapse after 7 days	Domes hold for 1 – 2 weeks		
900	Domes collapse after 6 – 8 days	Domes hold for 1 – 2 weeks		
1000	Domes collapse after 6 – 8 days	Domes hold for longer than 2 weeks		
	<b>Unsuccessful</b>	<b>Successful</b>		

According to Table 10 it was identified that approximately 1000 crypts that were seeded in Cultrex™ BME allowed for successful organoid growth and development. Possible causes for dome collapse are illustrated in Table 10. Therefore, based on the success of domes holding, Cultrex™ BME and 1000 crypts per 10 µL dome were selected for downstream applications.

## 5.2. Comparing Organoid Growth using STEMCELL™ Technologies media and in-house prepared Organoid Media

Another basic culture condition that had to be optimized was comparing organoid growth in STEMCELL™ Technologies media and in-house generated media. Organoid media is very expensive to procure and delays in shipments from overseas distributors can be detrimental to progress. Therefore, it was sought to generate media in-house by utilizing protocols found in previously published literature. Table 11 illustrates the comparisons between in-house media and purchased media from an international distributor.

**Table 11: Comparisons of procured media vs. generating in-house media**

	<b>STEMCELL™ Technologies media (purchased media)</b>	<b>Home-made media</b>
<b>Cost</b>	R45 000, 00 for 100 mL of media	Approximately R22 466,79 media for 100 mL of media (subject to slight variation based on exchange rate)
<b>Up scalability</b>	Limited due to cost of media.	More flexible as media can be produced at a cheaper cost
<b>Shipping</b>	Approximately R21 500 Delivery is 4 – 6 weeks.	Ranges from R200,00 to R2900,00 for international, expedited shipping. Delivery is 3 – 4 weeks.
<b>Availability of reagents</b>	No reagents listed, but media availability is limited due to cost.	Available from local distributors who usually have the reagents in stock or easily procured from international suppliers.
<b>Media availability</b>	Limited as media comes as two components; 50 mL of Basal media and 50 mL of Supplement to make 100 mL of complete organoid media for non-cancerous organoids. Cancer organoids require only Basal media supplied as a 50 mL bottle.	Largely available, individual components ordered can be used to make more than 100 mL for non-cancerous and cancer organoids.

Therefore, in-house media was prepared and organoid growth was monitored across several days in culture to compare the two media. Figure 6 illustrates the growth of non-cancerous and cancer organoids that were cultured in in-house prepared media and STEMCELL™ Technologies media, with the initial growth of non-cancerous organoids being slightly slower in the in-house prepared media but quite similar to the cancer organoids. The organoids used to compare the growth in the two different types of media were new organoid lines that were generated from fresh tissue biopsies.

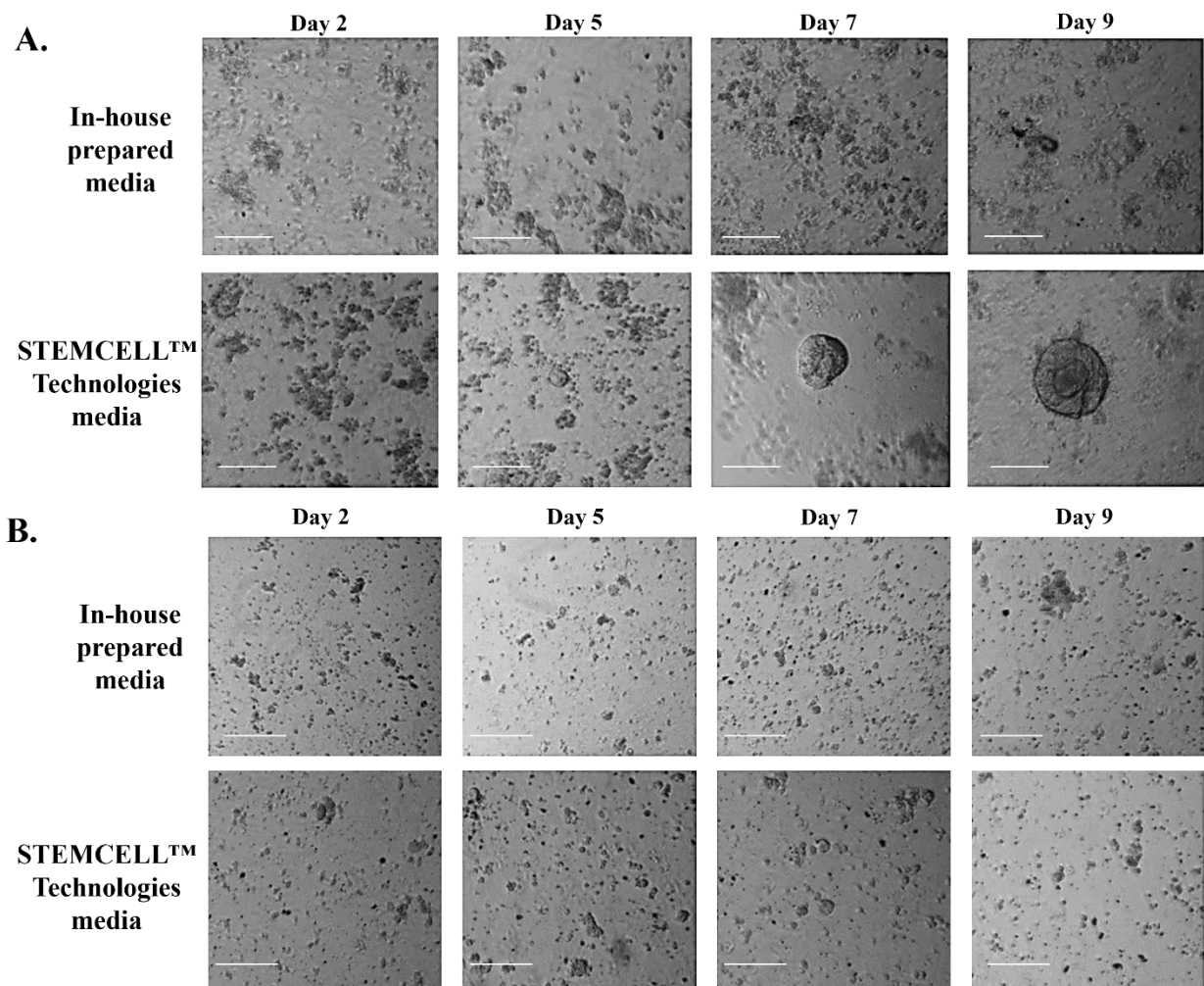


**Figure 6: Organoid growth of N-B043 of non-cancerous and C-B043 cancer organoids in STEMCELL™ Technologies organoid media vs. in-house prepared media. A) Non-cancerous organoid growth in STEMCELL™ Technologies media and in-house prepared media. As seen in**

day 2 for the sample in the two different mediums, clumps of single stem cells were visualised with some crypt-like structures. As culture progressed to day 5 in culture, the crypt-like structures developed into cyst-like structures, however in the STEMCELL™ Technologies media the cyst-like structures were larger in size. At day 7 in culture, organoids were visualised in both mediums but larger, more mature organoid structures were seen in the STEMCELL™ Technologies media.

B) Cancer organoid growth in STEMCELL™ Technologies media and in-house prepared media. Across both types of media used, single stem cells and clumps of single stem cells were visualised during the culture period with minimal growth. However, at day 9 in culture of the in-house prepared medium, larger clumps of cells were visualised. Images visualised using the Leica DMIL LED Inverted Microscope (Leica Microsystems, Germany), scale bar is 50 µm and at 10x magnification.

As seen in Figure 6 both the non-cancerous and cancer organoids progress from clumps of single stem cells to crypt-like structures from day 5-7. On day 9 of the non-cancerous sample, more organoid structures were visualised that grew larger in size. This suggests that the non-cancerous organoids grew at a faster rate in the STEMCELL™ Technologies media in comparison to the in-house produced media. The non-cancerous organoids in the in-house produced media grew at a much slower rate and more areas of cell aggregates were visualised. The cancerous organoids grew similarly in both types of media, where clumps of stem cells were visualised and the culture seemed stagnant. At day in culture of the in-house prepared media illustrated larger clumps of stem cells that had increased in size although no conclusion regarding which medium was more suitable. Furthermore, it has been reported that cancer organoid growth tends to be slower than non-cancerous organoids. However, considering the costs and more availability of in-house prepared media, it was acceptable to pursue the culture of organoids in the media prepared in-house.

### **5.2.1. Organoid Growth Monitoring across days at Passage 0**

Based on the first ever human intestinal organoids generated by Sato and colleagues (2009), the organoids should follow a basic growth pattern of individual stems cells that increase in size to become cyst-like structures that will undergo budding and eventually progress to large, cystic, mature organoids. Consistent with their research, Figure 7 depicts our organoid growth across several days from a single stem cell to a mature organoid. This figure was generated from the non-

cancerous organoids from sample N-B020 that was established to compare the growth of the organoids generated to that of previously published literature.

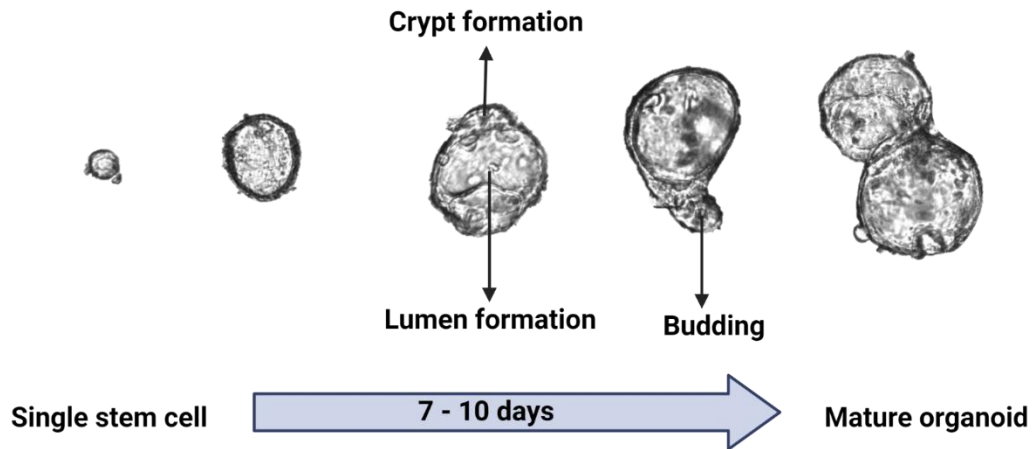


**Figure 7: Monitoring organoid growth to identify key development steps.** At day 0, the initial growth of the organoid presents as a clump of stem cells that will progress to form a cyst-like structure. The cyst-like structure is comprised of proliferating progenitor cells and a central lumen that will increase in size. Between days 3 and 4, budding of the cyst-like structure will appear, which marks the development of a crypt. Crypts present as budding structures around the central lumen and will progress to become larger. Organoids will reach maturity between days 7 and 10 in culture, where the structure of the organoid resembles that of the intestine. The lumen will also progress to become darker as this is the region in which villi will develop and dead cells are shed towards the lumen. Organoids visualised using the CytoSMART Lux3 FL (Axion Biosystems, USA) microscope and at 10x magnification.

As seen in Figure 7 it is evident that the organoids generated are first visible as a single stem cell, which develops into a cyst-like structure that contains the proliferating progenitor cells and a central lumen. The proliferating progenitor cells will be located towards the sides of the organoid and the lumen is located in the middle of the organoid. When a Wnt gradient is established the cyst-like structure will then undergo budding to give rise to future crypts. The central lumen is where villi would develop and will darken in colour as dead cells are shed towards the lumen. The

organoids continued to grow in size to produce mature organoids that maintain the original cystic structure as this form of organoid maintains the stem cell state. This growth pattern can be extended to the other non-cancerous organoid lines that were generated from different patient samples.

Organoid growth monitoring was performed from first day in culture across several days. This was done to determine the morphology and to ensure that morphology remains consistent with previous literature. Growth monitoring was performed using an inverted, phase-contrast light microscope and images were captured. Figure 8 illustrates the growth of organoids from non-cancerous tissue from samples N-B020, N-B026 and N-B027 across 7 – 10 days in culture. The non-cancerous samples used were derived from fresh tissue biopsies and were at p0.

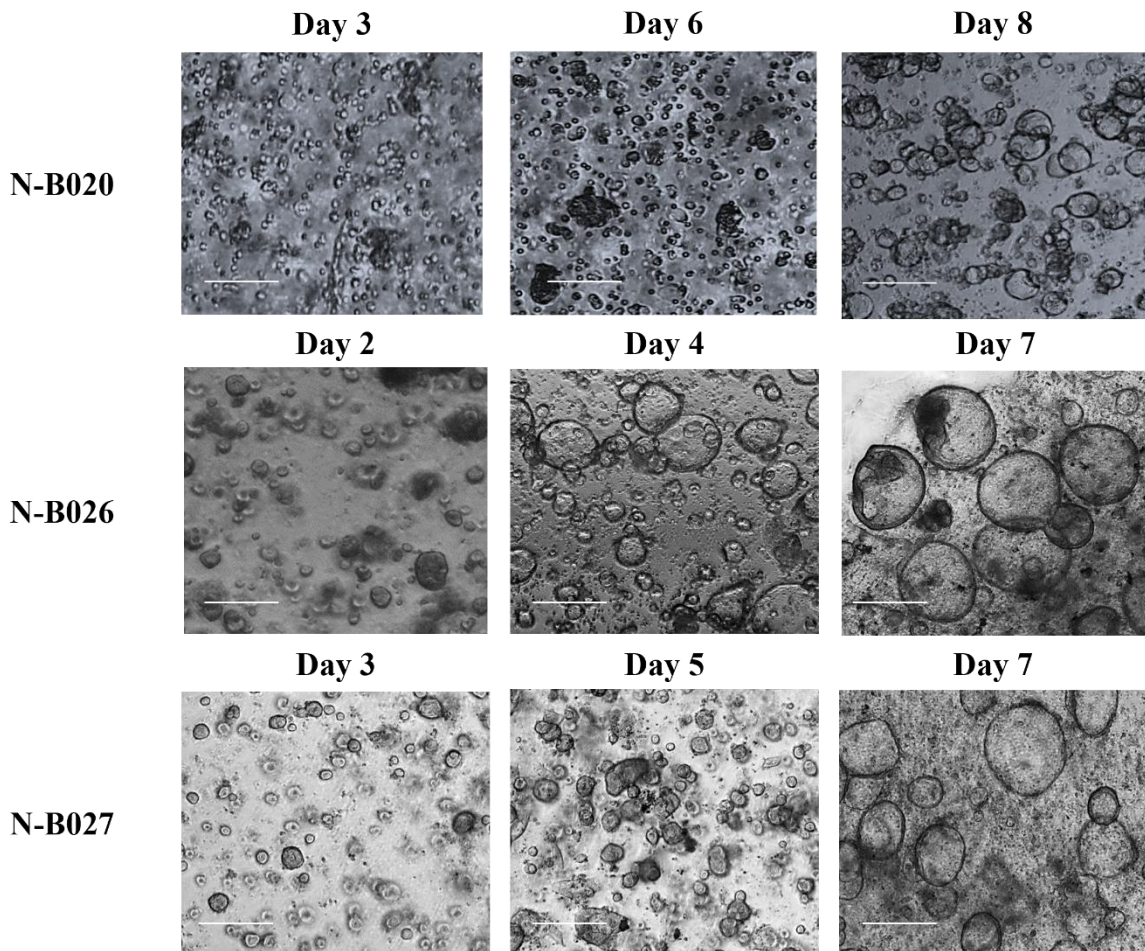


**Figure 8: Monitoring non-cancerous organoid growth across several days in culture at p0.** These panels of images depicts that the organoids in all three samples follow a similar growth pattern of cyst-like structures that eventually form budding and develop into large, mature

organoids as culture progresses. The single-stem cells form clumps of cells to produce round structures during days 2 – 3 of culture. This structures eventually increase in size as depicted on days 7 and 8. The organoids were grown in STEMCELL™ Technologies medium and were at p0. Visualised using the Leica DMIL LED Inverted Microscope (Leica Microsystems, Germany), scale bar is 50 µm and at 10x magnification.

As seen in Figure 8, the non-cancerous organoids followed through non-cancerous growth distribution across 7-10 days as expected in all samples. The first panel of images illustrates day 3 (N-B020 and N-B027)/day 2 (N-B026) in culture where the organoids present as round, cyst-like structures, as well as single stem cells. The second panel of images depicts day 6 (N-B020)/ day 4 (N-B026)/ day 5 (N-B027) in culture, where the cyst-like structures increased in size and budding is visualised in some of the cyst-like structures. The third panel of images depicts mature organoids in all three samples although N-B020 organoids are smaller in size.

### 5.2.2. Organoid Sub-culturing and Growth Monitoring across Passages

Once mature organoids were formed and were large in size, it is required to digest the organoids into crypt fragments. These crypt fragments can then be cultured once again to generate more organoids. Literature suggests that organoids can be digested employing 3-5-minute intervals at 37 °C in a water bath. Digestion was performed for 1 minute, 3 minutes and 5 minutes and images were captured and shown in Figure 9.

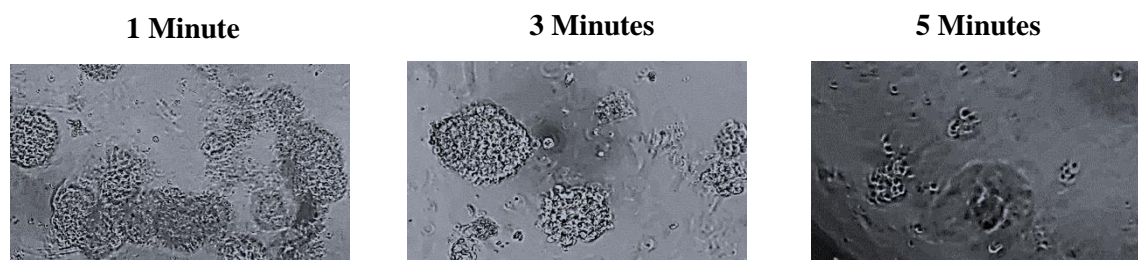


**Figure 9: Monitoring the organoids in TrypLE to identify optimal TrypLE incubation time.** Once the organoids were confluent and reached desired size, they were passaged by digesting the organoids down into crypt fragments to give rise to new organoids. The organoids were observed after 1 minute in TrypLE, which still showed whole organoid structures. Incubation was increased

*to 3 minutes and whole organoids were visualised once again. The 3-minute interval revealed that the organoids were becoming smaller and more digested revealing more single cells. However, the incubation period was increased to a total of 5 minutes and revealed clumps of single cells and crypts. This was satisfactory digestion and the single were seeded once again. Visualised using the Leica DMIL LED Inverted Microscope (Leica Microsystems, Germany), scale bar is 50  $\mu\text{m}$  and at 10x magnification.*

As seen in Figure 9, 5 minutes incubation time in TrypLE was satisfactory to digest the organoids into crypt fragments, however, dependent on the size of organoids, a maximum of 5 minutes can be utilized as well. Once the organoids were digested, the crypts were pelleted by centrifugation and seeded as 10  $\mu\text{L}$  domes with 1000 crypts per dome. The organoids were then cultured once again until large cystic organoids are seen and can be passaged indefinitely (Pleguezuelos-Manzano Cayetano *et al.*, 2020). Growth monitoring of the organoids was performed during passages as well to ensure morphology is maintained. Figure 10 illustrates the morphology of the non-cancerous organoids from 5.2.1 across 3 passages and it can be seen that the morphology remains consistent.

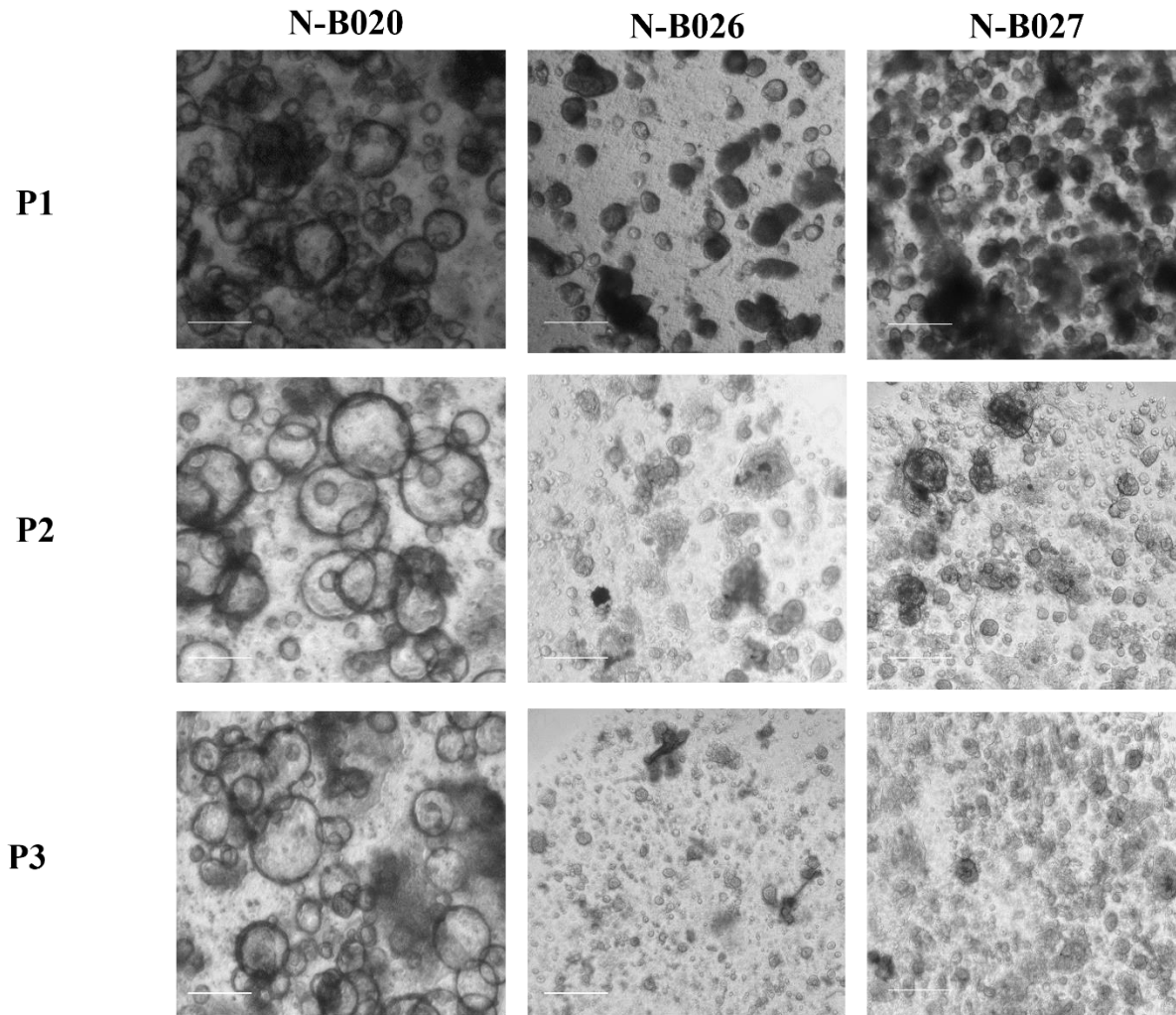


**Figure 10: Organoid growth during p1, p2 and p3.** It is illustrated the organoids maintain morphology as passage numbers increase. Images for N-B020 were taken prior to the organoids being passaged whereas images for N-B026 and N-B027 were taken during each passage. The organoids maintain the development of cyst-like structures that increase in size and produce budding until large, mature organoids are visualised. Visualised using the Leica DMIL LED Inverted Microscope (Leica Microsystems, Germany), scale bar is 50  $\mu\text{m}$  and at 10x magnification.

In Figure 10, the morphology of the organoids is maintained as round, cystic structures that increase in size as the organoids mature. Additionally, the organoids present with thin walls indicating that they are maintained in a stem cell state. N-B020 underwent passaging from p0 to p1 in 8 days, p1 to p2 in 10 days and p2 to p3 in 10 days. N-B026 underwent passaging from p0

to p1 in 7 days, p1 to p2 in 11 days and p2 to p3 in 10 days. N-B027 underwent passaging from p0 to p1 in 7 days, p1 to p2 in 11 days and p2 to p3 in 10 days. Additionally, the organoid growth, particularly in samples N-B026 and N-B027, seems to slow down across each passage that could be a direct result of it being a primary culture and indicating patient-to-patient variability.

The protocol of generating organoids was first optimized on non-cancerous tissue biopsies prior to cancer tissue biopsies. However, when attempting the same protocol on fresh cancer tissue biopsies it was unsuccessful as the cancer biopsy samples that were obtained were miniscule in comparison to the normal biopsy samples. Furthermore, the cancer tissue samples had more red blood cells/vessels around the tissue, tougher and looked more irregular in comparison to the normal biopsy samples. Cancer samples were seeded at 1000 crypts per 10  $\mu$ L dome and were cultured in in-house produced media without the addition of Human Recombinant Wnt3a. Figure 11 illustrates the failure of culturing cancer organoids from two fresh tissue biopsies, C-B042 and C-T006 at p0.

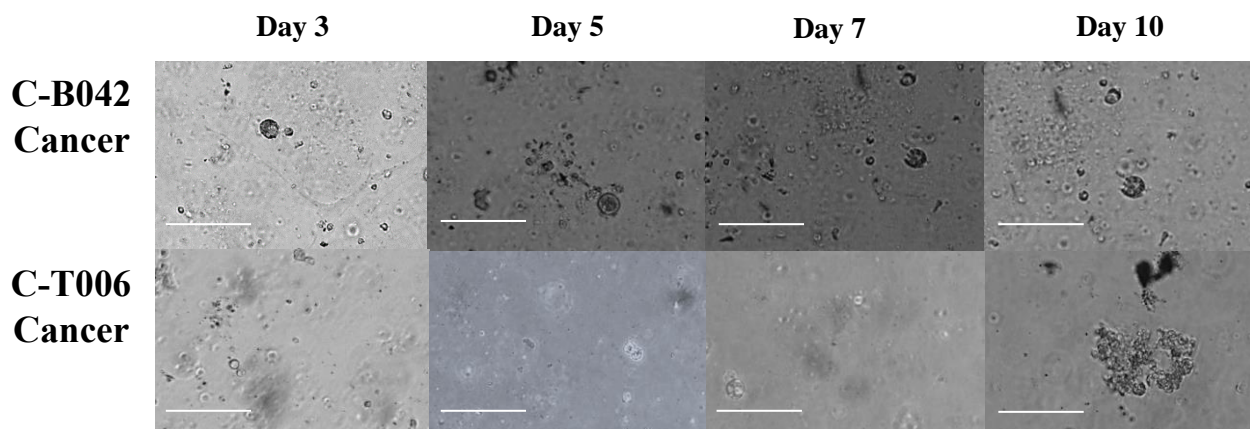


**Figure 11: Failure of cancer organoid growth from fresh tissue biopsies.** Two fresh cancer tissue biopsies, namely, C-B042 and C-T006 was used in an attempt to culture cancer organoids. C-B042 at day 3 in culture showed very few single stem cells or clumps of single stem cells present in the dome, with one small cyst-like structure. At day 5 in culture, very few cyst-like structures had developed and as culture progressed from day 7 to day 10, these structures did not increase in size. Similar observations were seen in C-T006, where few single stem cells were visualised and very few cyst-like structures were seen across days 3 to 7. However, on day 10 in culture a small cluster of cyst-like structures were seen but growth seemed to be stunted. Visualised using the Leica DMIL LED Inverted Microscope (Leica Microsystems, Germany), scale bar is 50  $\mu$ m and at 10x magnification.

Based on Figure 11, C-B042 and C-T006 illustrated similar growth patterns where few single stem cells were visualised and very few cyst-like structure had developed. Any cyst-like structures that were visualised remained stunted in growth suggesting that the non-cancerous organoids were not viable. Additionally, very few cell aggregates were visualised across the 10  $\mu$ L domes even when 1000 crypts per dome was seeded. Indicating a weak aggregation potential. Due to the failure of the two cancer organoid lines, a third sample was not attempted to prevent sample and media wastage. In order to generate cancer organoids, frozen cancer tissue biopsies were used.

### 5.3. Protocol generating organoids from frozen tissue biopsies

Since the conventional protocol failed to produce mature CRC organoids, frozen cancer tissue biopsies were used as literature indicated that frozen biopsies could also be used to generate organoids. This was performed by comparing two protocols that differed in the digestion of the biopsies. The first protocol utilized dispase dissolved in organoid media and the second protocol utilized collagenase II dissolved in organoid media. Figure 12 illustrates the monitoring of non-cancerous organoid growth (N-B046) across several days to compare which protocol was more successful in generating organoids. N-B046 was a new organoid line and at p0.

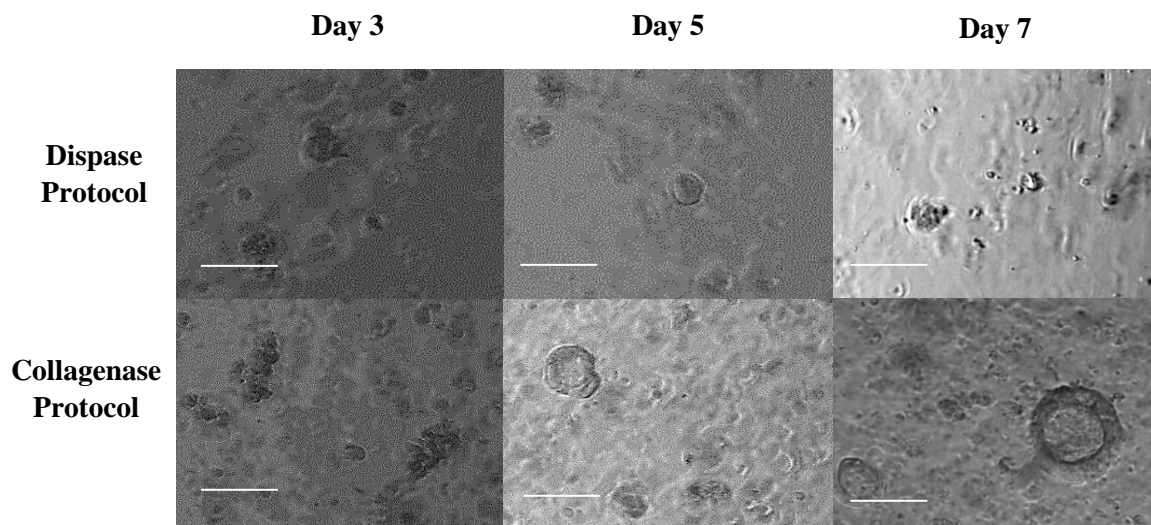


**Figure 12: Comparison of non-cancerous organoid growth from N-B046 frozen tissue biopsy.** The same tissue biopsy was used to be able to confidently compare the two different protocols of tissue digestion to harvest crypts for organoid culture. As seen from the dispase protocol for

*biopsy digestion, day 3 in culture produced round, cyst-like structures that increased slightly in size by day 5 in culture. However, as seen in day 7 in culture, these cyst-like structures did not increase further in size to produce mature organoids. As seen in the collagenase II protocol, more cyst-like structures were visualised at day 3 in culture in comparison to the dispase digestion protocol. At day 5 in culture, the cyst-like structure grew in size and by day 7 in culture, mature organoids could be visualised. Visualised using the Leica DMIL LED Inverted Microscope (Leica Microsystems, Germany), scale bar is 50  $\mu\text{m}$  and at 10x magnification.*

The protocol that utilized collagenase II dissolved in organoid media was more successful and organoid growth occurred quicker during the 7 days in culture (Figure 12). Despite small cyst-like structures being visualised following the dispase digestion, the growth of non-cancerous organoids decreased over days in culture under this digestion condition. Therefore, the protocol that was utilized to successfully generate non-cancerous organoids involves the use of frozen tissue biopsy digested in collagenase II that is reconstituted in organoid media. This protocol was applied on cancerous patient samples and as seen in Figure 13; it illustrates the monitoring of cancer organoids across several days in culture grown in in-house produced media. All cancerous samples used were new organoid lines and were at p0.

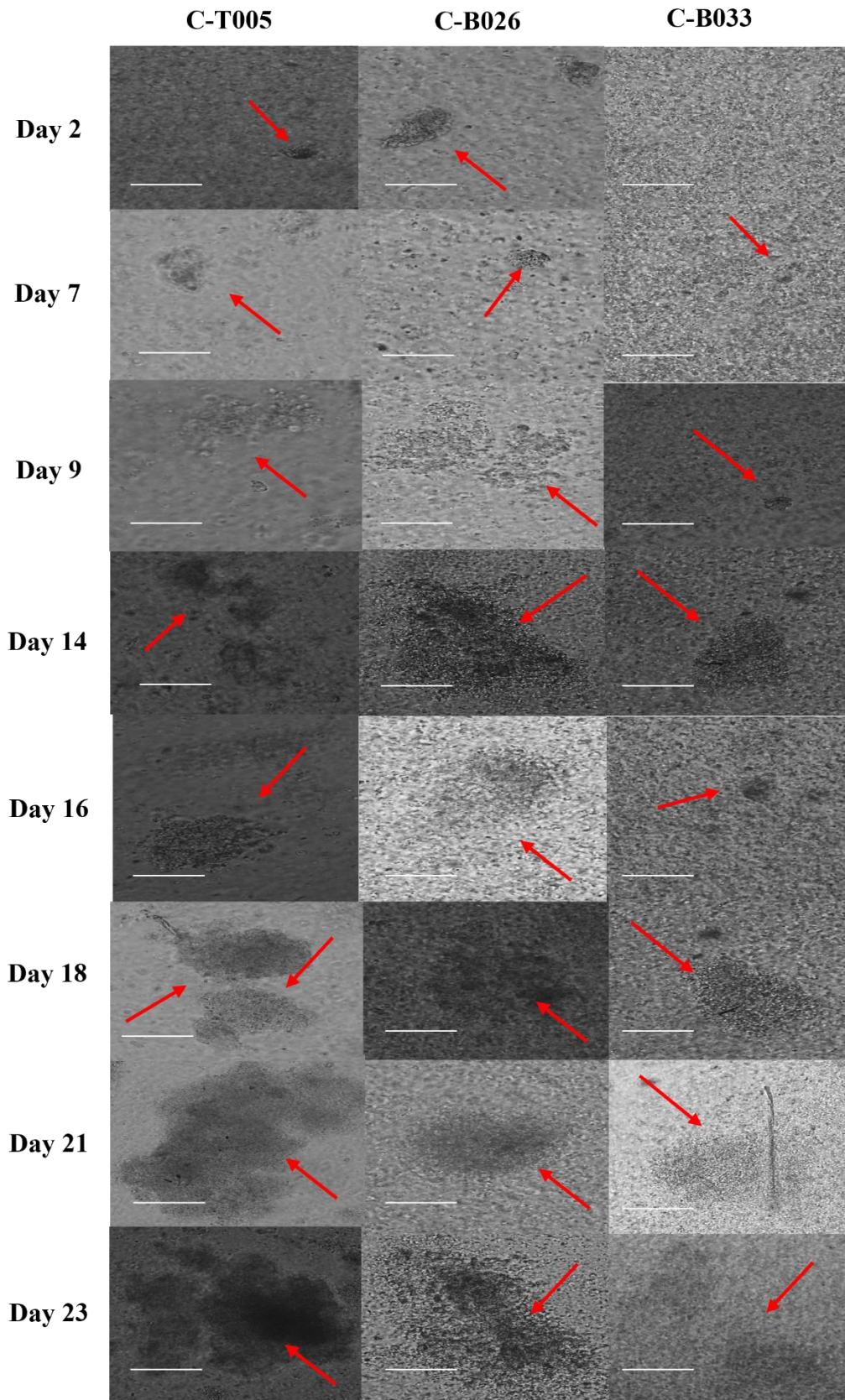


**Figure 13: Growth monitoring of cancer organoids in culture from frozen tissue biopsies.** As seen across all cancerous organoid samples, the organoids were maintained in culture for a period of 23 days. Sample C-T005 presented with small crypt-like structures from days 2 to 7 in culture. At day 9 in culture, the crypts had grown in size and developed into cell aggregates. The cell aggregates increased in size from days 14 to 23 in culture. The C-B026 sample presented with crypt-like structures from days 2 to 7. The crypt-like structures progressed to cell aggregate structures at day 9 that increased in size as culture progressed to day 23. Sample C-B033 presented as single cells from days 3 to day 7. On day 9, crypt-like structures were visualised, but from day 14 onwards, more cell aggregate structures were visualised that increased in size. Visualised using the Leica DMIL LED Inverted Microscope (Leica Microsystems, Germany), scale bar is 50  $\mu\text{m}$  and at 10x magnification. Red arrows indicate the cancerous organoids.

Each of the organoid cultures was maintained in culture for twenty-three days. The organoids in Figure 13 first resembled crypt structures which grew to form cell aggregates. The cell aggregates increased in size, suggesting sufficient aggregation potential but failed to form cystic structures. Furthermore, these cell aggregates were grainy and lacked a uniform shape, similar to the tissue from which they were derived. Additionally, the domes seemed smeared due to the large number of cells that failed to form aggregates and can affect organoid forming efficiency. The cell aggregates in the cancerous organoids were also darker in colour and may suggest that the viability of the culture is low. All three samples were used for immunofluorescence to generate a proof of concept and to ascertain if the organoids that were grown did present with cell types of interest.

#### **5.4. Organoids Accurately Recapitulate Genetic Composition and Spatial Localization of Cell Types in Primary Tissue**

In order to optimize the primer annealing temperatures gradient PCR was performed for each primer to establish the ideal annealing temperatures. The optimized annealing temperature for each primer is illustrated in Table 6. Agarose gel electrophoresis was used to visualise the PCR products from the gradient PCR and to determine the optimal annealing temperature for each primer. Agarose gels depicting PCR products can be found in Supplementary Figure 1, Annexure 1.

##### **5.4.1. Identification of the most suitable protocol to isolate RNA from organoids**

Once the non-cancerous organoids had reached confluency and passage 2, RNA extraction was performed. The RNA yield was evaluated using the Nanodrop 1000 spectrophotometer as well as

the purity by evaluating the  $A_{260}/A_{230}$  and  $A_{260}/A_{280}$  ratio. An  $A_{260}/A_{230}$  of 1.8 was deemed usable and absent of salt/phenol contamination. An  $A_{260}/A_{280}$  ratio of 2.0 was deemed usable and absent of protein contamination. RNA integrity was evaluated by using agarose gel electrophoresis, which separated the 28S and 18S ribosomal RNA (rRNA) bands. When two distinct bands for the rRNA was visualised on the ChemiDoc™ MP system (Bio-Rad, USA), the RNA was utilized to produce cDNA. Initially, the Qiagen RNeasy® Mini Kit was employed, however, this protocol yielded unsatisfactory RNA purity ratios and extremely low yields of 0.1 – 9.2 ng/ $\mu$ L. Therefore, in an attempt to extract RNA from the non-cancerous organoids, TRIzol® (Ambion®, Life Technologies, USA) RNA extraction was performed as well as using the Omega Bio-tek E.Z.N.A® Total RNA Kit I (double column extraction kit). The difference between using the TRIzol® method for RNA extraction and the Omega Bio-tek E.Z.N.A® Total RNA Kit I is the use of a spin-column for digestion. RNA extraction that is performed using the TRIzol® method involves lysing the cells using TRIzol® reagent and then separating the RNA, DNA and proteins into three different phases, namely the aqueous phase, interphase and organic phase using chloroform. TRIzol® is a monophasic solution of guanidium isothiocyanate and phenol that solubilizes biological material and denatures protein (Rio *et al.*, 2010). The addition of chloroform causes phase separation of the two liquids as it is miscible with phenol and has a higher density. RNA is then isolated to the aqueous phase due to pH and as it is more polar than DNA (due to it having a 2-hydroxyl group), which can be collected (Chomczynski and Sacchi, 2006). Therefore, the TRIzol® method relies on phase separation due to pH to extract RNA from cells. The Omega Bio-tek E.Z.N.A® Total RNA Kit I uses an on-column approach for RNA extraction, where the cells are lysed using a lysis buffer and homogenizer column and the cell lysate is then transferred to a binding column. This binding column allows for the binding of nucleic acid binding to the solid matrix of silica when in the presence of a high salt buffer. Once the nucleic acid is bound to the column, it is washed and eluted to isolate RNA. These two RNA isolation protocols were employed as they differ in principle of RNA extraction to determine a more suitable method to obtain high quality RNA and high yields. Table 12 illustrates the comparisons amongst the three RNA extraction methods.

**Table 12: Comparison across three different RNA isolation protocols tested.**

	<b>TRIzol® Method</b>	<b>Qiagen RNeasy® Mini Kit</b>	<b>Omega E.Z.N.A® RNA Kit I</b>	<b>Bio-tek Total</b>
<b>Ice cold DPBS wash</b>	√	√	√	
<b>Harvesting of organoids</b>	√	√	√	
<b>TrypLE organoids</b>			√	
<b>Vortex</b>		√	√	
<b>Addition of lysis buffer</b>		√	√	
<b>Homogenisation</b>		√		
<b>On column digestion</b>			√	
<b>Addition of RNA binding column</b>		√	√	
<b>Addition of B-Mercaptoethanol</b>		√	√	
<b>Addition of TRIzol®</b>	√			
<b>Addition of Chloroform</b>	√			
<b>Addition of Isopropanol</b>	√			
<b>Incubation on ice</b>	√			
<b>Inverting of tube in isopropanol</b>	√			
<b>Addition of ethanol</b>	√	√	√	
<b>Addition of wash buffer</b>		√	√	
<b>Heating of sample</b>	√			
<b>Addition of ice-cold RNase free water</b>		√	√	

<b>Range of 260/280 Ratios</b>	2.06 – 3.87	1.23 – 2.03	2.02 – 2.10
<b>Range of 260/230 Ratios</b>	0.01- 0.02	0.29 – 0.35	1.43 – 1.75
<b>Range of RNA concentrations obtained</b>	1.2 – 8.2 ng/ $\mu$ L	1.2 – 3.1 ng/ $\mu$ L	52.0 – 239.6 ng/ $\mu$ L
<b>Success of Extraction (Purity)</b>	Unsuccessful	Unsuccessful	Successful
<b>Success of Extraction (Quantification in ng/<math>\mu</math>l)</b>	Unsuccessful	Unsuccessful	Successful
<b>Success of Integrity (Integrity gel)</b>	Unsuccessful	Unsuccessful	Successful

Based on Table 12, the Omega Bio-tek E.Z.N.A® Total RNA Kit I yielded satisfactory RNA yields, ratios and integrities and was utilized for the extraction of RNA from the non-cancerous organoids. Once RNA extraction was completed for N-B020, N-B026 and N-B027, cDNA was synthesised for the preparation of RT-qPCR

### **5.5. Genetic Composition of Cell Types present in Normal Tissue is Recapitulated in Non-cancerous Organoids**

RT-qPCR was selected to quantify the mRNA extracted from the organoids and to identify the gene expression from specific cell types present in the organoids for characterization purposes. The genes of interest included *CHGA* (enteroendocrine cells), *EPCAM* (for epithelial cells), *LGR5* (for crypt base columnar cells), *LYZ* (for Paneth cells), *MKI67* (for actively proliferating cells), *MUC2* (for goblet cells) and *VILI* (for tuft cells). Additionally, RT-qPCR was performed on the matched non-cancerous tissue of the organoids to validate the fidelity of the model. The organoid lines (N-B020, N-B026 and N-B027) were at p2 in culture when they were harvested for RT-qPCR and the tissue used was organoid sample matched that was previously snap frozen and stored in liquid nitrogen. It can be stated that the cell types present in the organoids were present in a similar ratio when compared to the primary tissue. Figure 14 illustrates the normalized gene expression of the gene of interest to validate that the non-cancerous organoids cultured were those from the intestinal tract.

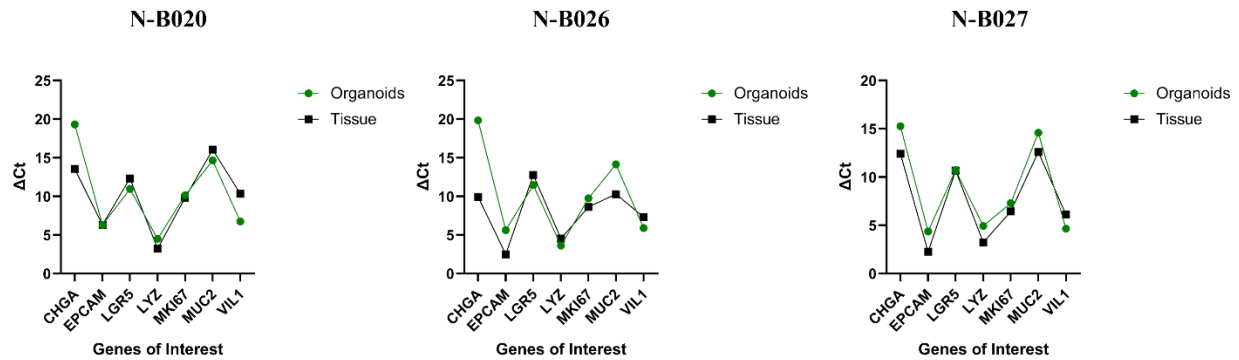


**Figure 14: Characterising non-cancerous organoid cell composition using RT-qPCR in comparison to matched tissue.** RT-qPCR analysis was performed on the organoids and the matched tissue and showed that both expressed the gene expression markers of interest. Each graph illustrates a similar trend in the expression of the genes between the organoids and the tissue from which they were derived. Gene expression is indicated relative to  $\beta$ -actin. Statistical analysis: Paired t-test. This was performed once in duplicate for each sample and the p-value for each sample was 0.9064 for N-B020, 0.2293 for N-B026 and 0.0824 for N-B027. Three biological repeats were used (3 different patient samples) and each was repeated in duplicate. Sample size was too small to perform statistical analysis.

Similar trends were observed in the cell types of the non-cancerous organoids when compared to the tissue as the organoids were derived from the same tissue. Slight variations in  $\Delta$ CT values are expected as the cells constituting the organoids would be in different stages of maturity and differentiation as compared to the tissue that was snap frozen. Additionally, the physical tissue sizes used were much larger than the number of organoids used and can affect the  $\Delta$ CT values obtained for the tissue in comparison to the organoids. However, as the tissue was used to generate the non-cancerous organoids, the  $\Delta$ Ct values could be deemed as the basal  $\Delta$ Ct value for each marker gene and a high  $\Delta$ Ct value would indicate a lower expression of the gene and a low  $\Delta$ Ct value would indicate a higher expression of the gene. Statistical analysis using a paired t-test indicated that the p-values across all three samples were non-significant between the organoids and the tissues. Furthermore, the  $2^{-\Delta\Delta C_t}$  was calculated by using the  $\Delta$ Ct value for each gene in the tissue samples and subtracting it from the  $\Delta$ Ct values for each gene of the organoids. These values are illustrated in Table 13.

**Table 13: The  $2^{-\Delta\Delta Ct}$  values obtained for each gene per sample when comparing the organoids to the tissue samples**

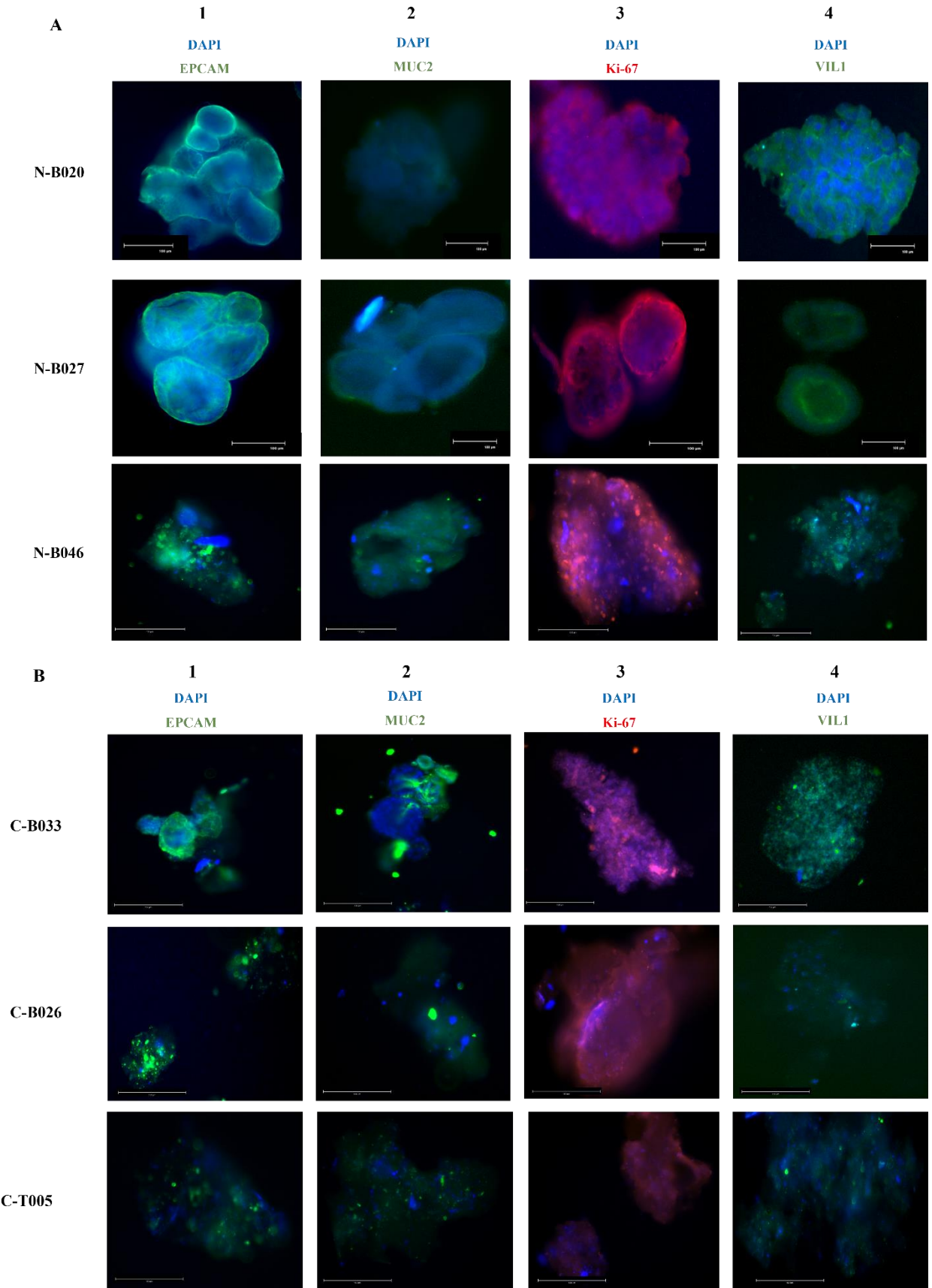
<b>N-B020</b>		
Gene of Interest	$2^{-\Delta\Delta Ct}$ value	Conclusion
<i>CHGA</i>	0.0185	Slight increase in organoid expression
<i>EpCAM</i>	1.0210	Increase in organoid expression
<i>LGR5</i>	2.5487	Increase in organoid expression
<i>LYZ</i>	0.4145	Slight increase in organoid expression
<i>MKI67</i>	0.8039	Slight increase in organoid expression
<i>MUC2</i>	2.6574	Increase in organoid expression
<i>VIL1</i>	12.000	High increase in organoid expression
<b>N-B026</b>		
<i>CHGA</i>	0.0011	Slight increase in organoid expression
<i>EpCAM</i>	0.1154	Slight increase in organoid expression
<i>LGR5</i>	2.4786	Increase in organoid expression
<i>LYZ</i>	1.8797	Increase in organoid expression
<i>MKI67</i>	0.4569	Slight increase in organoid expression
<i>MUC2</i>	0.0689	Slight increase in organoid expression
<i>VIL1</i>	2.6620	Increase in organoid expression
<b>N-B027</b>		
<i>CHGA</i>	0.1398	Slight increase in organoid expression
<i>EpCAM</i>	0.2295	Slight increase in organoid expression
<i>LGR5</i>	0.9666	Slight increase in organoid expression
<i>LYZ</i>	0.3077	Slight increase in organoid expression
<i>MKI67</i>	0.5481	Slight increase in organoid expression

<i>MUC2</i>	0.2529	Slight increase in organoid expression
<i>VIL1</i>	2.7673	Increase in organoid expression

The above table, Table 13 indicates the relative fold change of the gene expression between the organoids and the tissue from which the organoids were derived. All  $2^{-\Delta\Delta C_t}$  values indicate an increased expression of the genes of interest when comparing the organoids to the tissue. This is expected as the organoids were grown and expected to have slight increased expression depending on the maturity and differentiation of the organoids. However, RT-qPCR was not used to determine increased/decreased gene expression but to determine whether the organoids represent the tissue from which they were derived. Therefore, based on Figure 14, similar  $\Delta C_t$  trends were observed between the organoids and the tissue and based on Table 13, the increased gene expression fold change indicated that the organoids contained mature and differentiated cell types that are present in the intestine.

### **5.6. Spatial Localization of Characteristic Cell Types in Organoids using Immunofluorescence Microscopy**

Immunofluorescence is an immunochemical technique that allows for the detection and localization of antigens in the organoids. This technique was used as a characterization technique to identify the presence of specific proteins in the organoids, namely, EpCAM (for epithelial cells), MUC2 (for goblet cells), Ki-67 (for actively proliferating cells) and VIL1 (for Paneth cells). It allowed for the identification as well as localization of the proteins in the respective organoids. The intensity and extent of antibody staining can be used to infer the expression and localization of the proteins. Immunofluorescence was performed on three non-cancerous samples (N-B020, N-B027 and N-B046) that were at p3 in culture as well as on three cancer samples at p0 (C-B033, C-T005 and C-B026) as a proof of concept that the cancer organoids being cultured contained the specific cell types present in the intestinal tract. Visualization was performed using the Flouid™ Cell Imaging station (for non-cancerous samples N-B020 and N-B027) at 40 X magnification and the EVOS M7000 at 20 X magnification (for non-cancerous sample N-B046 and cancerous samples C-B033, C-B026 and C-T005) (Figure 15).



C

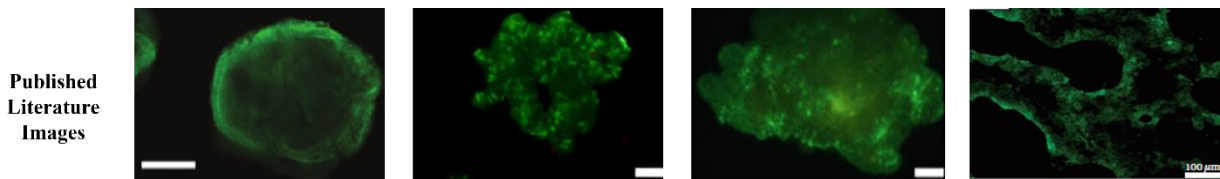


**Figure 15: Representative immunofluorescent images of non-cancerous and cancerous organoids in comparison to previously published literature.** A. Immunofluorescence images of the non-cancerous organoids. N-B020, N-B027 and N-B046 samples were used. Unfortunately, N-B026 didn't have enough sample to complete immunofluorescence and therefore N-B046 was used. B. Immunofluorescence images of cancerous organoids. C-B033, C-B026 and C-T005 samples were used. EpCAM (in green, refer to panel 1), was used to identify epithelial cells present in the organoids and across all three samples it was evident that there were epithelial cells present. MUC2 (in green, refer to panel 2,) was used to identify goblet cells present in the organoids and across all three samples it was evident that there were goblet cells present. Ki-67 (in red, refer to panel 3), was used to identify proliferating cells present in the organoids and the intensity of the red fluorescence indicates that there were numerous actively proliferating cells. VIL1 (in green, refer to panel 4), was used to identify Paneth cells present in the organoids. As seen across all three samples, there is evidence of Paneth cells. DAPI was used to stain the nuclei blue. Images from N-B026 and N-B027 were obtained using the FLoId Imaging Station (Thermo Fisher Scientific, USA) at 40 X magnification and images from N-B046 (non-cancerous), and cancerous samples (C-B033, C-B026 and C-T005) were obtained using the EVOS M7000 microscope (Thermo Fisher Scientific, USA) at 20 X magnification. Scale bar is 150  $\mu\text{m}$ . C. Panel C indicates the reference images from previously published literature and indicates that EpCAM (scale bar is 200  $\mu\text{m}$ ) in green in panel 1, MUC2 (scale bar is 50  $\mu\text{m}$ ) in green in panel 2, Ki-67(scale bar is 50  $\mu\text{m}$ ) in green in panel 3 and VIL1(scale bar is 100  $\mu\text{m}$ ) in green in panel 4. Panel C illustrates that the various cell types are expressed across the entire organoids (References: (Hahn et al., 2017; Han et al., 2023; Pineiro-Llanes et al., 2024))

As seen across all samples, all the organoids (non-cancerous and cancerous) presented with EpCAM, MUC2, Ki-67 and VIL1 protein expression (Figure 15). EpCAM (panel 1) indicates that the localization is present on the cell surface of the organoids as these 3D structures are composed of polarized epithelium as shown across all samples. MUC2 (panel 2) presents with a lower fluorescent intensity with less visualization of as localization should be present towards the interior

of the organoids as it contributes to the mucus layer that lines the intestine. The localization of Ki-67 (panel 3) is expected to be expressed throughout the organoids as this protein is associated with actively proliferating cells as shown across all samples. VIL1 protein expression (panel 4) is expected to be expressed on the apical surface of the organoids as it is a cytoskeletal protein that is localised to microvilli, this is evident in the organoids expressing VIL1 specifically around the cells (N-B020) or across the entire organoid (N-B027, N-B046, C-B033, C-B026 and C-T005). The reference images in panel C are used to compare the intestinal organoids derived from South African patients to that of previously published literature. It is evident that there are some similarities amongst the images with the proteins being expressed throughout the organoids. This is particularly evident when comparing EpCAM, MUC2 and Ki-67 expression in the South African derived organoids to the previously published literature. However, it is noted that there is decreased expression in MUC2 of the cancerous organoids across all three samples when comparing it to the representative image. When comparing VIL1 expression in N-B020 and N-B026 to the reference image there is similarities in VIL1 being expressed towards the interior of the organoids and the exterior of the organoids. Conversely, in N-B027 and the cancerous samples this is not clearly seen as there are numerous VIL1 expressing cells throughout the organoids and more so towards the exterior of the organoids. However, despite the localization of these proteins, it indicates that the organoids are composed of mature, differentiated cell types that are required for intestinal growth and development

## 6. Discussion

The use of patient-derived cells and tissue models is becoming an important tool in understanding cancer biology and drug discovery (Ng *et al.*, 2019). This is due to limitations that are associated with conventional cancer cell lines, particularly in predicting accurate clinical efficacy of cancer therapies, limited cell type heterogeneity, variations in primary tumour representation, cross-contamination with other cells and lack of correlation between clinical samples and established cell lines (Gillet *et al.*, 2011; Ng *et al.*, 2019). Therefore, focus has been placed on the use of patient-derived organoids that could potentially predict the outcome of therapeutics to specific patients and provide novel insights into patient-specific cancer biology (Clevers, 2016; Ng *et al.*, 2019). The purpose of the project to establish, characterize and validate the organoid cultures from the non-cancerous and cancerous tissues obtained from South African colorectal patients.

This project is the first of its kind that utilizes patient-derived tissue from South African patients to generate organoids. It is also one of the first reports of standardizing organoid culture protocols in South Africa. Patient-derived organoids from South African individuals can be used to understand CRC disease progression and development. Additionally, it can provide a more accurate drug treatment outcome prediction, thus bringing South Africa a step closer to a personalized medicine approach to develop novel treatment regimens that are tailored to each patient. Furthermore, the clinical data collected from each patient can be used to evaluate general trends in South African CRC development. The clinical data that was collected for the samples used in this study (Table 9) showed that only two patients out of the nine patients had been diagnosed with CRC over the age of 70 years old, one patient being white and the other being African. This supports the hypothesis that white South Africans present with earlier onset of CRC before the age of 70 years old, but a larger sample size is needed to confirm this (McCabe *et al.*, 2020). Unfortunately, no comment can be made on the South African black population as only one African sample was used. This was not based on a biased decision as samples were selected at random and clinical data was only reviewed afterwards to avoid bias towards particular samples. However, it is interesting to note that four patients (44.4% of patients) indicated that there is family history of CRC and the age of diagnosis was between 39 – 55 years old. This could indicate that earlier onset of CRC may be attributed to family history. Furthermore, 44.4 % (four out of nine, Table 9) of the patients presented with low grade adenocarcinomas meaning that the cancers are less aggressive and have a better prognosis. However, CRC tissues from more patients of all races would have to be evaluated before any inferences can be made regarding CRC disease development and progression in South African patients. Moreover, this project was aimed at establishing and standardizing organoid culture from South African individuals with particular focus on determining the appropriate BME and seeding density, evaluating organoid growth and the genetic and spatial characterization of intestinal cell types to validate the organoid cultures.

### **6.1. Success of Organoid Culture is Inherently Dictated by the Concentration of Reconstituted BME and Seeding Density of Organoids**

A key requirement for organoid culture is to recapitulate the ECM that plays a role in biochemical and biomechanical processes that aid in development and progression of tumours (Brogiere *et al.*, 2018; Ng *et al.*, 2019; Rezakhani *et al.*, 2021). The ECM components present in various types of BME matrices provide this 3D scaffold. The main components present in BME matrices is a

heterogeneous mixture of ECM proteins, proteoglycans and growth factors (Broguiere *et al.*, 2018). In general, the basement membrane consists of collagen IV, laminins and proteoglycans that vary depending on the type of tissue (Jeon *et al.*, 2022). Commercially available BME contain the aforementioned proteins, as well as tumour-derived proteins, such as TGF peptides and fibroblast growth factors and enzymes such as matrix metalloproteinases (MMPs) (Aisenbrey and Murphy, 2020). Three commercially available BME matrices are Matrigel®, Cultrex™ BME and Geltrex™. Matrigel® consists of laminin I, type IV collagen, entactin and heparan sulfate proteoglycans that is purified from mouse Engelbreth-Holm-Swarm tumour and is considered the gold standard BME matrix (Millesi *et al.*, 2023). Cultrex™ BME is similar to Matrigel® and contains the aforementioned proteins present in Matrigel® (Millesi *et al.*, 2023). Geltrex™ is also derived from mouse Engelbreth-Holm-Swam tumour, making it similar to Matrigel® but like Cultrex™ it also contains variations in the protein concentrations (Saari *et al.*, 2022). These BME matrices allow for organoid growth as they allow stem cells to grow in 3D by providing an ECM-like substrate.

Since organoids are grown in solid BME matrices, organoid growth is constrained due to solid stress accumulation, oxygen and nutrient delivery and therefore frequent passaging is required to maintain and expand cultures (Hirokawa *et al.*, 2021). The stiffness of BME matrices can cause organoids to become compressed and not undergo budding and the lack of specific ECM components for specific tissues can also reduce growth and budding of organoids (Rezakhani *et al.*, 2021). Therefore, understanding the tissue from which the organoids are derived and the ECM architecture remains vital in successful organoid growth. Another factor to consider when generating organoids in BME matrices is organoid seeding density. Organoid seeding density can be defined as seeding organoids at the optimal density to ensure growth and maturation of organoids without causing overcrowding and organoid death. According to Table 10 it was established that the optimal seeding density to generate organoids was 1000 crypts per 10  $\mu$ L dome, which yielded confluent organoid domes in 7 to 10 days in culture (refer to Figure 8). When the organoids are seeded at crypt densities below 700 crypts per 10  $\mu$ L dome, the resultant organoids are sparse across the domes with small, stunted organoid growth. This stunted growth is attributed to the fact that the organoid growth is also reliant on the growth factors produced by the organoids and if insufficient growth factors are produced, the organoids do not grow and the dome eventually collapses (Pleguezuelos-Manzano Cayetano *et al.*, 2020). Organoids that are

seeded at crypt densities above 700 crypts to 1000 crypts were densely packed (70% confluent domes) which provides the organoids with enough space to grow and sufficient numbers of organoids to produce growth factors that allowed for expansion. The upper limit of 1000 crypts per dome was used as the domes held for longer, especially when required for cancer organoid growth that is slower than non-cancerous organoid growth. The upper limit also ensures that if the crypt count is lower due to only a small volume being counted, there is still sufficient crypts within the 700 – 1000 crypt density that will give rise to organoids. However, if organoids are seeded at a crypt density of greater than 1000 crypts per 10  $\mu$ L dome, stunted growth is also observed due to competition for space and excessive consumption of media components (Pleguezuelos-Manzano Cayetano *et al.*, 2020). The paracrine signalling is another important factor to consider as the cells within the organoid will produce growth factors that will exert effects on the cell types within the organoid that will maintain the stem cell niche (Biswas *et al.*, 2015). Growth factors that are supplemented in the organoid media also act via the paracrine signalling mechanism to modulate the microenvironment (Wordinger and Clark, 2008), which will assist in maintaining signalling gradients that promote the proliferation of the intestinal cell types (Biswas *et al.*, 2015). Therefore, it is vital to determine the correct seeding density as it enables paracrine signalling to support organoid growth, ensures sufficient space for the organoids to grow, limits the excessive consumption of media components and ensures that there is adequate diffusion of growth factors to the core of the BME domes (Pleguezuelos-Manzano Cayetano *et al.*, 2020).

Organoids variability in terms of organoid formation efficiency, end-point morphology and function is largely attributed to the nature of *in vitro* self-organisation and cell fate (Hofer and Lutolf, 2021). The initial culture conditions that the organoids are subjected to can also contribute to organoid variability, especially the starting cell population, their positioning and aggregation ability (Hofer and Lutolf, 2021). The cell type heterogeneity affects the generation of viable organoids as not all the cells harvested from the tissue will aggregate and bud to form organoids (Shankaran *et al.*, 2021). Therefore, by being able to selectively culture the aggregate of cells that could potentially generate organoids would increase the generation and yield of organoid cultures (Shankaran *et al.*, 2021). The size of initial cell aggregates are important in commencement of culture conditions as literature varies in the required number of crypts or cells to seed (Hofer and Lutolf, 2021).

When crypts are seeded at a density of 200-600 crypts per dome, the cell aggregates remain small and the generation of small organoids that do not increase in size is observed. This can contribute to dome collapse as the organoids are not assisting in the maintenance of Cultrex™ stiffness. The decreased stiffness of the Cultrex™ ultimately affects the biological activities of the cells within the organoid and affects organoid formation (Kozłowski *et al.*, 2021). When crypts were seeded at densities of 700-1000 crypts (Refer to Figure 8 and 10), the domes held for longer and cell aggregates were larger and gave rise to larger, mature organoids. The increase in initial cell aggregates contributes to increased stiffness of the Cultrex™ domes that may assist in increased organoid formation, stem cell proliferation and expansion (Kozłowski *et al.*, 2021). Although time from crypt to mature organoid varies from each patient line as well as passaging time, there was no variation in the general organoid growth pattern at the standardized crypt density of 1000 as seen in Figures 8 and 10. Time variations in sample growth can be attributed to the fact that there are differences between laboratory conditions that can result in different rates of proliferation and differentiation, leading to variability (Shariati *et al.*, 2021). Sources of variability between laboratories and from one experiment to the next, can be the conditions in which the organoids were cultured, i.e. batch-to-batch variability in growth factor purity; differences in oxygen exposure, the degree of differentiated cell types and that the cells present in the organoids are at different cellular states (Lehmann *et al.*, 2019; Gehling *et al.*, 2022).

## **6.2. Components in organoid media and their effects on organoid growth and morphology**

The growth medium required for tumour organoids varies as some organoids require medium specific to tumour growth and development, whereas some organoids require a basic medium with several growth factors (Shariati *et al.*, 2021). In all organoid culture systems, a distinct growth factor combination is required to obtain organoids and more differentiated cells in the organoids, which results in two different culture mediums (Schutgens and Clevers, 2020). These two culture mediums are expansion medium, used to generate and maintain organoid growth, and differentiation medium, which is used to differentiate the organoids into specific cell types for various experiments (Schutgens and Clevers, 2020). Literature indicates slight variations in concentrations of the various growth factors and reagents as shown in Table 13 as surveyed from 8 different protocols

**Table 14: Media composition comparisons across 8 different protocols**

Reagents	Protocol Number							
	1	2	3	4	5	6	7	8
Advanced DMEM/F12	25 mL	1 x	1 x	1 x	1 x	1 x	1 x	80% (v/v)
Primocin	100 µg/mL	-	1 x	-	100 µg/mL	-	-	1 x
ROCKi	10 µM	-		10 µM	10 µM	10 µM	-	-
Glutamax	-	-	-	1 x	-	2 mM	10 mmol/L	1 x
HEPES	-	-	10 mM, pH 7.0	1 x	-	10 mmol/L	10 mmol/L	10 mM
B-27 Supplement	1 x	-	1 x	1 x	1%	1 x	1 x	1 x
EGF	-	50 ng/mL	50 µg/mL	50 ng/mL	50 ng/mL	50 ng/mL	50 ng/mL	100 ng/mL
Recombinant human R-spondin 1	20% (v/v) R-spondin 1 conditioned medium	1 µg/mL	25 nM	500 ng/ml	10% conditioned medium	1 µg/mL	10% R-spondin 1 conditioned medium	40% (v/v) conditioned medium
Noggin	2% (v/v) Noggin conditioned medium	100 ng/mL	-	100 ng/mL	2% conditioned medium	100 ng/mL	100 ng/mL	40% (v/v) conditioned medium
Gastrin	-	1 nM	10 mM	50 nM	-	10 nM	10 nM	10 nM
Prostaglandin E2	1 µM	-	10 mM	-	10 nM	-	-	100 nM
A83-01	-	500 mM	500 nM	-	500 nM	500 nM	500 nM	500 nM
Niacinamide	10 mM	10 mM	10 mM	10 µM	10 mM	10 mM	10 mM	10 mM
n-Acetylcysteine	1.25 mM	-	1 mM	10 µM	1,25 mM	1 mM	1 mM	500 µM

SB202190	10 $\mu$ M	10 $\mu$ M	10 $\mu$ M	10 $\mu$ M	3 $\mu$ M	10 $\mu$ M	10 $\mu$ M	10 $\mu$ M
Recombinant human Wnt 3a	50% (v/v) Wnt 3A conditioned medium	100 ng/mL	-	100 ng/mL	1 $\mu$ g/mL	100 ng/mL	50% Wnt3A conditioned medium	20% (v/v) conditioned medium
N2-supplement	-	-	1 x	1 x	-	1 x	1 x	1 x
Reference	(Pleguezuelos-Manzano Cayetano <i>et al.</i> , 2020)	(Zhang <i>et al.</i> , 2020)	(Urbischek <i>et al.</i> , 2019)	(Wilson <i>et al.</i> , 2021)	(He <i>et al.</i> , 2022)	(Sato <i>et al.</i> , 2011)	(Yokota <i>et al.</i> , 2021)	(Gwilt and Thiagarajah, 2023)

*\*Note: Concentrations highlighted in green are the concentrations that were used to formulate the organoid media in this project.*

Table 14 supports the need for a standardized media protocol to ensure efficient organoid generation. However, due to organoids being comprised of various tumour cell populations, it is vital to understand the stem cell niche and specific factors required to allow stem cells to proliferate and self-renew (Zhou *et al.*, 2023). In addition to the effects of the growth factors and how they have been produced on the growth of organoids, the interaction between the cells and the environment may also affect organoid growth.

The level of CRC tumour heterogeneity has been shown to be attributed to the interactions of the genetic background of tumour cells with their environment and the differences in genetic and epigenetic properties of each cell and their correlated tumours heterogeneity (Kashfi *et al.*, 2018). Kashfi and colleagues (2018), evaluated non-cancerous and cancer organoid growth and morphological changes in patients with CRC. They identified that non-cancerous patient-derived organoids maintained the budding and cystic structures that are commonly seen in many CRC organoid studies (Kashfi *et al.*, 2018). This coincides with the non-cancerous organoids that were generated, and images captured in Figures 7, 8 and 10 indicating that the non-cancerous organoids maintain these proliferating structures when cultured in controlled conditions. The authors further illustrated that tumour derived organoids did not display whole-crypt like structures on day zero of culture and only some aggregated structures of small cell populations were formed (Kashfi *et al.*, 2018). The tumour organoid cultures were monitored over a period of four to fourteen days and the authors noted that very few cystic-like structures with uneven borders appeared (Kashfi *et al.*, 2018). Moreover, these cystic-like structures failed to form budding or branching structures over the fourteen-day period (Kashfi *et al.*, 2018). These observations were also observed in this study where the cancer organoids failed to develop into cystic-structures (refer to Figure 13). The cancer biopsies that were obtained were minuscule and tissue quality was lower than that of the non-cancerous tissue biopsies. The cancerous tissue exhibited higher levels of blood presence, tougher in texture and had irregular tissue borders. When digesting the cancer biopsies, more single cells were also present with fewer crypts in comparison to the non-cancerous biopsies. The cancer organoids that were generated also maintained aggregated structures throughout the culture period but increased in size. The failure of cancer organoids to form cystic, budding structures may be due to the deregulation of essential molecular and cellular signalling pathways that are required for proper maintenance and function of the cancer organoids (Kashfi *et al.*, 2018). The published images by Kashfi and colleagues (2018) illustrated similar trends in cancer organoid structures and

growth as seen in Figure 13, where large aggregates of cells are visualised rather than organoids as culture progresses. Kashfi and colleagues (2018), also cultured the tumour organoids in the absence of Wnt3a conditions. In the absence of Wnt3a, the organoids were capable of growing and the number of buds from the original cystic shape had increased and the differentiation potential had improved in comparison to those grown with Wnt3a (Kashfi *et al.*, 2018). This suggests that cancer organoid formation can occur in a Wnt niche-independent signalling way (Kashfi *et al.*, 2018) and should be further examined. Additionally, tumour-derived organoids do not follow a similar growth pattern to non-cancerous organoids, which is likely a result of differences in age, medical history and genetic background amongst patients (Kashfi *et al.*, 2018).

### **6.3. Inherent Sample variation and its Effects on Organoid Growth**

Utilizing organoids generated from tumour biopsies preserve cancer gene mutations in culture, making them an attractive model (Kretzschmar, 2021). However, limited studies have assessed the variation between tissue-derived organoids from various individuals and cellular heterogeneity between individuals (Jensen and Little, 2023). Therefore, it is important to identify this across multiple labs, cell culture conditions and tissue donors to provide insight into cellular heterogeneity between individuals. It is also important to note that heterogeneity is a feature of adult stem cell derived organoids as it is inherent, therefore it is important to thoroughly characterize organoid cultures with diverse assays (Mohammadi *et al.*, 2021).

Variability in the organoid culture system can be due to differences amongst individuals such as age and genetic background, therefore it is important to identify if patient or population diversity exists when organoids are cultured from human-derived tissues (Kim *et al.*, 2020; Jensen and Little, 2023). The probability of genetic diversity in human samples is high and therefore it is expected to have batch-to-batch variation between organoids generated from different patients (Jensen and Little, 2023). Moreover, variability can be due to tumour heterogeneity which can be divided into inter- and intra-tumour heterogeneity (Zhou *et al.*, 2023). Inter-tumour heterogeneity includes the spatiotemporal and extracellular diversity from different patients each having alterations caused by different etiological and environmental factors. Intra-tumour heterogeneity describes the variability of different tumour, stromal and immune cell populations within the same tumour specimen (Zhou *et al.*, 2023). This inter- and intra-tumour heterogeneity can be used to probe for variations in phenotype, genotype and gene expression across different organoids

generated from a single patient and across different patients (Padmanaban *et al.*, 2020). Due to heterogeneity between individuals and individual organoids, organoid morphology can be visualised as thin-walled cystic structures or compact organoids devoid of a lumen (Van De Wetering *et al.*, 2015). Both types of morphology were visualised in these cultures derived from South African patients, specifically the derived non-cancerous organoids maintaining a thin-walled cystic structure (Figure 8 and 10) and the cancer organoids maintaining a compact structure devoid of a lumen (Figure 13). However, these observations were only seen in four non-cancerous patient samples and three cancer patient samples and cannot be extrapolated to all patients. It is expected that different patients will present with different morphologies that are dictated by various factors such as tumour site, metastasis, genetics and tumour heterogeneity.

#### **6.4. Organoids Recapitulate Cell Types Present in the Original Tissue and Spatial Localization**

Direct comparisons between control organoid lines and patient tissue will show differences and it is vital to establish whether the disparities are biologically relevant or a technical difference (Jensen and Little, 2023). The basal gene expression levels of the marker genes are referred to as the expression levels found in the original tissue of the patient that is used to evaluate the expression levels of the marker in the matched patient-derived organoids (refer to Figure 14). Although the trends in expression are similar when comparing the organoids to the tissue, there is slight variations. These slight variations are the increased expression of *CHGA*, *EPCAM* and *MKI-67*. Increased expression of *EPCAM* and *MKI-67* is expected as the cells are epithelial cell types and actively proliferating. Furthermore, using chemically-defined medium (use of recombinant growth factors) increases cell proliferation and may account for the increased expression of the other marker genes as these cells assist in the development of functional intestinal organoids (Wang *et al.*, 2022). Additionally, in studies performed by Wang *et al.*, 2022 and Yokota *et al.*, 2021, that examined expression of *MKI-67*, *MUC2*, *LGR5*, *LYZ*, *VIL1*, *EPCAM* and *CHGA*, it was noted that across different organoid lines, expression levels of these genes will vary from patient-to-patient samples (Yokota *et al.*, 2021; Wang *et al.*, 2022). The normalized expression levels of these genes in the non-cancerous organoids are not significantly different in comparison to the tissue from which they were derived and variations amongst patient samples are to be expected. Interestingly, *VIL1* expression was decreased by 0.25-0.46 amongst all three samples and may be a result of the intestinal stem cells have already undergone differentiation into the

different cell types and increased expression of *VILI* is not required (Maunoury *et al.*, 1992). However, expression trends remain similar and the organoids do express the intestinal markers of interest. In a study by Criss and colleagues (2021), using RNA sequencing data, it was shown that variations in human intestinal organoids can be attributed to the experiment/project that was to be completed. This observation indicates transcriptional variation that may be a result of batch-to-batch variations in conditioned-media, differences in incubator conditions, passaging rates, media changing intervals or potentially sequencing platforms (Criss *et al.*, 2021). However, their study highlighted that there is much greater transcriptomic variability between different individuals rather than that of experimental conditions (Criss *et al.*, 2021). It was also highlighted that variation between patients is due to variations in their basal gene expression as well as differences in their responses to stimuli (Criss *et al.*, 2021). It was further recommended that multiple patient lines are used in organoid experiments to obtain a more holistic view and to compare organoid lines to patient-matched tissue (Criss *et al.*, 2021; Jensen and Little, 2023).

An additional technique that can be used to evaluate organoid composition is immunofluorescence that uses specific cell marker antibodies to provide further information on the presence of various cell types, the spatial distribution of these cell types and their proportions (Zhao *et al.*, 2022). Figure 15A illustrates the immunofluorescence images of the non-cancerous organoids, specifically for EpCAM, MUC2, Ki-67 and VIL1. EpCAM is expected to be expressed by a large number of cells as the majority of the intestinal epithelial tissue is comprised of epithelial cells (De Santa Barbara *et al.*, 2003). This is evident as the green hue seen around the organoids (Figure 15A, panel 1). Another marker that should produce bright fluorescence is Ki-67 as the intestinal tract contains a vast amount of stem cells that are actively proliferating (Bahrami *et al.*, 2017; Boonekamp *et al.*, 2020). This is evident in Figure 15A panel 3, where Ki-67 is illustrated as a bright red hue in the organoids and also indicates that the epithelial cells within the organoids were actively proliferating. MUC2 (Figure 15A, panel 2) was another marker that was used to identify the presence of goblet cells in the organoids. The presence of goblet cells was indicated by the green hue, and the lower fluorescence could be attributed to the fact that MUC2 is required in the lumen of the digestive tract and that these organoids have not become differentiated requiring a lesser expression of MUC2. Tuft cells were also identified in the organoids in Figure 15A (panel 4) with the green hue for VIL1 not being as intense. This is attributed to the fact that tuft cells are a rare cell type involved in chemoreception which could also result in the fluorescence being

mostly around cell borders (Esmaelniakooshkghazi *et al.*, 2020). However, the purpose of characterization indicates that these cell populations were present in the non-cancerous organoids.

As a proof-of-concept and to verify whether the cancer organoids contained different cell populations, immunofluorescence was also performed on these organoids. Figure 15B illustrates the immunofluorescence images of the cancer organoids, specifically for EpCAM, MUC2, Ki-67 and VIL1. EpCAM (Figure 15, panel 1) was not as highly fluorescent when compared to the non-cancerous organoids which could be attributed to negative association of EpCAM expression with tumour grade, invasion and lymph node metastasis (Lugli *et al.*, 2010). This correlates with the patient data that all three patients did present with lymph node metastasis (Table 9). The fluorescence of Ki-67 (Figure 15B, panel 3) was brighter in the cancer organoids indicating a higher proportion of proliferating cells. The increased fluorescence of Ki-67 has been shown to be closely associated with poor patient prognosis in CRC and is increased in cancerous tissues as compared to normal tissues (Tong *et al.*, 2020; Liu *et al.*, 2023). This increased expression of Ki-67 is attributed to the organoids being derived from cancerous tissue but further validation using RT-qPCR is required. MUC2 (Figure 15B, panel 2) was also identified in the cancer organoids but the fluorescence intensity was lower than that of the non-cancerous organoids which could be attributed to the fact that the expression of MUC2 is decreased in cancer tissues as compared to normal tissue (Gan *et al.*, 2021). Furthermore, the expression of MUC2 is correlated with lymph node metastasis as shown by Gan and colleagues (2021), that investigated the expression of MUC2 in normal and CRC tissue as it may play a protective role by participating in the intestinal mucosal barrier (Gan *et al.*, 2021). It was also highlighted in the aforementioned study that in CRC the mucosal barrier becomes impaired that the expression of MUC2 decreases possibly due to suppressed immune system function (Gan *et al.*, 2021). Tuft cells were also present in the cancer organoids with the green hue representing VIL1 (Figure 15B, panel 4) being slightly more intense than the non-cancerous organoids. This is attributed to the fact that tuft cells can be converted to cancer-initiating cells when the surrounding cellular niche is altered (Westphalen *et al.*, 2014). Furthermore, the DAPI staining varies amongst the images in Figure 15 and could be attributed to the 3D nature of the organoids that prevents DAPI from efficiently accessing every single nuclei as well as the fact that literature has indicated that it preferentially binds to the adenine-thymine rich chromosomal regions and may provide inaccurate estimates of the genome content (Munyenyembe *et al.*, 2021). However, the purpose of characterization indicates that these

cell populations were present in the cancer organoids but requires further validation through RT-qPCR. To ensure the reproducibility of organoid experiments, standardised protocols of organoid culturing techniques are required to limit the intrinsic donor-to-donor variation, as well as batch-to-batch variation in culture reagents (Dotti *et al.*, 2022). Furthermore, additional experiments should be performed as an added security in organoid characterization to overcome the uncertainty in organoid culturing.

### **6.5. Successes of this study**

The study is novel as it reports the first establishment of non-cancerous organoid generation from South African CRC patients that follow similar trends in growth and morphology to those observed in global publications. Additionally, it includes the defined methodologies that have proven successful in generating non-cancerous organoids from fresh and frozen tissue and serves as a proof-of-concept of methodology for the establishment of cancer organoids by assessing cancer organoid morphology, and characterization through protein markers specific to the colon. This study provides a foundation for future intestinal organoid culture for South African patients that can be utilized for various applications such as drug screening, delineating population variance in CRC development and progression that can be compared to global data.

### **6.6. Limitations of organoids and this study**

A major limitation in organoid culture in general is the reproducibility of the research due to the variations mentioned above, as well as sample availability. Therefore, standardized protocols will assist in reducing discrepancies and reduce patient sample loss or wastage (Kim *et al.*, 2020; El Harane *et al.*, 2023). Significant efforts have been made to define organoid culturing protocols, as well as media and growth factor combinations required for different types of organoids, however, these combinations have not been standardized (Bose *et al.*, 2021). This can be attributed to different individual studies optimizing growth factor concentrations based on cost and availability (Bose *et al.*, 2021). This makes comparisons of organoid growth across different studies difficult due to variations in microenvironmental factors (Bose *et al.*, 2021). Although, complete organoid media can be commercially purchased, the media compositions should be standardized to ensure adequate reproducibility (Bose *et al.*, 2021). Moreover, the distribution of tissue sources that are renewable and are comparable between laboratories affect the long-term advancement of organoids (Lehmann *et al.*, 2019). The development of tissue and organoid biobanks can assist in

this regard and can be generated from various individuals from various populations which can be used to understand and delineate the development of diseases in affected and non-affected individuals (Lehmann *et al.*, 2019). Researchers should also be willing to share different organoid lines to compare results to gauge an understanding of the potential effects of genetic background on organoid cultures and experimental responses (Lehmann *et al.*, 2019). Currently, the cost of organoid culturing is largely determined by the time and labour consuming process of establishing cultures and passaging them as well as the materials used to develop and maintain culture, i.e. BME matrices and the expensive combination of growth factors required for media (Bose *et al.*, 2021).

The success rate of generating organoids and the rate of establishment varies greatly amongst tumour types, for example, the success rate of generating organoids spans from 70 – 90% for CRC tumours (Booij *et al.*, 2022). Standardized protocols need to be developed for the derivation and culture conditions of organoids and provide sufficient details to ensure reproducibility and high establishment rates (Lehmann *et al.*, 2019). In order to generate an established, novel organoid protocol, rigorous characterization should be performed (Jensen and Little, 2023). Examples of rigorous characterization includes characterising the cell types present, histological structure comparisons between organoids and tissue as well as omics profiling (Jensen and Little, 2023). In this study, we have successfully standardized crypt seeding density, in-house prepared organoid media, non-cancerous organoid growth as well as RT-qPCR for non-cancerous organoids and immunofluorescence for cancerous and non-cancerous organoids which have never been completed in our laboratory before. As these protocols have now been standardized, they can be used for further experiments, such as optimizing RT-qPCR for cancerous organoids, co-culturing and drug screening. However, in terms of limitations of this study, H&E staining was not performed on the organoids and the tissue from which they were derived which is an additional characterization method that should be performed in future studies. Additionally, RT-qPCR was not performed on cancer organoids due to insufficient RNA yields, time and tissue constraints. Additionally, this study did not perform experiments on the matched tissue which could have been used to compare the gene expression and spatial localization of the cell types and should be performed in future. Omics profiling was also not performed in this study, which is another limitation and could be applied in future experiments to further study the genomics and metabolomics of the organoids. The availability of fresh tissue to generate intestinal organoids is

also a limitation as fresh tissue provides better organoid yields. Therefore, the use of frozen tissue was also attempted to mitigate the limitations of fresh tissue.

Numerous publications recommend the use of frozen tissue biopsies due to the fact that fresh tissue biopsies may not be easily obtained or readily available. Organoids can be established from frozen biopsies that have been stored in liquid nitrogen for several months (Saito *et al.*, 2020). The generation of organoids from fresh tissues can be difficult to obtain due to limited access of fresh sample and the viability of human samples has a short window, which limits the time for which patient samples can be used for organoid and research purposes (Tsai *et al.*, 2018). Therefore, frozen tissue biopsies are an advantageous alternative to fresh tissues. In a study performed by Walsh and colleagues (2016), it was established that organoids can be successfully grown from frozen tissue biopsies and that the resultant organoids are identical to the organoids grown from fresh tissue biopsies (Walsh *et al.*, 2016). Hence, the use of frozen tissue biopsies to generate cancer organoids is beneficial especially when fresh tissue biopsies are not always available. In this study, the generation of cancer organoids from frozen tissue biopsies was not successful in obtaining cancer organoids that demonstrated a cyst-like morphology and the growth of the cancer organoids became stunted after 16 days in culture (refer to Figure 13). The ability for the cell types to aggregate and form differentiated cancer organoids could be due to the fact that the tissue was digested in organoid culture medium that would assist in maintaining the different cell types as compared to the tissue dissociation buffer which does not contain the growth factors required to maintain the different cell types.

## **6.7. Future research and recommendations**

During the early stages of organoid culture, it is recommended to use haematoxylin and eosin (H&E) staining and immunohistochemistry to determine similarities between the cultured organoids and the tissue from which the organoids were derived (Fang *et al.*, 2023). Additionally, gene expression validation and high-throughput whole-genome transcriptome analysis is traditionally performed (Zhao *et al.*, 2022). RT-qPCR is one of the most commonly used techniques as it is easy, fast and provides a quantitative readout on marker genes that provides an indication of cell identity (Zhao *et al.*, 2022). Furthermore, comparisons to the tissue of origin is also important to validate that the organoids derived from the tissue maintain histology and immunochemistry profiles as well as transcriptomic and genomic profiles (Zhao *et al.*, 2022).

Therefore, future studies should include at least two wells of cancer organoids to potentially yield sufficient RNA for RT-qPCR characterization. However, immunofluorescence images obtained from the organoids did indicate the presence of several cell types of interest, but further validation is required. Lastly, the inclusion of more samples for non-cancerous and cancer organoid generation should be done to ensure consistency amongst samples and the use of matched non-cancerous and cancer organoids should also be included.

Future recommendations for the establishment and characterization of intestinal organoids using this experimental design have been summarised in Table 15.

**Table 15: Variables to consider when generating organoids and the recommendations based on this experimental design.**

Variable	Recommendation	
BME Used	Cultrex™.	
Number of Crypts to seed	1000 crypts per 10 µL dome.	
TrypLE incubation period	5 minutes, ensured organoids digested into crypts and single cells that can be used to generate more organoids.	
Frozen or fresh tissue biopsies	Organoids were successfully generated from fresh and frozen non-cancerous biopsies in relatively similar time periods. However, the generation of cancer tissues still requires further evaluation as fresh and frozen samples yielded similar results in terms of organoid growth and development.	
Organoid morphological features	Cystic morphology should be observed at approximately day 3 – 4 in culture with budding occurring. Cancer organoids can present with this cystic morphology or compact organoids devoid of a lumen. This is dependent on sample variation.	
Media, purchase commercial media or make in-house	Generate media in-house as larger volumes of media can be made with a reduced cost. This also assists in scalability of organoid cultures. Additionally, the use of growth factors from conditioned medium is recommended specifically for Wnt3a, R-spondin1 and Noggin.	
Media components required	Non-cancerous organoid requirements (concentration)	Cancer organoid requirements (concentration)
	<ul style="list-style-type: none"> <li>• Advanced DMEM/F12 (1 x)</li> <li>• Glutamax (1 x)</li> </ul>	<ul style="list-style-type: none"> <li>• Advanced DMEM/F12 (1 x)</li> <li>• Glutamax (1 x)</li> </ul>

	<ul style="list-style-type: none"> <li>• HEPES (10 mM)</li> <li>• B27 (1 x)</li> <li>• EGF (50 ng/mL)</li> <li>• R-spondin1 (500 ng/mL)</li> <li>• Noggin (100 ng/mL)</li> <li>• Gastrin (10 nM)</li> <li>• Prostaglandin E2 (10 nM)</li> <li>• A83-01 (500 nM)</li> <li>• Niacinamide (10 mM)</li> <li>• n-Acetylcysteine (1,25 mM)</li> <li>• SB202190 (3 <math>\mu</math>M)</li> <li>• Wnt3a (200 ng/mL)</li> <li>• N-2 supplement (1 x)</li> </ul>	<ul style="list-style-type: none"> <li>• HEPES (10 mM)</li> <li>• B27 (1 x)</li> <li>• EGF (50 ng/mL)</li> <li>• Noggin (100 ng/mL)</li> <li>• Gastrin (10 nM)</li> <li>• Prostaglandin E2 (10 nM)</li> <li>• A83-01 (500 nM)</li> <li>• Niacinamide (10 mM)</li> <li>• n-Acetylcysteine (1,25 mM)</li> <li>• SB202190 (3 <math>\mu</math>M)</li> <li>• Wnt3a (200 ng/mL)</li> <li>• N-2 supplement (1 x)</li> </ul>
RNA Extraction protocol	Omega Bio-tek E.Z.N.A® Total RNA Kit I resulted in sufficient RNA integrity and yields from both the non-cancerous organoids and tissue.	
Marker genes for characterization	<i>EpCAM</i> , <i>VIL1</i> , <i>MKi-67</i> , <i>CHGA</i> , <i>MUC2</i> , <i>LGR5</i> and <i>LYZ</i> as these genes assess the major cell types present in the intestinal tract. <i>ACTB</i> is also a suitable reference gene in both tissue and non-cancerous organoid samples.	
Immunofluorescence markers for characterization	EpCAM, VIL1, MUC2 and Ki-67. Additional immunofluorescence markers that can be included are LGR5 and CHGA.	

Based on the recommendations from Table 15, intestinal organoids were successfully established from South African non-cancerous patient samples and cancer samples, where latter require more rigorous evaluation and culture attempts. Furthermore, basic characterization techniques are also demonstrated in Table 14 that can be used to characterize the organoids generated.

## **7. Conclusion**

In conclusion, this study is the first one reported within South Africa, contributing to the novelty of this study as well as to the use of 3D models to explore CRC disease development and progression in South African patients. Organoids are an attractive model for studying cancer in general and the applications of such a model is expanding. The use of organoids in studying disease progression, development and treatment is endless and this is evident in the growing amount of literature reporting novel outcomes. In terms of future applications for intestinal organoids, drug screening of chemotherapeutic treatments, currently used and novel, can be employed to elucidate patient treatment responses for a more personalised medicine approach. Additionally, these intestinal organoids can be used for co-culturing with patient-derived immune cells and microorganisms. This application can be used to study interactions of organoids with their TME to further elucidate the effects of TME on cancer development, progression and treatment response.

Despite the potential use of organoids, there are a number of considerations and limitations that need to be overcome for this to be a more robust model with a variety of clinical applications. One of the major limitations of this model is the cost and standardization of protocols used for organoid generation. Optimistically, as this model becomes more widely used and resource availability increases, the cost of this culture method would decrease and more laboratories from developing countries could contribute to the use of organoids to study disease biology. However, despite these limitations, organoid models still present with a unique opportunity to investigate complex cellular pathways in cancer with the potential to facilitate patient-centred translational benefits.

## 8. Annexure 1

### 8.1. Reconstitution Methodologies for Reagents

**Table S 1: Reagents and concentrations required to generate the media for sample collection**

Reagent	Concentration
DMEM (Thermo Fischer Scientific, USA)	1 x
Primocin (Davies Diagnostics, RSA)	2.5 mg/mL
Glutamax Supplement (Thermo Fischer Scientific, USA)	1 x
HEPES (Thermo Fischer Scientific, USA)	10 mM

#### **Reconstitution of ROCKi (Y-27632 dihydrochloride) to 10 mM stock solution**

- Dilute 1 mg of Y-27632 dihydrochloride in 312,25 µl distilled water
- Store as 13 µl aliquots at -20°C

#### **Generation of 25% BSA in PBS**

- Weigh 5 g of BSA and mix with 20 mL of PBS

#### **Tip pre-wetting solution, 10 mL**

- Add 400 µL of 25% BSA to 9.6 mL of DMEM/F12

#### **Dispase Reconstitution as 10 mg/mL aliquots**

- Weigh 100 mg of Dispase
- Combine 100 mg of Dispase with 10 mL of DPBS

**Table S 2: Reagents and concentrations required to generate tissue dissociation buffer (TDB)**

Reagents	Concentration
<b>DMEM with 1 mM Glutamax, 15 mM HEPES and 2.5% FBS</b>	
DMEM	1 x
Glutamax supplement	1mM
HEPES	15mM
FBS	2.5%
<b>Dispase</b>	
	10 mg/mL

<b>Collagenase II</b>	
Weigh 15mg and add directly to TDB	-
<b>Primocin™</b>	2.5 mg/mL
<b>ROCK Inhibitor</b>	10 $\mu$ M

\*Note: before adding Primocin™ and ROCK inhibitor, sterile filter the tissue dissociation buffer and then add

**Table S 3: Reagents and concentration required to generate collagenase IV digestion buffer.**

<b>Reagent</b>	<b>Concentration</b>
Organoid media	1 x
Collagenase	100 mg/mL

**Table S 4: Reagents and concentrations required to generate Complete Intesticult™ Organoid medium (non-cancerous organoid media).**

<b>Reagent</b>	<b>Concentration</b>
<b>Complete Intesticult™ Organoid Growth Medium</b>	
Intesticult™ Organoid Growth Medium Basal media	1 x
Intesticult™ Organoid Growth Medium Organoid Supplement	1 x
<b>Primocin™</b>	
Primocin™	2.5 mg/mL
<b>ROCK Inhibitor</b>	
ROCK Inhibitor	10 $\mu$ M

**Table S 5: Reagents and concentrations required to make Basal Intesticult™ Organoid Growth Medium (cancer organoid media).**

<b>Reagent</b>	<b>Concentration</b>
<b>Intesticult™ Organoid Growth Medium Basal</b>	
Intesticult™ Organoid Growth Medium Basal media	1 x
<b>Primocin™</b>	
Primocin™	2.5 mg/mL
<b>ROCK Inhibitor</b>	
ROCK Inhibitor	10 $\mu$ M

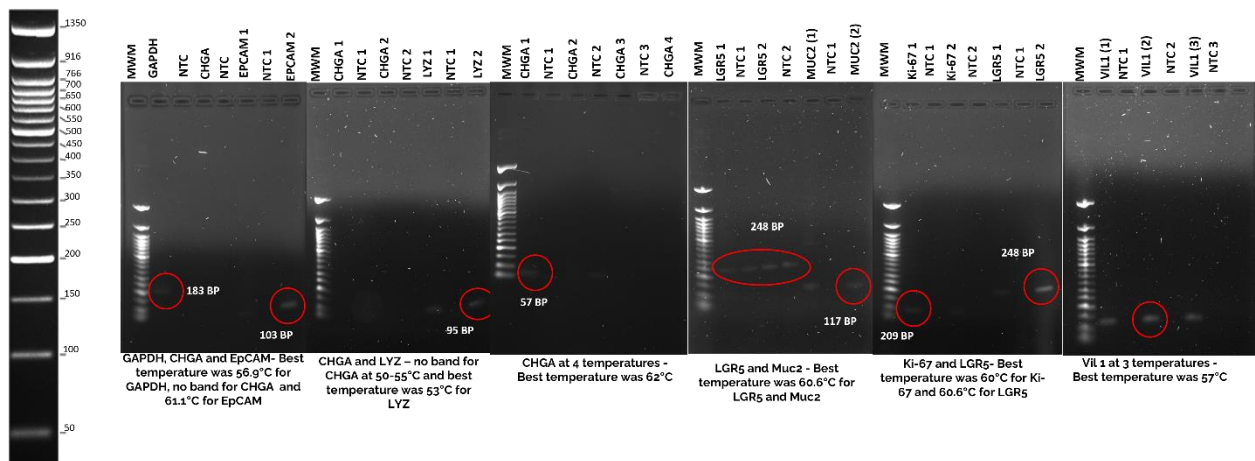
**Table S 6: Reagents and volumes used to make washing solution for organoid immunofluorescence.**

Reagent	Volume (mL)
DPBS (Thermo Fischer Scientific, USA)	14.849
Tween-20 (Sigma, UK)	0.001 (0.1%)
BSA (VWR, USA)	0.15 (1%)
<b>Final Volume</b>	<b>15</b>

### Preparation of TBE buffer for agarose gel electrophoresis

- Weigh 108 g of Tris(hydroxymethyl)aminomethane (SRL Chem, India, pH 10.5 – 11, Molecular weight 121.14)
- Weigh 55 g of Boric acid (Calbiochem, USA, pH 3.6 - 4, Molecular weight 61.83)
- Weigh 7.5 g of EDTA (Ethylenediaminetetraacetic acid tetrasodium salt dihydrate) (Sigma Aldrich, UK, Molecular weight 416.20)
- Dissolve above components in 900 mL of distilled water
- pH to 8.0
- Make to 1 L

## 8.2. Agarose Gel Electrophoresis RT-qPCR Optimization



**Supplementary Figure 1: Representative gel images for PCR optimization.** These sets of gel images are the PCR results we have obtained thus far for the genes that was used to characterize the organoids. The approximate PCR product lengths that would be obtained was generated using *in silico* PCR. The first gel image depicts GAPDH was loaded into the first well and produced a faint band at the expected product size of 183 base pairs. The middle wells contained CHGA and no band was produced and the last well contained EpCAM, which

*produced a faint band when run at 61.1°C. The faint band for EpCAM was correlated to the expected product size of 103 base pairs. The second gel depicts the results for CHGA and LYZ. No band was evident for CHGA in the range of 50-55°C, however, a brighter band was produced for LYZ at 53°C. at the expected PCR product size which was 95 base pairs. The third gel depicts the results of CHGA that was run at 4 different temperatures, a range from 56-62°C and it is evident that a faint band was produced at 62°C. The size of the PCR product also correlates to the expected product size of 57bp. The fourth gel depicts the results for LGR5 and MUC2. The LGR5 sample contained bands present in both the sample and no template control indicating contamination, despite the size being correlated to the expected product length. MUC2 correlated to the expected PCR product size being 117 base pairs as well as produced a brighter band at 60.6°C so this was selected as the temperature moving forward. The fifth gel depicts the results of Ki-67 and LGR5. The Ki-67 sample approximately correlated to the expected size, which is 209 base pairs and produced a band only at 60°C. A fresh LGR5 sample was made and the size correlated to that of the expected PCR product length, which was 248 base pairs as well as produced a bright band at 60.6°C without contamination of the NTC. The sixth gel depicts the PCR products for VIL1. VIL1, being lowly expressed, was run at a temperature range of 55-60°C and it was noted that the brightest band was present at 57°C so this was selected as the optimal temperature for this gene and the obtained size correlated to the expected PCR product size that was 122 base pairs.*

## 9. References

- Aisenbrey, E. A. and Murphy, W. L. (2020). ‘Synthetic alternatives to Matrigel’, *Nature Reviews Materials*. doi: 10.1038/s41578-020-0199-8.
- Ali, A., Tan, H. Y. and Kaiko, G. E. (2020). ‘Role of the Intestinal Epithelium and Its Interaction With the Microbiota in Food Allergy’, *Frontiers in Immunology*, pp. 1–12. doi: 10.3389/fimmu.2020.604054.
- Almeqdadi, M., Mana, M. D., Roper, J. and Yilmaz, Ö. H. (2019). ‘Gut organoids: Mini-tissues in culture to study intestinal physiology and disease’, *American Journal of Physiology - Cell Physiology*, 317(3), pp. C405–C419. doi: 10.1152/ajpcell.00300.2017.
- Arya, M., Shergill, I. S., Williamson, M., Gommersall, L., Arya, N. and Patel, H. R. H. (2005). ‘Basic principles of real-time quantitative PCR’, *Expert Review of Molecular Diagnostics*, 5(2), pp. 209–219. doi: 10.1586/14737159.5.2.209.
- Bahrami, A., Amerizadeh, F., ShahidSales, S., Khazaei, M., Ghayour-Mobarhan, M., Sadeghnia, H. R., Maftouh, M., Hassanian, S. M. and Avan, A. (2017). ‘Therapeutic Potential of Targeting Wnt/ $\beta$ -Catenin Pathway in Treatment of Colorectal Cancer: Rational and Progress’, *Journal of Cellular Biochemistry*, 118(8), pp. 1979–1983. doi: 10.1002/jcb.25903.
- Baker, B. M. and Chen, C. S. (2012). ‘Deconstructing the third dimension – how 3D culture microenvironments alter cellular cues’, *Journal of Cell Science*. Company of Biologists, 125(13), p. 3015. doi: 10.1242/JCS.079509.
- Barbosa, M. A. G., Xavier, C. P. R., Pereira, R. F., Petrikaitė, V. and Vasconcelos, M. H. (2022). ‘3D Cell Culture Models as Recapitulators of the Tumor Microenvironment for the Screening of Anti-Cancer Drugs’, *Cancers*, 14(1), pp. 1–30. doi: 10.3390/cancers14010190.
- Barker, N., Van Es, J. H., Kuipers, J., Kujala, P., Van Den Born, M., Cozijnsen, M., Haegebarth, A., Korving, J., Begthel, H., Peters, P. J. and Clevers, H. (2007). ‘Identification of stem cells in small intestine and colon by marker gene *Lgr5*’, *Nature*, 449(7165), pp. 1003–1007. doi: 10.1038/nature06196.
- Bel, S., Pendse, M., Wang, Y., Li, Y., Ruhn, H. A., Hassel, B., Leal, T., Winter, S. E., Xavier, R. R. and Hooper, L. V. (2017). ‘Bacterial infection of the renal allograft’, *Bacterial Infections and the Kidney*, 357(6355), pp. 195–209. doi: 10.1007/978-3-319-52792-5\_8.
- Bergdorf, K. N., Phifer, C. J., Bechard, M. E., Lee, M. A., McDonald, O. G., Lee, E. and Weiss, V. L. (2021). ‘Immunofluorescent staining of cancer spheroids and fine-needle aspiration-derived organoids’, *STAR Protocols*. Elsevier Inc., 2(2), p. 100578. doi: 10.1016/j.xpro.2021.100578.
- Białkowska, K., Komorowski, P., Bryszewska, M. and Miłowska, K. (2020). ‘Spheroids as a type of three-dimensional cell cultures—examples of methods of preparation and the most important application’, *International Journal of Molecular Sciences*, 21(17), pp. 1–17. doi: 10.3390/ijms21176225.
- Biju, T. S., Priya, V. V. and Francis, A. P. (2023). ‘Role of three-dimensional cell culture in therapeutics and diagnostics: an updated review’, *Drug Delivery and Translational Research*. Springer US, 13(9), pp. 2239–2253. doi: 10.1007/s13346-023-01327-6.
- Biswas, S., Davis, H., Irshad, S., Sandberg, T., Worthley, D. and Leedham, S. (2015). ‘Microenvironmental control of stem cell fate in intestinal homeostasis and disease’, *Journal of Pathology*, 237(2), pp. 135–145. doi: 10.1002/path.4563.
- Bonis, V., Rossell, C. and Gehart, H. (2021). ‘The Intestinal Epithelium – Fluid Fate and Rigid Structure From Crypt Bottom to Villus Tip’, *Frontiers in Cell and Developmental Biology*, 9(May), pp. 1–20. doi: 10.3389/fcell.2021.661931.
- Booij, T. H., Cattaneo, C. M. and Hirt, C. K. (2022). ‘Tumor Organoids as a Research Tool: How to

Exploit Them', *Cells*, 11(21), pp. 1–18. doi: 10.3390/cells11213440.

Booij, T. H., Price, L. S. and Danen, E. H. J. (2019). '3D Cell-Based Assays for Drug Screens: Challenges in Imaging, Image Analysis, and High-Content Analysis', *SLAS Discovery*, 24(6), pp. 615–627. doi: 10.1177/2472555219830087.

Boonekamp, K. E., Dayton, T. L. and Clevers, H. (2020). 'Intestinal organoids as tools for enriching and studying specific and rare cell types: advances and future directions', *Journal of Molecular Cell Biology*, 12(8), pp. 562–568. doi: 10.1093/jmcb/mjaa034.

Bose, S., Clevers, H. and Shen, X. (2021). 'Promises and challenges of organoid-guided precision medicine', *Med*, 2(9), pp. 1011–1026. doi: 10.1016/j.medj.2021.08.005.

Brand, M., Gaylard, P. and Ramos, J. (2018). 'Colorectal cancer in South Africa: An assessment of disease presentation, treatment pathways and 5-year survival', *South African Medical Journal*, 108(2), pp. 118–122. doi: 10.7196/SAMJ.2018.v108i2.12338.

Broguiere, N., Isenmann, L., Hirt, C., Ringel, T., Placzek, S., Cavalli, E., Ringnalda, F., Villiger, L., Züllig, R., Lehmann, R., Rogler, G., Heim, M. H., Schüller, J., Zenobi-Wong, M. and Schwank, G. (2018). 'Growth of Epithelial Organoids in a Defined Hydrogel', *Advanced Materials*, 30(43). doi: 10.1002/adma.201801621.

Calà, G., Sina, B., De Coppi, P., Giobbe, G. G. and Gerli, M. F. M. (2023). 'Primary human organoids models: Current progress and key milestones', *Frontiers in Bioengineering and Biotechnology*, 11(March), pp. 1–17. doi: 10.3389/fbioe.2023.1058970.

CANSA (2023). *Prevalence Cancer - CANSA - The Cancer Association of South Africa | CANSA – The Cancer Association of South Africa, CANSA Statistics webpage*. Available at: <https://cansa.org.za/south-african-cancer-statistics/> (Accessed: 20 February 2022).

Caputo, F., Santini, C., Bardasi, C., Cerma, K., Casadei-Gardini, A., Spallanzani, A., Andrikou, K., Cascinu, S. and Gelsomino, F. (2019). 'BRAF-mutated colorectal cancer: Clinical and molecular insights', *International Journal of Molecular Sciences*, 20(21). doi: 10.3390/ijms20215369.

Chen, H., Wu, Z., Gong, Z., Xia, Y., Li, J., Du, L., Zhang, Y., Gao, X., Fan, Z., Hu, H., Qian, Q., Ding, Z. and Guo, S. (2022). 'Acoustic Bioprinting of Patient-Derived Organoids for Predicting Cancer Therapy Responses', *Advanced Healthcare Materials*. John Wiley & Sons, Ltd, 11(13), p. 2102784. doi: 10.1002/ADHM.202102784.

Chen, S. F., Chang, Y. C., Nieh, S., Liu, C. L., Yang, C. Y. and Lin, Y. S. (2012). 'Nonadhesive culture system as a model of rapid sphere formation with cancer stem cell properties', *PLoS ONE*, 7(2). doi: 10.1371/journal.pone.0031864.

Chomczynski, P. and Sacchi, N. (2006). 'The single-step method of RNA isolation by acid guanidinium thiocyanate-phenol-chloroform extraction: Twenty-something years on', *Nature Protocols*, 1(2), pp. 581–585. doi: 10.1038/nprot.2006.83.

Clevers, H. (2016). 'Modeling Development and Disease with Organoids', *Cell*. Elsevier Inc., 165(7), pp. 1586–1597. doi: 10.1016/j.cell.2016.05.082.

Conder, R., Chew, L. H., Elstone, F., Lankhorst, M., Añonuevo, A., Simmini, S., Chang, W., Eaves, A. C., Thomas, T. E. and Louis, S. A. (2020). 'Organoid culture systems: Products supporting one of the biggest revolutions in biological research', *Biomedical Science and Engineering*, 3(102), pp. 40–41. doi: 10.4081/bse.2019.

Costa, E. C., Moreira, A. F., de Melo-Diogo, D., Gaspar, V. M., Carvalho, M. P. and Correia, I. J. (2016). '3D tumor spheroids: an overview on the tools and techniques used for their analysis', *Biotechnology Advances*. Elsevier, 34(8), pp. 1427–1441. doi: 10.1016/J.BIOTECHADV.2016.11.002.

Criss, Z. K. *et al.* (2021). 'Deconstructing Organs: Single-Cell Analyses, Decellularized Organs,

Organoids, and Organ-on-a-Chip Models Drivers of transcriptional variance in human intestinal epithelial organoids', *Physiological Genomics*, 53(11), pp. 486–508. doi: 10.1152/physiolgenomics.00061.2021.

D'Costa, K., Kasic, M., Lam, A., Moradipour, A., Zhao, Y. and Radisic, M. (2020). 'Biomaterials and Culture Systems for Development of Organoid and Organ-on-a-Chip Models', *Annals of Biomedical Engineering*, 48(7), pp. 2002–2027. doi: 10.1007/s10439-020-02498-w.

Dallas, N. A., Xia, L., Fan, F., Gray, M. J., Gaur, P., Buren, G. Van, Samuel, S., Kim, M. P., Lim, S. J. and Ellis, L. M. (2009). 'Chemoresistant Colorectal Cancer Cells, the Cancer Stem Cell Phenotype and Increased Sensitivity to Insulin-like Growth Factor Receptor-1 Inhibition', *Cancer Research*, 69(5), pp. 1951–1957. doi: 10.1158/0008-5472.CAN-08-2023.Chemoresistant.

Dao, D.-P. D. and Le, P. H. (2021). 'Histology, Goblet Cells', *StatPearls*. StatPearls Publishing. Available at: <https://www.ncbi.nlm.nih.gov/books/NBK553208/> (Accessed: 28 February 2022).

Dijkstra, K. K. *et al.* (2018). 'Generation of Tumor-Reactive T Cells by Co-culture of Peripheral Blood Lymphocytes and Tumor Organoids', *Cell*. Elsevier Inc., 174(6), pp. 1586-1598.e12. doi: 10.1016/j.cell.2018.07.009.

Dotti, I., Mayorgas, A. and Salas, A. (2022). 'Generation of human colon organoids from healthy and inflammatory bowel disease mucosa', *PLoS ONE*, 17(10 October), pp. 1–16. doi: 10.1371/journal.pone.0276195.

Drost, Jarno, Richard H. Van Jaarsveld, Bas Ponsioen, Cheryl Zimmerlin, Ruben Van Boxtel, Arjan Buijs, Norman Sachs, *et al.* 2015. "Sequential Cancer Mutations in Cultured Human Intestinal Stem Cells." *Nature* 521 (7550): 43–47. <https://doi.org/10.1038/nature14415>.

Du, Y., Gao, H., He, C., Xin, S., Wang, B., Zhang, S., Gong, F., Yu, X., Pan, L., Sun, F., Wang, W. and Xu, J. (2023). 'An update on the biological characteristics and functions of tuft cells in the gut', *Frontiers in Cell and Developmental Biology*, pp. 1–17. doi: 10.3389/fcell.2022.1102978.

Engevik, M. A., Yacyshyn, M. B., Engevik, K. A., Wang, J., Darien, B., Hassett, D. J., Yacyshyn, B. R. and Worrell, R. T. (2014). 'Human *Clostridium difficile* infection: Altered mucus production and composition', *American Journal of Physiology - Gastrointestinal and Liver Physiology*, 308(6), pp. G510–G524. doi: 10.1152/ajpgi.00091.2014.

Esmailniakooshkghazi, A., George, S. P., Biswas, R. and Khurana, S. (2020). 'Mouse intestinal tuft cells express advillin but not villin', *Scientific Reports*. Springer US, 10(1), pp. 1–11. doi: 10.1038/s41598-020-65469-0.

Ettayebi, K., Salmen, W., Imai, K., Hagi, A., Neill, F. H., Atmar, R. L., Prasad, B. V. V. and Estes, M. K. (2022). 'Antiviral Activity of Olanexidine-Containing Hand Rub against Human Noroviruses', *mBio*. American Society for Microbiology, 13(2), pp. 1–13. doi: 10.1128/mbio.02848-21.

Fang, Z., Li, P., Du, F., Shang, L. and Li, L. (2023). 'The role of organoids in cancer research', *Experimental Hematology and Oncology*, 12(1), pp. 1–21. doi: 10.1186/s40164-023-00433-y.

Fearon, E. and Vogelstein, B. (1990). 'A genetic model for colorectal tumorigenesis', *Cell*. Cell, 61(5), pp. 759–767. doi: 10.1016/0092-8674(90)90186-I.

Fei, K., Zhang, J., Yuan, J. and Xiao, P. (2022). 'Present Application and Perspectives of Organoid Imaging Technology', *Bioengineering*, 9(3). doi: 10.3390/bioengineering9030121.

Franchi-Mendes, T., Eduardo, R., Domenici, G. and Brito, C. (2021). '3D cancer models: Depicting cellular crosstalk within the tumour microenvironment', *Cancers*, 13(18), pp. 1–49. doi: 10.3390/cancers13184610.

Fujii, M., Matano, M., Toshimitsu, K., Takano, A., Mikami, Y., Nishikori, S., Sugimoto, S. and Sato, T. (2018). 'Human Intestinal Organoids Maintain Self-Renewal Capacity and Cellular Diversity in

Niche-Inspired Culture Condition', *Cell Stem Cell*. Elsevier Inc., 23(6), pp. 787-793.e6. doi: 10.1016/j.stem.2018.11.016.

Gan, G. L., Wu, H. T., Zheng, Y. F., Chen, W. J., Li, C. L., Ye, Q. Q. and Liu, J. (2021). 'Diverse expression patterns of mucin 2 in colorectal cancer indicates its mechanism related to the intestinal mucosal barrier', *World Journal of Gastroenterology*, 27(25), pp. 3888–3900. doi: 10.3748/wjg.v27.i25.3888.

Gehling, K., Parekh, S., Schneider, F., Kirchner, M., Kondylis, V., Nikopoulou, C. and Tessarz, P. (2022). 'RNA-sequencing of single cholangiocyte-derived organoids reveals high organoid-to-organoid variability', *Life Science Alliance*, 5(12), pp. 1–12. doi: 10.26508/lsa.202101340.

Gillet, J. P., Calcagno, A. M., Varma, S., Marino, M., Green, L. J., Vora, M. I., Patel, C., Orina, J. N., Eliseeva, T. A., Singal, V., Padmanabhan, R., Davidson, B., Ganapathi, R., Sood, A. K., Rueda, B. R., Ambudkar, S. V. and Gottesman, M. M. (2011). 'Redefining the relevance of established cancer cell lines to the study of mechanisms of clinical anti-cancer drug resistance', *Proceedings of the National Academy of Sciences of the United States of America*, 108(46), pp. 18708–18713. doi: 10.1073/pnas.1111840108.

Gjorevski, N., Avignon, B., Gérard, R., Cabon, L., Roth, A. B., Bscheider, M. and Moisan, A. (2020). 'Neutrophilic infiltration in organ-on-a-chip model of tissue inflammation', *Lab on a Chip*. The Royal Society of Chemistry, 20(18), pp. 3365–3374. doi: 10.1039/D0LC00417K.

Groves, T., Corley, C., Byrum, S. D. and Allen, A. R. (2021). 'The Effects of 5-Fluorouracil/Leucovorin Chemotherapy on Cognitive Function in Male Mice', *Frontiers in Molecular Biosciences*, 8(October), pp. 1–13. doi: 10.3389/fmolb.2021.762116.

Gu, Y., Zhang, W., Wu, X., Zhang, Y., Xu, K. and Su, J. (2023). 'Organoid assessment technologies', *Clinical and Translational Medicine*, 13(12). doi: 10.1002/ctm2.1499.

Gunti, S., Hoke, A. T. K., Vu, K. P. and London, N. R. (2021). 'Organoid and spheroid tumor models: Techniques and applications', *Cancers*, 13(4), pp. 1–18. doi: 10.3390/cancers13040874.

Gwilt, K. B. and Thiagarajah, J. R. (2023). 'Overcoming problematic growth phenotypes in organoids from patients with monogenic GI disease', pp. 1–11.

Hahn, S., Nam, M. O., Noh, J. H., Lee, D. H., Han, H. W., Kim, D. H., Hahm, K. B., Hong, S. P., Yoo, J. H. and Yoo, J. (2017). 'Organoid-based epithelial to mesenchymal transition (OEMT) model: From an intestinal fibrosis perspective', *Scientific Reports*. Springer US, 7(1), pp. 1–11. doi: 10.1038/s41598-017-02190-5.

Haisler, W. L., Timm, D. M., Gage, J. A., Tseng, H., Killian, T. C. and Souza, G. R. (2013). 'Three-dimensional cell culturing by magnetic levitation', *Nature Protocols* 2013 8:10. Nature Publishing Group, 8(10), pp. 1940–1949. doi: 10.1038/nprot.2013.125.

Han, S. J., Kwon, S. and Kim, K. S. (2021). 'Challenges of applying multicellular tumor spheroids in preclinical phase', *Cancer Cell International*. BioMed Central, 21(1), pp. 1–19. doi: 10.1186/s12935-021-01853-8.

Han, W., Lu, G., Zhao, S., Wang, R., Liu, K., Nie, Y. and Dong, J. (2023). 'Rapid , Efficient , and Universally Applicable Genetic Engineering of Intestinal Organoid with a Sequential Monolayer to Three-Dimensional Strategy', *Wiley Stem Cells International*, 2024.

El Harane, S., Zidi, B., El Harane, N., Krause, K.-H., Matthes, T. and Preynat-Seauve, O. (2023). 'Cancer Spheroids and Organoids as Novel Tools for Research Precision Medicine', *Cells*, 12(7), p. 1001.

He, Gui Wei, Lin Lin, Jeff DeMartino, Xuan Zheng, Nadzeya Staliarova, Talya Dayton, Harry Begthel, et al. 2022. "Optimized Human Intestinal Organoid Model Reveals Interleukin-22-Dependency of Paneth Cell Formation." *Cell Stem Cell* 29 (9): 1333-1345.e6.

<https://doi.org/10.1016/j.stem.2022.08.002>.

- Hendel, S. K., Kellermann, L., Hausmann, A., Bindslev, N., Jensen, K. B. and Nielsen, O. H. (2022). ‘Tuft Cells and Their Role in Intestinal Diseases’, *Frontiers in Immunology*, pp. 1–13. doi: 10.3389/fimmu.2022.822867.
- Herath, M., Hosie, S., Bornstein, J. C., Franks, A. E. and Hill-Yardin, E. L. (2020). ‘The Role of the Gastrointestinal Mucus System in Intestinal Homeostasis: Implications for Neurological Disorders’, *Frontiers in Cellular and Infection Microbiology*. Frontiers Media S.A., 10, p. 248. doi: 10.3389/FCIMB.2020.00248/BIBTEX.
- Hickman, J. A., Graeser, R., de Hoogt, R., Vidic, S., Brito, C., Gutekunst, M., van der Kuip, H. and Imi Predelect consortium (2014). ‘Three-dimensional models of cancer for pharmacology and cancer cell biology: Capturing tumor complexity in vitro/ex vivo’, *Biotechnology Journal*. John Wiley & Sons, Ltd, 9(9), pp. 1115–1128. doi: 10.1002/BIOT.201300492.
- Hirokawa, Y., Clarke, J., Palmieri, M., Tan, T., Mouradov, D., Li, S., Lin, C., Li, F., Luo, H., Wu, K., Faux, M., Tan, C. W., Lee, M., Gard, G., Gibbs, P., Burgess, A. W. and Sieber, O. M. (2021). ‘Low-viscosity matrix suspension culture enables scalable analysis of patient-derived organoids and tumoroids from the large intestine’, *Communications Biology*. Springer US, 4(1), pp. 1–17. doi: 10.1038/s42003-021-02607-y.
- Ho-Pun-Cheung, A., Bascoul-Molleivi, C., Assenat, E., Boissière-Michot, F., Bibeau, F., Cellier, D., Ychou, M. and Lopez-Crapez, E. (2009). ‘Reverse transcription-quantitative polymerase chain reaction: Description of a RIN-based algorithm for accurate data normalization’, *BMC Molecular Biology*, 10, pp. 1–10. doi: 10.1186/1471-2199-10-31.
- Hoarau-Véchet, J., Rafii, A., Touboul, C. and Pasquier, J. (2018). ‘Halfway between 2D and animal models: Are 3D cultures the ideal tool to study cancer-microenvironment interactions?’, *International Journal of Molecular Sciences*, 19(1). doi: 10.3390/ijms19010181.
- Hoevenaer, W. H. M., Janssen, A., Quirindongo, A. I., Ma, H., Klaasen, S. J., Teixeira, A., van Gerwen, B., Lansu, N., Morsink, F. H. M., Offerhaus, G. J. A., Medema, R. H., Kops, G. J. P. L. and Jelluma, N. (2020). ‘Degree and site of chromosomal instability define its oncogenic potential’, *Nature Communications*. Springer US, 11(1), pp. 1–11. doi: 10.1038/s41467-020-15279-9.
- Hofer, M. and Lutolf, M. P. (2021). ‘Engineering organoids’, *Nature Reviews Materials*. Springer US, 6(5), pp. 402–420. doi: 10.1038/s41578-021-00279-y.
- Hong, Q., Li, B., Cai, X., Lv, Z., Cai, S., Zhong, Y. and Wen, B. (2021). ‘Transcriptomic Analyses of the Adenoma-Carcinoma Sequence Identify Hallmarks Associated With the Onset of Colorectal Cancer’, *Frontiers in Oncology*, pp. 1–18. doi: 10.3389/fonc.2021.704531.
- Hossain, M. S., Karuniawati, H., Jairoun, A. A., Urbi, Z., Ooi, D. J., John, A., Lim, Y. C., Kibria, K. M. K., Mohiuddin, A. K. M., Ming, L. C., Goh, K. W. and Hadi, M. A. (2022). ‘Colorectal Cancer : A Review of Carcinogenesis , Global’, *Cancer*, 14(1732), pp. 1–25.
- Hu, T., Li, Z., Gao, C. Y. and Cho, C. H. (2016). ‘Mechanisms of drug resistance in colon cancer and its therapeutic strategies’, *World Journal of Gastroenterology*, 22(30), pp. 6876–6889. doi: 10.3748/wjg.v22.i30.6876.
- Huang, L., Yang, Y., Yang, F., Liu, S., Zhu, Z., Lei, Z. and Guo, J. (2018). ‘Functions of EpCAM in physiological processes and diseases (Review)’, *International Journal of Molecular Medicine*, 42(4), pp. 1771–1785. doi: 10.3892/ijmm.2018.3764.
- Hughes, C. S., Postovit, L. M. and Lajoie, G. A. (2010). ‘Matrigel: a complex protein mixture required for optimal growth of cell culture.’, *Proteomics*, 10(9), pp. 1886–1890. doi: 10.1002/pmic.200900758.
- Imamura, Y., Mukohara, T., Shimono, Y., Funakoshi, Y., Chayahara, N., Toyoda, M., Kiyota, N., Takao, S., Kono, S., Nakatsura, T. and Minami, H. (2015). ‘Comparison of 2D- and 3D-culture models

as drug-testing platforms in breast cancer’, *Oncology Reports*, 33(4), pp. 1837–1843. doi: 10.3892/or.2015.3767.

In, J., Foulke-Abel, J., Zachos, N. C., Hansen, A. M., Kaper, J. B., Bernstein, H. D., Halushka, M., Blutt, S., Estes, M. K., Donowitz, M. and Kovbasnjuk, O. (2016). ‘Enterohemorrhagic Escherichia coli Reduces Mucus and Intermicrovillar Bridges in Human Stem Cell-Derived Colonoids’, *Cmgh*. Elsevier Inc, 2(1), pp. 48-62.e3. doi: 10.1016/j.jcmgh.2015.10.001.

Iqbal, S., Rezaul Karim, M., Yang, D. C., Mathiyalagan, R. and Chan Kang, S. (2023). ‘Tuft cells - the immunological interface and role in disease regulation’, *International Immunopharmacology*. Elsevier, 118, p. 110018. doi: 10.1016/J.INTIMP.2023.110018.

Jensen, C. and Teng, Y. (2020). ‘Is It Time to Start Transitioning From 2D to 3D Cell Culture?’, *Frontiers in Molecular Biosciences*, pp. 1–15. doi: 10.3389/fmolb.2020.00033.

Jensen, K. B. and Little, M. H. (2023). ‘Organoids are not organs: Sources of variation and misinformation in organoid biology’, *Stem Cell Reports*, 18(6), pp. 1255–1270. doi: 10.1016/j.stemcr.2023.05.009.

Jeon, E. Y., Sorrells, L. and Abaci, H. E. (2022). ‘Biomaterials and bioengineering to guide tissue morphogenesis in epithelial organoids’, *Frontiers in Bioengineering and Biotechnology*, pp. 1–18. doi: 10.3389/fbioe.2022.1038277.

Jovic, D., Liang, X., Zeng, H., Lin, L., Xu, F. and Luo, Y. (2022). ‘Single-cell RNA sequencing technologies and applications: A brief overview’, *Clinical and Translational Medicine*, 12(3). doi: 10.1002/ctm2.694.

Kapałczyńska, M., Kolenda, T., Przybyła, W., Zajączkowska, M., Teresiak, A., Filas, V., Ibbs, M., Bliźniak, R., Łuczewski, Ł. and Lamperska, K. (2016). ‘2D and 3D cell cultures – a comparison of different’, *Archives of Medical Science*, 14(4), pp. 910–919.

Karve, S. S., Pradhan, S., Ward, D. V. and Weiss, A. A. (2017). ‘Intestinal organoids model human responses to infection by commensal and Shiga toxin producing Escherichia coli’, *PLoS ONE*, 12(6), pp. 1–20. doi: 10.1371/journal.pone.0178966.

Kashfi, S. M. H., Almozyan, S., Jinks, N., Koo, B. K. and Nateri, A. S. (2018). ‘Morphological alterations of cultured human colorectal matched tumour and healthy organoids’, *Oncotarget*, 9(12), pp. 10572–10584. doi: 10.18632/oncotarget.24279.

Kasprzak, A. and Adamek, A. (2019). ‘Insulin-like growth factor 2 (IGF2) signaling in colorectal cancer—from basic research to potential clinical applications’, *International Journal of Molecular Sciences*, 20(19), pp. 1–28. doi: 10.3390/ijms20194915.

Khan, U., Chowdhury, S., Billah, M. M., Islam, K. M. D., Thorlacius, H. and Rahman, M. (2021). ‘Neutrophil Extracellular Traps in Colorectal Cancer Progression and Metastasis’, *International Journal of Molecular Sciences*, 22(14), p. 7260. doi: 10.3390/IJMS22147260.

Khetan, S. and Burdick, J. A. (2010). ‘Patterning network structure to spatially control cellular remodeling and stem cell fate within 3-dimensional hydrogels’, *Biomaterials*. Elsevier, 31(32), pp. 8228–8234. doi: 10.1016/j.biomaterials.2010.07.035.

Khiavi, M. A., Safary, A. and Somi, M. H. (2019). ‘Recent advances in targeted therapy of colorectal cancer: impacts of monoclonal antibodies nanoconjugates’, *BioImpacts : BI*. Tabriz University of Medical Sciences, 9(3), p. 123. doi: 10.15171/BI.2019.16.

Kim, J., Koo, B. K. and Knoblich, J. A. (2020). ‘Human organoids: model systems for human biology and medicine’, *Nature Reviews Molecular Cell Biology*. Springer US, 21(10), pp. 571–584. doi: 10.1038/s41580-020-0259-3.

Kozłowski, M. T., Crook, C. J. and Ku, H. T. (2021). ‘Towards organoid culture without Matrigel’,

*Communications Biology*. Springer US, 4(1). doi: 10.1038/s42003-021-02910-8.

Kretzschmar, K. (2021). ‘Cancer research using organoid technology’, *Journal of Molecular Medicine*. *Journal of Molecular Medicine*, 99(4), pp. 501–515. doi: 10.1007/s00109-020-01990-z.

Krüger, J., Groß, R., Conzelmann, C., Müller, J. A., Koepke, L., Sparrer, K. M. J., Weil, T., Schütz, D., Seufferlein, T., Barth, T. F. E., Stenger, S., Heller, S., Münch, J. and Kleger, A. (2021). ‘Drug Inhibition of SARS-CoV-2 Replication in Human Pluripotent Stem Cell–Derived Intestinal Organoids’, *Cmgh*. Elsevier Inc, 11(4), pp. 935–948. doi: 10.1016/j.jcmgh.2020.11.003.

Laguerre, F., Anouar, Y. and Montero-Hadjadje, M. (2020). ‘Chromogranin A in the early steps of the neurosecretory pathway’, *IUBMB Life*, 72(4), pp. 524–532. doi: 10.1002/iub.2218.

Lamarca, A., Foster, L., Valle, J. W., Satyadas, T. and Siriwardena, A. (2020). ‘FOLFIRINOX or FOLFOXIRI in locally advanced duodenal adenocarcinoma: Are we missing out?’, *ESMO Open*. Elsevier Masson SAS, 5(5), p. e000633. doi: 10.1136/esmoopen-2019-000633.

Langhans, S. A. (2018). ‘Three-dimensional in vitro cell culture models in drug discovery and drug repositioning’, *Frontiers in Pharmacology*, pp. 1–14. doi: 10.3389/fphar.2018.00006.

Lehmann, R., Lee, C. M., Shugart, E. C., Benedetti, M., Charo, R. A., Gartner, Z., Hogan, B., Knoblich, J., Nelson, C. M. and Wilson, K. M. (2019). ‘Human organoids: A new dimension in cell biology’, *Molecular Biology of the Cell*, 30(10), pp. 1129–1137. doi: 10.1091/mbc.E19-03-0135.

Leslie, J. L., Huang, S., Opp, J. S., Nagy, M. S., Kobayashi, M., Young, V. B. and Spence, J. R. (2015). ‘Persistence and toxin production by *Clostridium difficile* within human intestinal organoids result in disruption of epithelial paracellular barrier function’, *Infection and Immunity*, 83(1), pp. 138–145. doi: 10.1128/IAI.02561-14.

Liu, Q., Ran, D., Wang, L., Feng, J., Deng, W., Mei, D., Peng, Y. and Du, C. (2023). ‘Association between Ki67 expression and therapeutic outcome in colon cancer’, *Oncology Letters*, 25(6), pp. 1–6. doi: 10.3892/ol.2023.13858.

Livak, K. J. and Schmittgen, T. D. (2001). ‘Analysis of Relative Gene Expression Data Using Real-Time Quantitative PCR and the 2<sup>-</sup> $\Delta\Delta$ CT Method’, *Methods*. Academic Press, 25(4), pp. 402–408. doi: 10.1006/METH.2001.1262.

Lueschow, S. R. and McElroy, S. J. (2020). ‘The Paneth Cell: The Curator and Defender of the Immature Small Intestine’, *Frontiers in Immunology*, pp. 1–12. doi: 10.3389/fimmu.2020.00587.

Lugli, A., Iezzi, G., Hostettler, I., Muraro, M. G., Mele, V., Tornillo, L., Carafa, V., Spagnoli, G., Terracciano, L. and Zlobec, I. (2010). ‘Prognostic impact of the expression of putative cancer stem cell markers CD133, CD166, CD44s, EpCAM, and ALDH1 in colorectal cancer’, *British Journal of Cancer*. Nature Publishing Group, 103(3), pp. 382–390. doi: 10.1038/sj.bjc.6605762.

Malki, A., Elruz, R. A., Gupta, I., Allouch, A., Vranic, S. and Al Moustafa, A. E. (2021). ‘Molecular mechanisms of colon cancer progression and metastasis: Recent insights and advancements’, *International Journal of Molecular Sciences*, 22(1), pp. 1–24. doi: 10.3390/ijms22010130.

Marinucci, M. *et al.* (2022). ‘Standardizing Patient-Derived Organoid Generation Workflow to Avoid Microbial Contamination From Colorectal Cancer Tissues’, *Frontiers in Oncology*, pp. 1–13. doi: 10.3389/fonc.2021.781833.

Mármol, I., Sánchez-de-Diego, C., Dieste, A. P., Cerrada, E. and Yoldi, M. J. R. (2017). ‘Colorectal carcinoma: A general overview and future perspectives in colorectal cancer’, *International Journal of Molecular Sciences*, 18(1). doi: 10.3390/ijms18010197.

Matano, M., Date, S., Shimokawa, M., Takano, A., Fujii, M., Ohta, Y., Watanabe, T., Kanai, T. and Sato, T. (2015). ‘Modeling colorectal cancer using CRISPR-Cas9-mediated engineering of human intestinal organoids’, *Nature Medicine*. Nature Publishing Group, 21(3), pp. 256–262. doi:

10.1038/nm.3802.

Maubach, G., Vieth, M., Boccellato, F. and Naumann, M. (2022). 'Helicobacter pylori-induced NF- $\kappa$ B: trailblazer for gastric pathophysiology', *Trends in Molecular Medicine*. Elsevier Ltd, 28(3), pp. 210–222. doi: 10.1016/j.molmed.2021.12.005.

Maunoury, R., Robine, S., Pringault, E., Léonard, N., Gaillard, J. A. and Louvard, D. (1992). 'Maunoury et al 1992 1425351', 728, pp. 717–728.

Mboko, W. P., Chhabra, P., Valcarce, M. D., Costantini, V. and Vinjé, J. (2022). 'Advances in understanding of the innate immune response to human norovirus infection using organoid models', *Journal of General Virology*, 103(1), pp. 1–18. doi: 10.1099/jgv.0.001720.

McCabe, M., Perner, Y., Magobo, R., Mirza, S. and Penny, C. (2020). 'Descriptive epidemiological study of South African colorectal cancer patients at a Johannesburg Hospital Academic institution', *JGH Open*, 4(3), pp. 360–367. doi: 10.1002/jgh3.12248.

McQuade, R. M., Stojanovska, V., Bornstein, J. C. and Nurgali, K. (2017). 'Colorectal Cancer Chemotherapy: The Evolution of Treatment and New Approaches', *Current Medicinal Chemistry*, 24(15), pp. 1537–1557. doi: 10.2174/092986732466617011152436.

Mei, X., Gu, M. and Li, M. (2020). 'Plasticity of Paneth cells and their ability to regulate intestinal stem cells', *Stem Cell Research and Therapy*. Stem Cell Research & Therapy, 11(1), pp. 1–13. doi: 10.1186/s13287-020-01857-7.

Millesi, F., Mero, S., Semmler, L., Rad, A., Stadlmayr, S., Borger, A., Supper, P., Haertinger, M., Ploszczanski, L., Windberger, U., Weiss, T., Naghilou, A. and Radtke, C. (2023). 'Systematic Comparison of Commercial Hydrogels Revealed That a Synergy of Laminin and Strain-Stiffening Promotes Directed Migration of Neural Cells', *ACS Applied Materials and Interfaces*, 15(10), pp. 12678–12695. doi: 10.1021/acsami.2c20040.

Miron, N. and Cristea, V. (2012). 'Enterocytes: Active cells in tolerance to food and microbial antigens in the gut', *Clinical and Experimental Immunology*, 167(3), pp. 405–412. doi: 10.1111/j.1365-2249.2011.04523.x.

Misiakos, E., Karidis, N. and Kouraklis, G. (2011). 'Current treatment for colorectal liver metastases', *World journal of gastroenterology*. World J Gastroenterol, 17(36), pp. 4067–4075. doi: 10.3748/WJG.V17.I36.4067.

Mohammadi, S., Morell-Perez, C., Wright, C. W., Wyche, T. P., White, C. H., Sana, T. R. and Lieberman, L. A. (2021). 'Assessing donor-to-donor variability in human intestinal organoid cultures', *Stem Cell Reports*. ElsevierCompany., 16(9), pp. 2364–2378. doi: 10.1016/j.stemcr.2021.07.016.

Morey, P., Pfannkuch, L., Pang, E., Boccellato, F., Sigal, M., Imai-Matsushima, A., Dyer, V., Koch, M., Mollenkopf, H. J., Schlaermann, P. and Meyer, T. F. (2018). 'Helicobacter pylori Depletes Cholesterol in Gastric Glands to Prevent Interferon Gamma Signaling and Escape the Inflammatory Response', *Gastroenterology*. Elsevier, Inc, 154(5), pp. 1391-1404.e9. doi: 10.1053/j.gastro.2017.12.008.

Mseka, T., Bamburg, J. R. and Cramer, L. P. (2007). 'ADF/cofilin family proteins control formation of oriented actin-filament bundles in the cell body to trigger fibroblast polarization', *Journal of Cell Science*, 120(24), pp. 4332–4344. doi: 10.1242/jcs.017640.

Munyenembe, K., Timmons, C., Weiner, A. K. M., Katz, L. A. and Yan, Y. (2021). 'DAPI staining and DNA content estimation of nuclei in uncultivable microbial eukaryotes (Arcellinida and Ciliates)', *European Journal of Protistology*, 81. doi: 10.1016/j.ejop.2021.125840.

Nazari, S. S. (2020). 'Generation of 3D Tumor Spheroids with Encapsulating Basement Membranes for Invasion Studies', *Current Protocols in Cell Biology*, 87(1), pp. 1–14. doi: 10.1002/cpcb.105.

- Ng, S., Tan, W. J., Pek, M. M. X., Tan, M. H. and Kurisawa, M. (2019). 'Mechanically and chemically defined hydrogel matrices for patient-derived colorectal tumor organoid culture', *Biomaterials*. Elsevier, 219(July), p. 119400. doi: 10.1016/j.biomaterials.2019.119400.
- Nguyen, H. T. and Duong, H. Q. (2018). 'The molecular characteristics of colorectal cancer: Implications for diagnosis and therapy (review)', *Oncology Letters*, 16(1), pp. 9–18. doi: 10.3892/ol.2018.8679.
- Nguyen, L. H., Goel, A. and Chung, D. C. (2020). 'Pathways of Colorectal Carcinogenesis', *Gastroenterology*, 158(2), pp. 291–302. doi: 10.1053/j.gastro.2019.08.059.Pathways.
- Noel, G., Baetz, N. W., Staab, J. F., Donowitz, M., Kovbasnjuk, O., Pasetti, M. F. and Zachos, N. C. (2017). 'A primary human macrophage-enteroid co-culture model to investigate mucosal gut physiology and host-pathogen interactions', *Scientific Reports*. Nature Publishing Group, 7(September 2016), pp. 1–14. doi: 10.1038/srep45270.
- Padmanaban, V., Tsehay, Y., Cheung, K. J., Ewald, A. J. and Bader, J. S. (2020). 'Between-tumor and within-tumor heterogeneity in invasive potential', *PLoS Computational Biology*, 16(1), pp. 1–27. doi: 10.1371/journal.pcbi.1007464.
- Pape, J., Emberton, M. and Cheema, U. (2021). '3D Cancer Models: The Need for a Complex Stroma, Compartmentalization and Stiffness', *Frontiers in Bioengineering and Biotechnology*, 9(April), pp. 1–8. doi: 10.3389/fbioe.2021.660502.
- Patil, H., Saxena, S. G., Barrow, C. J., Kanwar, J. R., Kapat, A. and Kanwar, R. K. (2017). 'Chasing the personalized medicine dream through biomarker validation in colorectal cancer', *Drug Discovery Today*. Elsevier Ltd, 22(1), pp. 111–119. doi: 10.1016/j.drudis.2016.09.022.
- Pineiro-Llanes, J., da Silva, L., Huang, J. and Cristofolletti, R. (2024). 'Comparative Study of Basement-membrane Matrices for Human Stem Cell Maintenance and Intestinal Organoid Generation', *Journal of Visualized Experiments*, 2024(205), pp. 1–22. doi: 10.3791/66277.
- Pleguezuelos-Manzano, C. *et al.* (2020). 'Mutational signature in colorectal cancer caused by genotoxic pks + E. coli', *Nature*, 580(7802), pp. 269–273. doi: 10.1038/s41586-020-2080-8.
- Pleguezuelos-Manzano Cayetano, Puschhof, J., van den Brink, S., Geurts, V., Beumer, J. and Clevers, H. (2020). 'Establishment and Culture of Human Intestinal Organoids Derived from Adult Stem Cells', *Current Protocols in Immunology*, 130(1), pp. 1–24. doi: 10.1002/cpim.106.
- Pradhan, S., Karve, S. S., Weiss, A. A., Hawkins, J., Poling, H. M., Helmrath, M. A., Wells, J. M. and McCauley, H. A. (2020). 'Tissue Responses to Shiga Toxin in Human Intestinal Organoids', *Cmgh*. Elsevier Inc, 10(1), pp. 171–190. doi: 10.1016/j.jcmgh.2020.02.006.
- Prince, E., Cruickshank, J., Ba-Alawi, W., Hodgson, K., Haight, J., Tobin, C., Wakeman, A., Avoulov, A., Topolskaia, V., Elliott, M. J., McGuigan, A. P., Berman, H. K., Haibe-Kains, B., Cescon, D. W. and Kumacheva, E. (2022). 'Biomimetic hydrogel supports initiation and growth of patient-derived breast tumor organoids', *Nature Communications*. Springer US, 13(1). doi: 10.1038/s41467-022-28788-6.
- Quirke, P., Williams, G. T., Ectors, N., Ensari, A., Piard, F. and Nagtegaal, I. (2007). 'The future of the TNM staging system in colorectal cancer: time for a debate?', *Lancet Oncology*, 8(7), pp. 651–657. doi: 10.1016/S1470-2045(07)70205-X.
- Ramani, S., Atmar, R. L. and Estes, M. K. (2014). 'Epidemiology of human noroviruses and updates on vaccine development', *Current Opinion Gastroenterology*, 30(1), pp. 25–33. doi: 10.1097/MOG.000000000000022.Epidemiology.
- Ravi, M., Paramesh, V., Kaviya, S. R., Anuradha, E. and Paul Solomon, F. D. (2015). '3D Cell Culture Systems: Advantages and Applications', *Journal of Cellular Physiology*. John Wiley & Sons, Ltd, 230(1), pp. 16–26. doi: 10.1002/JCP.24683.

- Rezakhani, S., Gjorevski, N. and Lutolf, M. P. (2021). 'Extracellular matrix requirements for gastrointestinal organoid cultures', *Biomaterials*. Elsevier Ltd, 276, p. 121020. doi: 10.1016/j.biomaterials.2021.121020.
- Rio, D. C., Ares, M., Hannon, G. J. and Nilsen, T. W. (2010). 'Purification of RNA using TRIzol (TRI reagent)', *Cold Spring Harbor protocols*. Cold Spring Harb Protoc, 2010(6). doi: 10.1101/PDB.PROT5439.
- Rizzo, G., Bertotti, A., Leto, S. M. and Vetrano, S. (2021). 'Patient-derived tumor models: a more suitable tool for pre-clinical studies in colorectal cancer', *Journal of Experimental and Clinical Cancer Research*. Journal of Experimental & Clinical Cancer Research, 40(1), pp. 1–18. doi: 10.1186/s13046-021-01970-2.
- Ryu, N. E., Lee, S. H. and Park, H. (2019). 'Spheroid Culture System Methods and Applications for Mesenchymal Stem Cells', *Cells*. NLM (Medline). doi: 10.3390/cells8121620.
- Saari, J., Siddique, F., Korpela, S., Mäntylä, E., Ihalainen, T. O., Kaukinen, K., Aalto-Setälä, K., Lindfors, K. and Juuti-Uusitalo, K. (2022). 'Toward Xeno-Free Differentiation of Human Induced Pluripotent Stem Cell-Derived Small Intestinal Epithelial Cells', *International Journal of Molecular Sciences*, 23(3). doi: 10.3390/ijms23031312.
- Saito, Y., Muramatsu, T. and Saito, H. (2020). 'Establishment and Long-Term Culture of Organoids Derived from Human Biliary Tract Carcinoma', *STAR Protocols*. Elsevier, 1(1), p. 100009. doi: 10.1016/j.xpro.2019.100009.
- Sakr, A., Elsherbeiny, M., Moneim, R. A., Shaaban, S. and Aldaly, M. (2020). 'Neoadjuvant FOLFIRINOX followed by chemoradiotherapy for middle and lower rectal cancer', *Asian Pacific Journal of Cancer Prevention*, 21(6), pp. 1717–1723. doi: 10.31557/APJCP.2020.21.6.1717.
- De Santa Barbara, P., Van Den Brink, G. R. and Roberts, D. J. (2003). 'Development and differentiation of the intestinal epithelium', *Cellular and Molecular Life Sciences*. Inseam, 60(7), p. 1322. doi: 10.1007/S00018-003-2289-3.
- Sato, T. and Clevers, H. (2013). 'Growing self-organizing mini-guts from a single intestinal stem cell: Mechanism and applications', *Science*, 340(6137), pp. 1190–1194. doi: 10.1126/science.1234852.
- Sato, T., Stange, D. E., Ferrante, M., Vries, R. G. J., Van Es, J. H., Van Den Brink, S., Van Houdt, W. J., Pronk, A., Van Gorp, J., Siersema, P. D. and Clevers, H. (2011). 'Long-term expansion of epithelial organoids from human colon, adenoma, adenocarcinoma, and Barrett's epithelium', *Gastroenterology*. Elsevier Inc., 141(5), pp. 1762–1772. doi: 10.1053/j.gastro.2011.07.050.
- Sato, T., Vries, R. G., Snippert, H. J., Wetering, M. van de, Barker, N., Stange, D. E., Es, J. H. van, Abo, A., Kujala, P., Peters, P. J. and Clevers, H. (2009). 'Single Lgr5 stem cells build crypt-villus structures in vitro without a mesenchymal niche', *Nature* 2009 459:7244. Nature Publishing Group, 459(7244), pp. 262–265. doi: 10.1038/nature07935.
- Schlaermann, P., Toelle, B., Berger, H., Schmidt, S. C., Glanemann, M., Ordemann, J., Bartfeld, S., Mollenkopf, H. J. and Meyer, T. F. (2016). 'A novel human gastric primary cell culture system for modelling Helicobacter pylori infection in vitro', *Gut*, 65(2), pp. 202–213. doi: 10.1136/gutjnl-2014-307949.
- Schnalzger, T. E., Groot, M. H., Zhang, C., Mosa, M. H., Michels, B. E., Röder, J., Darvishi, T., Wels, W. S. and Farin, H. F. (2019). '3D model for CAR-mediated cytotoxicity using patient-derived colorectal cancer organoids', *The EMBO Journal*, 38(12), pp. 1–15. doi: 10.15252/embj.2018100928.
- Schutgens, F. and Clevers, H. (2020). 'Human Organoids: Tools for Understanding Biology and Treating Diseases', *Annual Review of Pathology: Mechanisms of Disease*, 15, pp. 211–234. doi: 10.1146/annurev-pathmechdis-012419-032611.
- Schwank, G., Koo, B. K., Sasselli, V., Dekkers, J. F., Heo, I., Demircan, T., Sasaki, N., Boymans, S.,

- Cuppen, E., Van Der Ent, C. K., Nieuwenhuis, E. E. S., Beekman, J. M. and Clevers, H. (2013). 'Functional repair of CFTR by CRISPR/Cas9 in intestinal stem cell organoids of cystic fibrosis patients', *Cell Stem Cell*. Elsevier Inc., 13(6), pp. 653–658. doi: 10.1016/j.stem.2013.11.002.
- Shankaran, A., Prasad, K., Chaudhari, S., Brand, A. and Satyamoorthy, K. (2021). 'Advances in development and application of human organoids', *3 Biotech*. Springer International Publishing, 11(6), pp. 1–22. doi: 10.1007/s13205-021-02815-7.
- Shariati, L., Esmaili, Y., Haghjooy Javanmard, S., Bidram, E. and Amini, A. (2021). 'Organoid technology: Current standing and future perspectives', *Stem Cells*, 39(12), pp. 1625–1649. doi: 10.1002/stem.3379.
- Sharma, R., Aashima, Nanda, M., Fronterre, C., Sewagudde, P., Ssentongo, A. E., Yenney, K., Arhin, N. D., Oh, J., Amponsah-Manu, F. and Ssentongo, P. (2022). 'Mapping Cancer in Africa: A Comprehensive and Comparable Characterization of 34 Cancer Types Using Estimates From GLOBOCAN 2020', *Frontiers in Public Health*, 10(April), pp. 1–14. doi: 10.3389/fpubh.2022.839835.
- Siegel, R. L., Miller, K. D., Fuchs, H. E. and Jemal, A. (2021). 'Cancer Statistics, 2021', *CA: A Cancer Journal for Clinicians*, 71(1), pp. 7–33. doi: 10.3322/caac.21654.
- Simian, M. and Bissell, M. J. (2017). 'Organoids: A historical perspective of thinking in three dimensions', *Journal of Cell Biology*, 216(1), pp. 31–40. doi: 10.1083/jcb.201610056.
- Smit, W. L., Spaan, C. N., De Boer, R. J., Ramesh, P., Garcia, T. M., Meijer, B. J., Vermeulen, J. L. M., Lezzerini, M., MacInnes, A. W., Koster, J., Medema, J. P., Van Den Brink, G. R., Muncan, V. and Heijmans, J. (2020). 'Driver mutations of the adenoma-carcinoma sequence govern the intestinal epithelial global translational capacity', *Proceedings of the National Academy of Sciences of the United States of America*, 117(41), pp. 25560–25570. doi: 10.1073/pnas.1912772117.
- Sung, D. J. and Sung, C. K. (2010). 'AJCC CANCER STAGING MANUAL', in Edge, S. B., Byrd, D. R., Compton, C. C., Fritz, A. G., Greene, F. L., and Trotti, A. (eds) *Springer*. 7th edn. New York: Springer New York Dordrecht Heidelberg London, pp. 143–164. doi: 10.1007/978-3-642-05322-1\_33.
- Sung, H., Ferlay, J., Siegel, R. L., Laversanne, M., Soerjomataram, I., Jemal, A. and Bray, F. (2021). 'Global cancer statistics 2020: GLOBOCAN estimates of incidence and mortality worldwide for 36 cancers in 185 countries', *CA: A Cancer Journal for Clinicians*, pp. 1–41. doi: 10.3322/caac.21660.
- Taelman, J., Diaz, M. and Guiu, J. (2022). 'Human Intestinal Organoids: Promise and Challenge', *Frontiers in Cell and Developmental Biology*, 10(March), pp. 1–9. doi: 10.3389/fcell.2022.854740.
- Tian, C. mei, Yang, M. feng, Xu, H. ming, Zhu, M. zheng, Yue, N. N., Zhang, Y., Shi, R. yue, Yao, J., Wang, L. sheng, Liang, Y. jie and Li, D. feng (2023). 'Stem cell-derived intestinal organoids: a novel modality for IBD', *Cell Death Discovery*. Springer US, 9(1). doi: 10.1038/s41420-023-01556-1.
- Tong, G., Zhang, G., Liu, J., Zheng, Z., Chen, Y., Niu, P. and Xu, X. (2020). 'Cutoff of 25% for Ki67 expression is a good classification tool for prognosis in colorectal cancer in the AJCC-8 stratification', *Oncology Reports*, 43(4), pp. 1187–1198. doi: 10.3892/or.2020.7511.
- Tsai, Y. H., Czerwinski, M., Wu, A., Dame, M. K., Attili, D., Hill, E., Colacino, J. A., Nowacki, L. M., Shroyer, N. F., Higgins, P. D. R., Kao, J. Y. and Spence, J. R. (2018). 'A Method for Cryogenic Preservation of Human Biopsy Specimens and Subsequent Organoid Culture', *Cmgh*, 6(2), pp. 218–222.e7. doi: 10.1016/j.jcmgh.2018.04.008.
- Tuveson, D. and Clevers, H. (2019). 'Cancer modeling meets human organoid technology', *Science*, 364(6444), pp. 952–955. doi: 10.1126/science.aaw6985.
- Urbischek, M., Rannikmae, H., Foets, T., Ravn, K., Hyvönen, M. and de la Roche, M. (2019). 'Organoid culture media formulated with growth factors of defined cellular activity', *Scientific Reports*, 9(1), pp. 1–11. doi: 10.1038/s41598-019-42604-0.

- Valderrama-Treviño, A. I., Barrera-Mera, B., Ceballos-Villalva, J. C. and Montalvo-Javé, E. E. (2017). ‘Hepatic Metastasis from Colorectal Cancer’, *Euroasian Journal of Hepato-Gastroenterology*. Jaypee Brothers Medical Publishing (P) Ltd., 7(2), p. 166. doi: 10.5005/JP-JOURNALS-10018-1241.
- Verhoeckx, K., Cotter, P., Kleiveland, C., Lea, T., Mackie, A. and Requena, T. (2015). *In vitro fermentation models: General introduction, The Impact of Food Bioactives on Health: In Vitro and Ex Vivo Models*. doi: 10.1007/978-3-319-16104-4.
- Vitale, S., Picascia, S. and Gianfrani, C. (2016). ‘The cross-talk between enterocytes and intraepithelial lymphocytes’, *Molecular and Cellular Pediatrics*. Molecular and Cellular Pediatrics, 3(1), pp. 0–3. doi: 10.1186/s40348-016-0048-4.
- Vlachogiannis, Georgios, Somaieh Hedayat, Alexandra Vatsiou, Yann Jamin, Javier Fernández-mateos, Khurum Khan, Andrea Lampis, et al. 2018. “Patient-Derived Organoids Model Treatment Response of Metastatic Gastrointestinal Cancers.” *Science* 359: 920–26.
- Vodenkova, S., Buchler, T., Cervena, K., Veskrnova, V., Vodicka, P. and Vymetalkova, V. (2020). ‘5-fluorouracil and other fluoropyrimidines in colorectal cancer: Past, present and future’, *Pharmacology and Therapeutics*. Elsevier Inc., 206, p. 107447. doi: 10.1016/j.pharmthera.2019.107447.
- Vonk, A. M., van Mourik, P., Ramalho, A. S., Silva, I. A. L., Statia, M., Kruisselbrink, E., Suen, S. W. F., Dekkers, J. F., Vlegaar, F. P., Houwen, R. H. J., Mullenders, J., Boj, S. F., Vries, R., Amaral, M. D., de Boeck, K., van der Ent, C. K. and Beekman, J. M. (2020). ‘Protocol for Application, Standardization and Validation of the Forskolin-Induced Swelling Assay in Cystic Fibrosis Human Colon Organoids’, *STAR Protocols*. Elsevier, 1(1), p. 100019. doi: 10.1016/j.xpro.2020.100019.
- Walsh, A. J., Cook, R. S., Sanders, M. E., Arteaga, C. L. and Skala, M. C. (2016). ‘Drug response in organoids generated from frozen primary tumor tissues’, *Scientific Reports*. Nature Publishing Group, 6(June 2015), pp. 1–12. doi: 10.1038/srep18889.
- Wang, R., Mao, Y., Wang, Wendong, Zhou, X., Wang, Wei, Gao, S., Li, J., Wen, L., Fu, W. and Tang, F. (2022). ‘Systematic evaluation of colorectal cancer organoid system by single-cell RNA-Seq analysis’, *Genome Biology*. BioMed Central, 23(1), pp. 1–22. doi: 10.1186/s13059-022-02673-3.
- Wang, S., Guan, X., Ma, M., Zhuang, M., Ma, T., Liu, Z., Chen, H., Jiang, Z., Chen, Y., Wang, G. and Wang, X. (2020). ‘Reconsidering the prognostic significance of tumour deposit count in the TNM staging system for colorectal cancer’, *Scientific Reports*, 10(1), pp. 1–8. doi: 10.1038/s41598-019-57041-2.
- Watanabe, T. (2021). ‘The emerging roles of chromogranins and derived polypeptides in atherosclerosis, diabetes, and coronary heart disease’, *International Journal of Molecular Sciences*, 22(11). doi: 10.3390/ijms22116118.
- Westphalen, C. B., Asfaha, S., Hayakawa, Y., Takemoto, Y., Lukin, D., Nuber, A., Brandtner, A., Setlik, W., Remotti, H., Muley, A., Chen, X., May, R., Houchen, C., Fox, J., Gershon, M., Quante, M. and Wang, T. (2014). ‘Long-lived intestinal tuft cells serve as colon cancer–initiating cells’, *Journal of Clinical Investigation*, 124(3), pp. 1283–1295. doi: 10.1172/JCI73434DS1.
- Van De Wetering, M. et al. (2015). ‘Prospective derivation of a living organoid biobank of colorectal cancer patients’, *Cell*. Elsevier Inc., 161(4), pp. 933–945. doi: 10.1016/j.cell.2015.03.053.
- Wilson, S. S., Mayo, M., Melim, T., Knight, H., Patnaude, L., Wu, X., Phillips, L., Westmoreland, S., Dunstan, R., Fiebiger, E. and Terrillon, S. (2021). ‘Optimized Culture Conditions for Improved Growth and Functional Differentiation of Mouse and Human Colon Organoids’, *Frontiers in Immunology*, 11(February), pp. 1–18. doi: 10.3389/fimmu.2020.547102.
- Wordinger, R. J. and Clark, A. F. (2008). ‘Growth Factors and Neurotrophic Factors as Targets’, *Ocular Therapeutics*. Academic Press, pp. 87–116. doi: 10.1016/B978-012370585-3.50007-8.
- Worthington, J. J., Reimann, F. and Gribble, F. M. (2018). ‘Enteroendocrine cells-sensory sentinels of

- the intestinal environment and orchestrators of mucosal immunity', *Mucosal Immunology*. Nature Publishing Group, 11(1), pp. 3–20. doi: 10.1038/mi.2017.73.
- Wright, N. A. (2012). 'Stem Cells in the Gastrointestinal Tract', *Physiology of the Gastrointestinal Tract, Two Volume Set*. Academic Press, pp. 359–378. doi: 10.1016/B978-0-12-382026-6.00012-9.
- Yamada, K. M., Doyle, A. D. and Lu, J. (2022). 'Cell–3D matrix interactions: recent advances and opportunities', *Trends in Cell Biology*. Elsevier Ltd, 32(10), pp. 883–895. doi: 10.1016/j.tcb.2022.03.002.
- Yan, H. H. N. *et al.* (2018). 'A Comprehensive Human Gastric Cancer Organoid Biobank Captures Tumor Subtype Heterogeneity and Enables Therapeutic Screening', *Cell Stem Cell*. Elsevier Inc., 23(6), pp. 882–897.e11. doi: 10.1016/j.stem.2018.09.016.
- Yao, X. and Smolka, A. J. (2019). 'Gastric Parietal Cell Physiology and Helicobacter pylori–Induced Disease', *Gastroenterology*, 156(8), pp. 2158–2173. doi: 10.1053/j.gastro.2019.02.036.Gastric.
- Yokota, J., Yamashita, T., Inui, T., Nomoto, R., Kishimoto, W., Nakase, H. and Mizuguchi, H. (2021). 'Comparison of culture media for human intestinal organoids from the viewpoint of pharmacokinetic studies', *Biochemical and Biophysical Research Communications*. Elsevier Ltd, 566, pp. 115–122. doi: 10.1016/j.bbrc.2021.06.007.
- Yu, S. *et al.* (2020). 'Paneth Cell-Derived Lysozyme Defines the Composition of Mucolytic Microbiota and the Inflammatory Tone of the Intestine', *Immunity*, 53(2), pp. 398–416.e8. doi: 10.1016/j.immuni.2020.07.010.
- Yuan, J., Li, X. and Yu, S. (2023). 'Cancer organoid co-culture model system: Novel approach to guide precision medicine', *Frontiers in Immunology*. doi: 10.3389/fimmu.2022.1061388.
- Zhang, M., Liu, Y. and Chen, Y. G. (2020). 'Generation of 3D human gastrointestinal organoids: principle and applications', *Cell Regeneration*. Cell Regeneration, 9(1), pp. 1–13. doi: 10.1186/s13619-020-00040-w.
- Zhao, C. (2023). 'Cell culture: in vitro model system and a promising path to in vivo applications', *Journal of Histotechnology*. Taylor & Francis, pp. 1–4. doi: 10.1080/01478885.2023.2170772.
- Zhao, Z., Chen, X., Dowbaj, A. M., Sljukic, A., Bratlie, K., Lin, L., Fong, E. L. S., Balachander, G. M., Chen, Z., Soragni, A., Huch, M., Zeng, Y. A., Wang, Q. and Yu, H. (2022). 'Organoids', *Nature Reviews Methods Primers*, 2(1). doi: 10.1038/s43586-022-00174-y.
- Zhou, C., Wu, Y., Wang, Z., Liu, Y., Yu, J., Wang, W., Chen, S., Wu, W., Wang, J., Qian, G. and He, A. (2023). 'Standardization of organoid culture in cancer research', *Cancer Medicine*, 12(13), pp. 14375–14386. doi: 10.1002/cam4.5943.
- Zhou, C., Zhang, Y., Bassey, A., Huang, J., Zou, Y. and Ye, K. (2022). 'Expansion of Intestinal Secretory Cell Population Induced by Listeria monocytogenes Infection: Accompanied With the Inhibition of NOTCH Pathway', *Frontiers in Cellular and Infection Microbiology*, 12(March), pp. 1–9. doi: 10.3389/fcimb.2022.793335.
- Zhou, C., Zou, Y., Zhang, Y., Teng, S. and Ye, K. (2022). 'Involvement of CCN1 Protein and TLR2/4 Signaling Pathways in Intestinal Epithelial Cells Response to Listeria monocytogenes', *International Journal of Molecular Sciences*, 23(5), pp. 1–14. doi: 10.3390/ijms23052739.
- Zhu, G. X., Gao, D., Shao, Z. Z., Chen, L., Ding, W. J. and Yu, Q. F. (2021). 'Wnt/ $\beta$ -catenin signaling: Causes and treatment targets of drug resistance in colorectal cancer (Review)', *Molecular Medicine Reports*, 23(2), pp. 1–13. doi: 10.3892/mmr.2020.11744.